Durham E-Theses

Fluid lubrication of soft surface layers

Cudworth, Christopher J.

How to cite:

Cudworth, Christopher J. (1974) *Fluid lubrication of soft surface layers*, Durham theses, Durham University. Available at Durham E-Theses Online: http://etheses.dur.ac.uk/8280/

Use policy

The full-text may be used and/or reproduced, and given to third parties in any format or medium, without prior permission or charge, for personal research or study, educational, or not-for-profit purposes provided that:

- a full bibliographic reference is made to the original source
- a link is made to the metadata record in Durham E-Theses
- the full-text is not changed in any way

The full-text must not be sold in any format or medium without the formal permission of the copyright holders.

Please consult the full Durham E-Theses policy for further details.

UNIVERSITY OF DURHAM

DEPARTMENT OF ENGINEERING SCIENCE

FLUID LUBRICATION OF SOFT SURFACE

LAYERS

A Thesis submitted for the Degree of Doctor of Philosophy in

University of Durham

by

CHRISTOPHER J. CUDWORTH

October 1974

ACKNOWLEDGEMENTS

I would like to express my appreciation to Professor
G. R. Higginson for his advice and guidance throughout
this research project. I wish also to thank all those who
were involved in the building and adaption of experimental
rigs and in the production of this thesis.

ABSTRACT

The performance of a lubricated, elastomer lined bearing is dependent upon the surface deformations of the liner. This investigation is concerned with the prediction of influence co-efficients for rigidly backed, soft[*] layers by the finite element method. These are applied in the pure-sliding, elastohydro-dynamic lubrication problem, of a rotating rigid cylinder loaded against a thin elastic layer, which covers the plane surface of a rigid solid.

Theoretical solutions showing the influence of elastic distortions upon friction, pressure and film shape are presented. These are supported by experiments upon the same type of bearing. Pressure measurements and the tangential force on the plane surface for layers of various thicknesses are recorded as obtained from two experimental rigs.

The persistence of hydrodynamic or boundary lubrication for a soft layer compared to a rigid plane, under conditions of low speed or low viscosity lubricant, is also illustrated by the friction measurements.

[*] The term "soft" refers throughout to materials of low-elastic modulus.

CONTENTS

I tax not you, you elements, with unkindness;

I never gave you kingdom, call'd you children,

You owe me no subscription: then, let fall

Your horrible pleasure; here I stand, your slave,

A poor, infirm, weak, and despis'd old man.

But yet I call you servile ministers,

That have with two pernicious daughters join'd

Your high-engender'd battles 'gainst a head

So old and white as this. O! O! 'tis foul.

LEAR, Scene II, Act III,

King Lear.

CHAPTER 1

INTRODUCTION

1.1 Tribology of Elastic Layers

The study of the lubrication of moving contacts (tribology) has attracted interest over the last ninety years. The effects of elasticity and pressure-dependent viscosity have been combined in an elasto-hydrodynamic analysis of rolling and sliding surfaces, the result of work by a series of investigators as summarised by Dowson and Higginson, Ref. 47,48.

For materials of low stiffness, elastic deformations within the bearing affect the lubrication mechanism for relatively low pressures. In comparison, the small variation of viscosity with pressure through the bearing has a negligible effect. Such conditions occur in bearings containing surface layers of low elastic modulus, supported by a relatively rigid backing. The difficulty arises in predicting the surface deflections, as it is inappropriate to treat the layer as an infinite elastic solid.

It was the object of the present work to provide a numerical solution to the deformation of such layers. Finite element techniques were used to determine influence displacements for uniform, linear and quadratic pressures applied to the surface of the elastomer. A combination of these can be approximated to any pressure curve. They were used in the elastohydrodynamic theory to calculate lubricant film shapes, pressure distributions and friction properties of a simple bearing. The theory was supported by pressure and friction experiments on the pure sliding of a rigid cylinder against a plane elastomer layer.

1.2 Bibliography

Research on bearings with compliant liners gained impetus with the growing interest in animal joints. Jones, (1934), Ref. 2, in a simple static friction experiment remarked upon the low co-efficient of friction of a joint. Later, several investigators report values of 0.003 to 0.025, Ref. 4-6, 12, 13.

Reynolds, (1886), Ref. 1, remarked upon the "self-acting system of lubrication ...... of reciprocating joints". Simple hydrodynamic lubrication of joints was proposed by MacConaill, (1932), Ref. 3. Charnley, (1959), Ref. 4, disputed this due to the conditions of load, etc. and suggested a form of boundary lubrication. To explain the low coefficient of friction McCutchen et al., (1959), Ref. 5-7, introduced the concept of "weeping" lubrication. Dintenfass, (1963), Ref. 8, discussed the possibility of elastohydrodynamic lubrication and was supported by an analysis by Tanner, (1966), Ref. 9. Fein, (1966), Ref. 10, in experiments on squeeze films and Dowson et al., (1966), Ref. 11,12, indicated that the main method of lubrication would be elastohydrodynamic in sliding or squeeze film conditions. They suggested that boundary lubrication would occur only in cases of severe loading.

The effects of the properties of synovial fluid have also been considered. As well as the fluid being thixotropic, Ref. 8, two "enrichment" mechanisms have been postulated, Ref. 14-16. These result in an increase of viscosity with decreasing film thickness on normal approach, due to the retention of the hyaluronic acid molecules in the contact zone as the base fluid flows away.

Higginson and Norman, (1974), Ref. 17, have shown that the permeability of cartilage, allowing "weeping" and one of the enrichment processes, is ineffective in the lubrication of joints,

except perhaps for very thin films indicative of boundary lubrication. The analysis indicated that the second enrichment mechanism, relying upon adsorption of the hyaluronic acid on the cartilage surface, would be effective. The conclusion was "that the mere presence of the soft impermeable layer has a greater effect than do either of the more complicated mechanisms of weeping or enrichment". The present investigation should provide an insight into this aspect of elastohydrodynamic lubrication.

The frictional behaviour of elastomers has been extensively studied, Ref. 18-22. Cohen and Tabor, (1965), Ref. 22, illustrated the effects of lubricant and polymer properties on the friction under conditions of dry contact and hydrodynamic lubrication. A coefficient of friction as low as 0.001 was obtained for experiments in full film lubrication of rubber on glass.

In the engineering field, bearings with elastomer liners were first used in 1927 for water lubricated ships' stern tubes, Ref. 23,24. Their success over lignum vitae was widely reported, Ref. 25,26. Busse and Denton, (1932), Ref. 27, and Fogg and Hunwicks, (1937), Ref. 28, found the coefficient of friction for water lubricated fluted and plain rubber bearings, to be 0.01 to 0.05 compared to 0.02 to 0.25 for their metal counterparts. Hother-Lushington and Sellors, (1963), Ref. 29, reported on wear experiments in boundary lubrication using water in plain journal bearings of various materials including plastics.

In a pure sliding experiment involving a metal cylinder and rubber plane, Higginson, (1962), Ref. 30, related the pressures to elastohydrodynamic behaviour. This was supported by film thickness and friction measurements on crossed perspex cylinders by Archard and Kirk, (1962-63), Ref. 31,32. Roberts et al, (1969), Ref. 33,

used optical interference and Swales et al, (1972), Ref. 34, capacitance techniques to measure film thickness of a lubricated sliding rubber cylinder. Pressures were also obtained by the latter using piezoelectric transducers. Jagger and Walker, (1966), Ref. 35, measured the coefficient of friction of synthetic rubber seals operating in boundary lubrication conditions.

Experiments directly referring to the thickness of the elastic layer have been performed on several types of bearing. Dowson and Taylor, (1967), Ref. 36, and Castelli et al., (1967), Ref. 37, reported on the pressures found in circular plate thrust bearings covered by thin elastic layers. Brighton et al., (1968), Ref. 44, measured pressures in a journal bearing containing a thick Delrin plastic liner. The friction variation for several layer thicknesses was studied by Bennett and Higginson, (1969-70), Ref. 38,39, in a pure sliding experiment on a cylinder and plane apparatus.

The first theoretical analysis, applied to an elastomer lined journal bearing, was by Higginson, (1965), Ref. 40. The surface deformation was determined from the local pressure. This assumption was later used for pure sliding by Bennett, (1969-70), Ref. 38,39, and for thrust bearings by Dowson and Taylor, (1967), Ref. 36. Castelli et al., (1967), Ref. 37, also considered the axisymmetric thrust bearing and gave an exact solution for the displacements under any pressure (when described as superimposed Bessel functions). Brighton, Hooke and O'Donoghue, (1967-69), Ref. 41-44, analysed journal bearing liners in a similar manner by approximating the pressures to a limited Fourier series. For highly deformed surfaces Hooke and O'Donoghue, (1972), Ref. 45, assumed the "dry contact" pressure curve, with alterations at inlet and outlet for the hydrodynamic conditions. Non-dimensional film

thicknesses are given for pure sliding, journal bearings and O-ring seals. Baglin and Archard, (1972), Ref. 46, using a similar method introduced a "tilting pad" modification to the Hertzian pressure curves; although layers were not considered.

CHAPTER 2

EXPERIMENTAL WORK

2.1   Introduction

The aim of the experiments was to study the lubrication
characteristics of bearings containing elastomer layers of low
elastic modulus. A two-dimensional model was adopted. It consisted
of a rotating cylinder loaded against a stationary plane. The
cylinder was considered rigid, whereas the plane was constructed of
an elastic layer adhered to a rigid backing. The tangential forces
on the plane, the lubricant pressures within the contact zone and
the film shape were to be measured in various lubrication conditions.
However, it proved impractical to measure the film thickness
directly. Comparisons between the experimental and theoretical
pressures could be made, and then the film shape found from theory.
A series of experiments was also required to find the elastic
constants of the "soft" layer.

2.2 Friction

The experimental apparatus to measure the tangential forces
acting on the plane, had been developed in previous research, Ref.
38. Results had been obtained for starved and full lubrication,
Ref. 39. The new work involved an extension to the experiments in
full lubrication. Lubricants of two different viscosities were
used to study the region close to break-down of the full film where
"dry friction" began.

The rig consisted of two, contra-rotating, identical cylinders,
whose axes were nominally parallel and in the same horizontal plane.
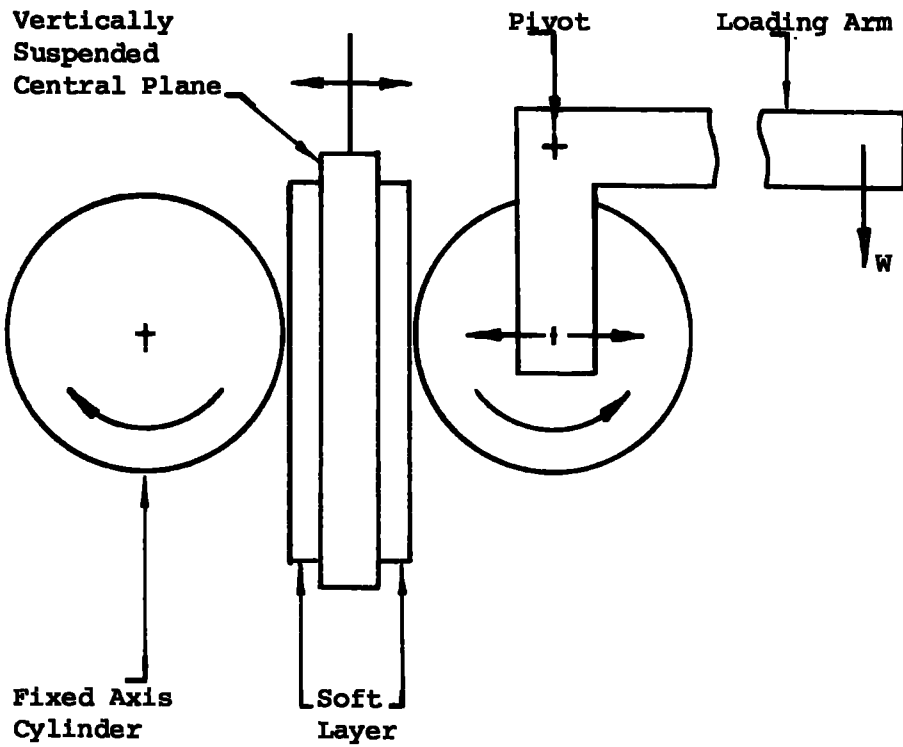
Vertically
Suspended
Central Plane

Pivot

Loading Arm

Fixed Axis
Cylinder

Soft
Layer

W

Fig. 2.1 **Friction Rig**

Pivot

Pressure
Tapping

Steel
Ball

Loading
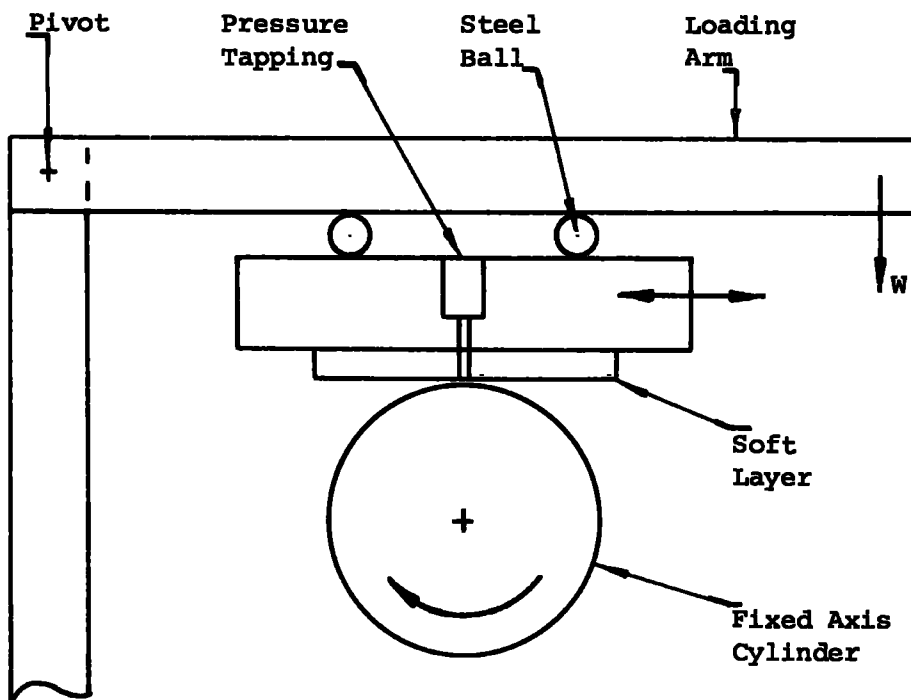Arm

W

Soft
Layer

Fixed Axis
Cylinder

Fig. 2.2 **Pressure Rig**

A vertical plane block, free to move horizontally, was suspended between the two, Fig. 2.1. The axis of one cylinder was fixed. The other cylinder was mounted on self-aligning bell-crank arms, through which a load could be applied. The plane block experienced a normal load from each cylinder. Any tangential friction force was indicated as a deflection of the beam supporting the vertical plane. The arrangement had the advantages of doubling the friction force, and overcoming the difficulties in measuring it when applying a relatively large normal load to the same body. The whole assembly was immersed in the lubricant to ensure full lubrication.

The cylinders were 115 mm diameter ground steel and could be considered rigid. The central block consisted of a composite of "rigid" Tufnol with elastic surface layers of polythene (Young's modulus approximately 40 MN/m^2). Plane layers of various thicknesses from 1 mm to 10 mm were used. In all cases it was important to build the block up to the thickness of 40 mm (the design separation between the two cylinders). The surfaces had to be straight and parallel to each other. Shell "Tellus 29" and paraffin of viscosities 10^{-1} and 1.5×10^{-3} kg/ms respectively, were the two lubricants employed. The friction variation with cylinder speed over a range of loads, was plotted for various soft layer thicknesses.

2.3 Pressure

A new rig was designed for the experiments for measuring pressure, Fig. 2.2. The simple model of pure sliding of a roller and plane was retained. A single steel cylinder 115 mm diameter rotated about a fixed horizontal axis. A perspex block 120 x 100 x 25 mm was loaded on top of the cylinder. A uniform soft layer firmly attached to the block, formed the bearing surface with

the cylinder. The steel and perspex could be considered rigid compared to the soft layer, a transparent silicone rubber of Young's modulus 1.0 MN/m^2.

The normal load was applied in the following manner. Two steel balls were positioned on the centre line of the top surface of the perspex symmetrically about the cylinder/block "line of contact". A pivoted cantilever set perpendicular to the axis of the cylinder rested on the two balls, so that a weight on its free end would apply a load to the block. The height of the pivot could be adjusted to ensure that the loading arm and block were horizontal.

Pressure measurement was by a mercury manometer. A vertical hole through the centre of the block and soft layer provided the main pressure tapping, diameter 0.5 mm. The block could be traversed through the contact zone. The rig was immersed in Shell "Tellus 29", viscosity approximately 0.1 kg/ms, to a level close to the top of the block.

The pressure distributions for various loads and speeds were found for a number of soft layer thicknesses. Even with the small pressures the width of the "contact zone" was relatively large, up to 15 mm. Thermal effects could be ignored as the temperature rise through the bearing was small due to large film thicknesses. Changes in viscosity of the lubricant due to temperature and pressure variations were negligible. As the surface layer was stationary the hysteresis characteristics of the elasticity of rubber under dynamic conditions was avoided. The contact region could be viewed easily, as the whole block was transparent.

2.4 Film thickness
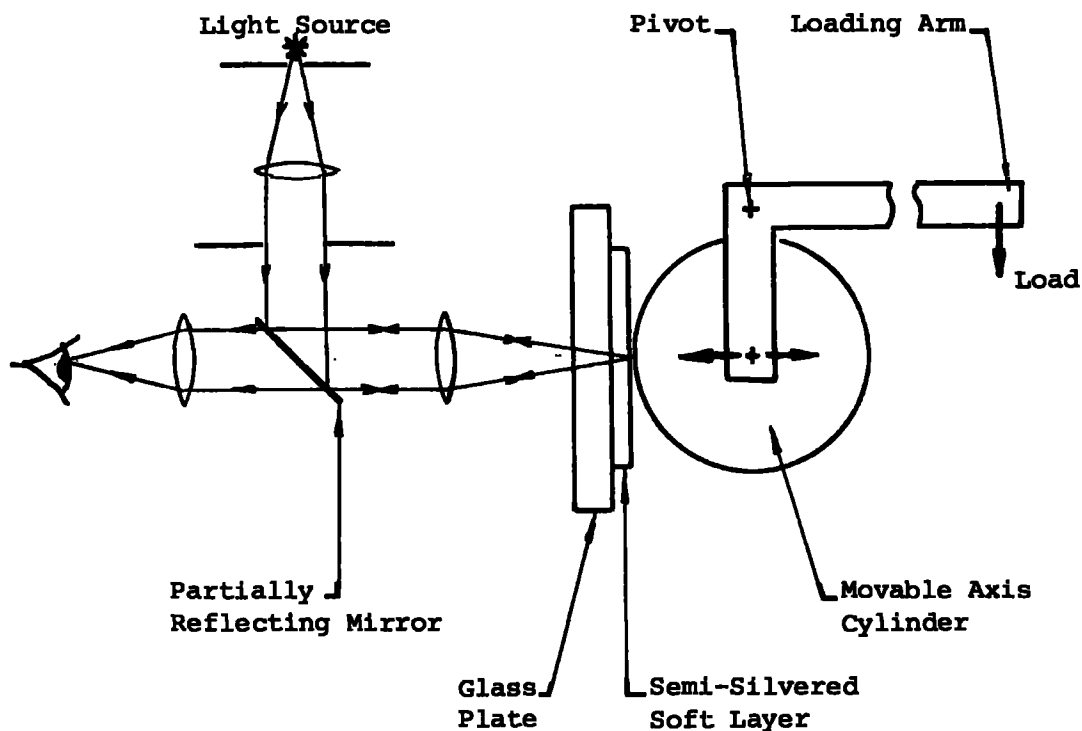
Fig 2.3 Film Thickness Rig

The friction rig was adapted to enable film thickness to be measured, but due to various difficulties results could not be obtained. Optical interference fringes developed in the gap between the cylinder and plane were to be employed; hence it was necessary to view the contact zone. The fixed axis cylinder and the suspended plane were replaced by a fixed plane. The moveable axis cylinder, which had been diamond polished to an optical finish, bore directly onto the plane. The latter consisted of a soft, surface layer of transparent, silicone rubber backed by a "rigid" glass sheet. A coating of silver was deposited on the surface of the rubber.

A suitable light source was used to produce the interference fringes between the partially reflecting silver and the polished

cylinder, Fig. 2.3. Fringes of equal thickness (e.g. Newton's rings) would provide information on variation of film thickness. On viewing the lubricant film through a spectroscope, fringes of equal chromatic order would give the absolute separation of the surfaces at that point.

Although both types of fringes could be seen for the static condition, when the cylinder was rotating none were apparent. The film shape and thickness make both types of fringes difficult to see. Due to the presence of the soft layer, the lubricant film was nearly parallel in the central region and then diverged rapidly. The fringes of equal thickness would be very widely spaced at the centre and become merged at the divergence. With the large film thicknesses the fringes of equal chromatic order would be close together in the spectrum. It was found that small, localised variations at a point in the film thickness, whilst the cylinder was rotating, disrupted the interference fringes so drastically as to make them indistinguishable. This was caused by imperfections in the overall geometry of the cylinder and inherent vibrations transmitted through the rig. These could not be reduced satis-factorily, so measurement of film thickness had to be abandoned.

2.5   Elastic Constants, Experiments and Results

The Young's modulus and Poisson's ratio of the soft layers were required for use in the computer programme. In a paper on the contact elasticity of seal elastomers, Drutowski, Ref. 49, reported a dependence of the modulus on strain life and an interaction of elastomer and fluid. However, a "before and after" test showed that the strain conditions and the lubricants in the pressure/friction experiments had a negligible effect on the elastic
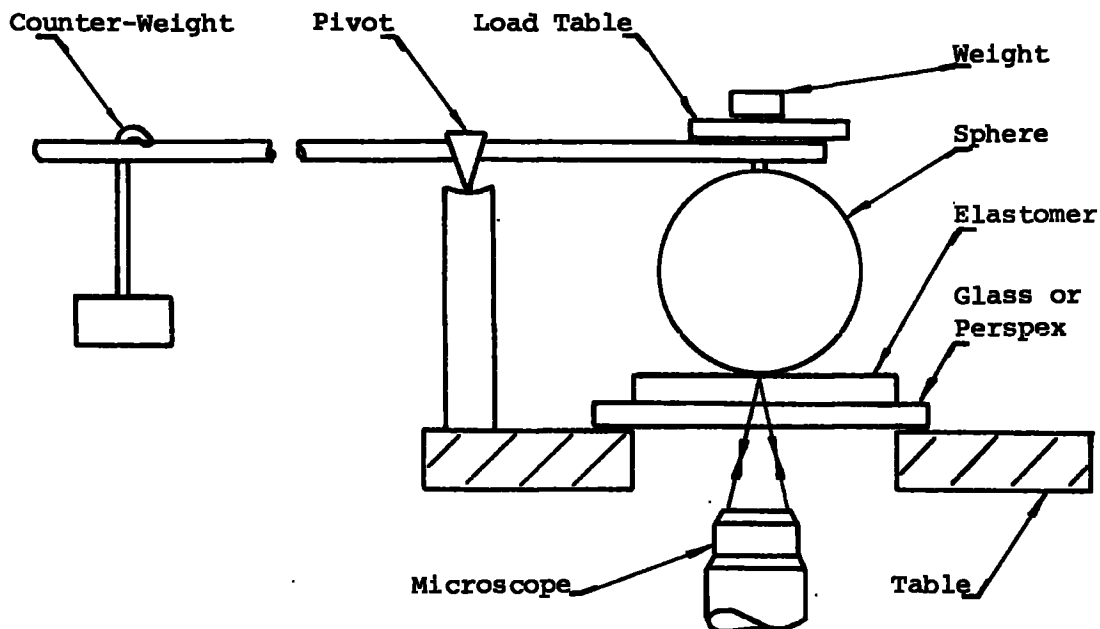
Counter-Weight   Pivot   Load Table   Weight

Sphere

Elastomer

Glass or
Perspex

Microscope   Table

Fig. 2.4 Apparatus For Measuring The Contact Area Of A

Spherical Indenter.

constants. Young's modulus was measured under similar conditions

of strain to those found in the main experiments.

The calculation of the modulus was based upon the optical

measurement of the contact between a loaded, spherical indenter and

the plane elastomer. The relationship for a sphere contacting a

plane can be developed from an analysis by Hertz, Ref. 50. The

diameter d, of the contact area is given by

$$d^3 = 6RP \frac{(1 - \nu^2)}{E}$$

(2.1)

where P is the indenting force, R the indenter's radius, E the

Young's modulus and ν the Poisson's ratio. Combined with results

from a confined compression test, the modulus can be found and an

approximate Poisson's ratio obtained.

The main part of the apparatus was a pivoted lever carrying a

45 mm diameter steel ball at one end and counter-weights at the

other, Fig 2.4. The sphere rested upon the transparent elastic

sample under test, which in turn was supported by a glass or perspex

plate. The whole could be loaded by adding weights to a small table above the sphere. The contact area was viewed and measured from below, through a microscope using normal incident illumination.

The contact area diameter to the third power was plotted against load. The slope of the linear portion of the graph G2.1 was proportional to the inverse of the elastic constants term in Eq. (2.1). The Young's modulus for the polythene used in the friction rig was known, only the properties of the silicone rubber were required. In combination with a confined compression test the results indicated a Poisson's ratio between 0.49 and 0.5.

The method had the advantage that the actual soft layers used in the lubrication experiments could be tested. The initial slope of Graph G2.1 and hence Young's modulus was identical for each layer. Only the thinnest layer deviated from a straight line; an indication of the effect of the rigid backing plate on the strain. The curves were reproducible before and after the lubrication experiments showing that the material was homogeneous and unaffected by the lubricant or strain conditions. The Young's modulus of the silicone rubber was found to be 1.02 MN/m^2; that of the polythene was of the order of 40 MN/m^2.

14
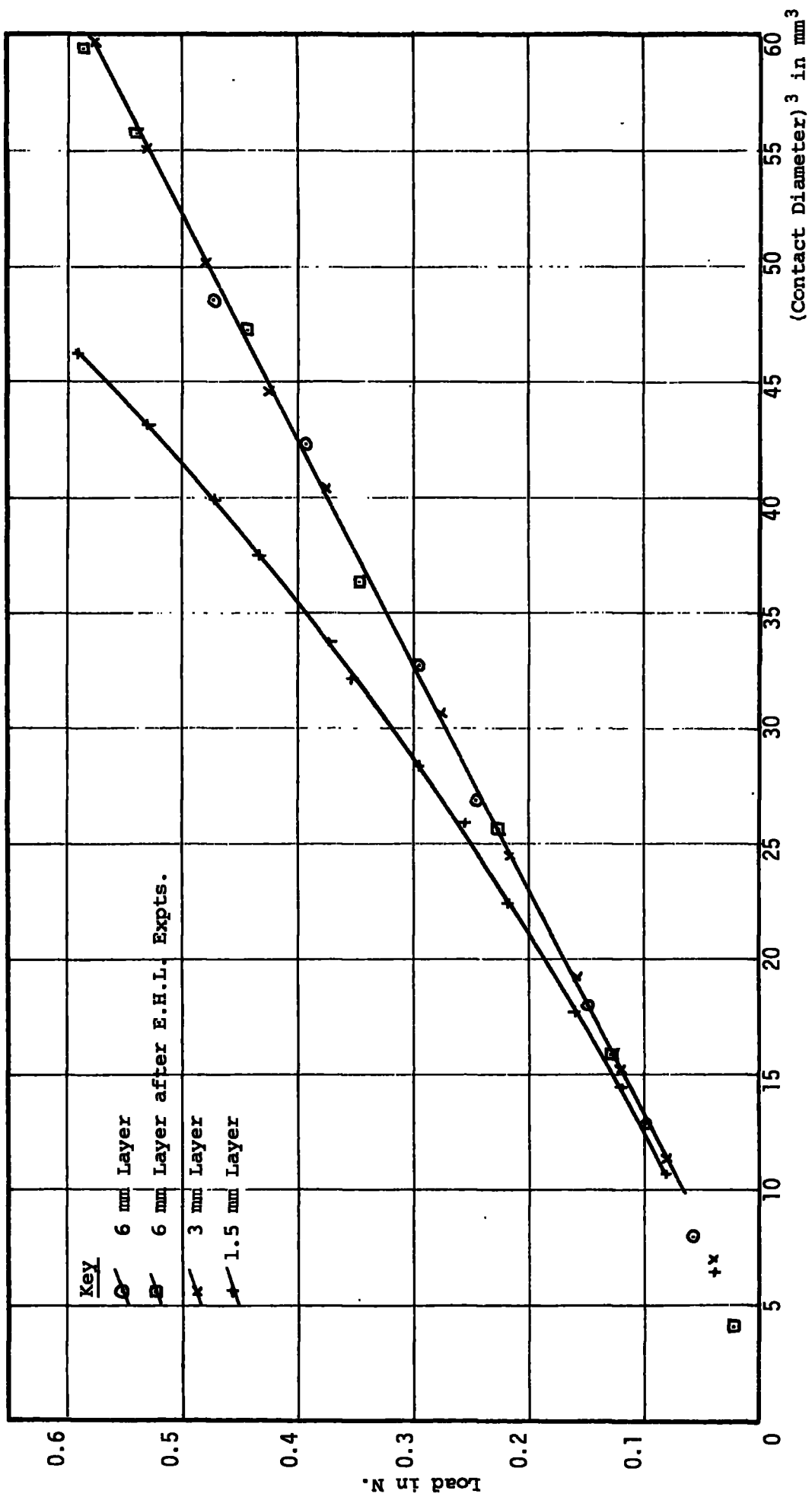
GRAPH G2.1 LOAD AGAINST (CONTACT DIAMETER)³ FOR A SPHERICAL INDENTER ON VARIOUS PLANE ELASTOMERS

CHAPTER 3

ELASTOHYDRODYNAMIC THEORY

3.1   Introduction

The investigation was aimed at bearings with surface layers of low elastic modulus, e.g. rubber, plastics, articular cartilage. The "zone of contact" was of the same order as the thickness of the soft layer; the deformations of the bearing surface being affected by the layer thickness. In the lubrication analysis, the effect of the elastic distortions predominated over the variation of lubricant viscosity, due to the relatively small temperature and pressure changes. The bearing was considered long enough to neglect side-leakage of lubricant.

The pressure distribution, friction force and film shape, in the simple pure-sliding case of a cylinder and plane, were to be predicted from the theory for a given speed and lubricant. All solids were considered rigid compared to the elastic surface layer firmly attached to the plane, Fig. 3.1.
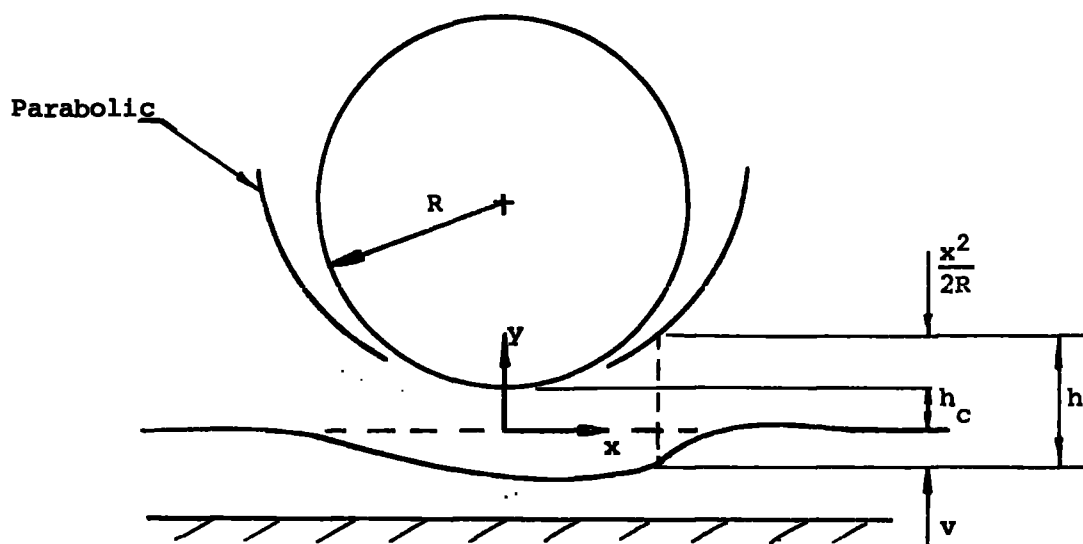
Fig. 3.1a Coordinates
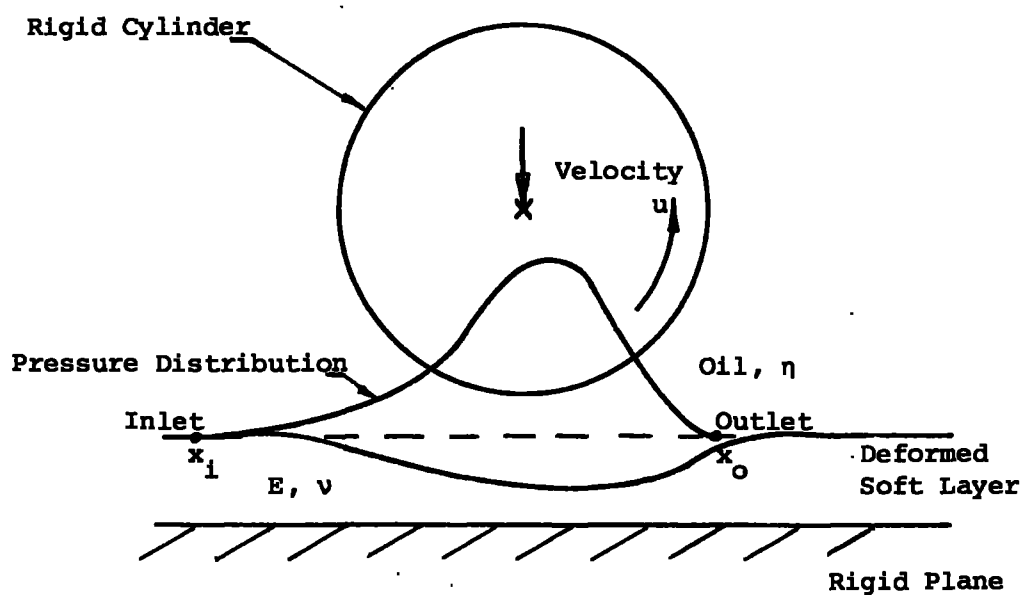
Fig. 3.1b Physical System

Fig. 3.1 Lubrication of a Rigid Cylinder and an Elastic Layer

3.2 Notation

b	Half width of pressure zone
E	Young's Modulus of elastic layer
f	Friction force per unit length of cylinder
F	f/ER
h	Film thickness
h'	Film thickness where $dp/dx = 0$
h_a	Central film thickness including deformation
h_c	Central film thickness excluding deformation
H H'	h/ER h'/ER
H_a H_c	h_a/ER h_c/ER
p	Pressure
P	p/ER
R	Radius of cylinder
t	Thickness of soft layer
T	t/R
u	Surface velocity of cylinder
U	$\eta u/ER$
v	Surface deformation of soft layer
V	v/R
w	Load per unit length of cylinder
W	w/ER
x	Distance through bearing
X	x/R
$\bar{z}$	Proportion of length occupied by lubricant in cavitation
η	Viscosity
θ	Angle around cylinder
μ	F/W, Coefficient of Friction
τ	Tangential shear stress
ν	Poisson's Ratio

3.3 Theory; Pressure and Film Shape

If the bearing is long compared with the width of contact so that the side leakage can be neglected, the pressure in the axial direction is constant and the problem is reduced to two dimensions. The integrated form of the Reynolds equation is then

$$\frac{dp}{dx} = 6\eta u \left(\frac{h - h'}{h^3} \right) \tag{3.1}$$

The expression for film thickness in Fig. 3.1 is

$$h = h_c + \frac{x^2}{2R} + v \tag{3.2}$$

for a parabolic representation of the cylinder. The material to which the soft elastic layer is attached and the cylinder are rigid. The deformation v is due solely to the surface deflection of the elastic layer. Equations (3.1) and (3.2) can be rewritten in dimensionless parameters

$$\frac{dP}{dX} = 6U \left(\frac{H - H'}{H^3} \right) \tag{3.3}$$

and

$$H = H_c + \frac{x^2}{2} + V \tag{3.4}$$

The boundary conditions for pressure are, at inlet P = O at a large distance from the contact zone; at outlet dP/dX=O, P = P_o for the cavitation boundary condition. The cavitation pressure P_o is taken usually to be zero.

The pressure distribution and film shape for a particular lubricant, speed of rotation, elastic layer and centre line separation were evaluated by the following method:

(1) The elastic distortions and hence lubricant film shape

    (Eq. 3.4) were derived from influence displacement coefficients

    assuming an initial pressure distribution.

(2) Reynolds equation was numerically integrated to provide a new
      pressure curve.

(3) The curve was segmented into quadratics suitable for the
      influence coefficients, and applied in Step (1). All
      procedures were repeated until two successive pressure dis-
      tributions were identical.

Reynolds equation was integrated by Simpson's rule. The
problem took the boundary conditions of $P = P_o$ (usually zero) and
$dP/dX = 0$, at the outlet point and was solved to find the pressure
at the inlet. As the position of the downstream, outlet point was
unknown, a trial value was selected. In general the inlet boundary
condition $P = 0$ was not satisfied so the chosen location was
modified accordingly. The iteration continued until the inlet
pressure was an acceptably small value.

The elastic distortions of the soft layer for a given bearing
geometry and pressure curve were obtained from influence displace-
ment coefficients. As described in Chapter 4, these were derived
by finite element methods for uniform, linear and quadratic pressure
variations of unit non-dimensional amplitude. The actual pressure
distribution was applied as a series of quadratics; the surface
deformation of the soft layer being the summation of the individual
distortions due to each quadratic, as determined from the influence
coefficients.

For each set of solutions the elasticity, undeformed geometry,
centre line film thickness H_a and speed-viscosity parameter U, of
the bearing were specified. The latter two could be altered for
successive problems. The process began with an estimated pressure
distribution equal to either zero or a related solution. The
resultant distortion and thence a new pressure curve were found by

the procedure described earlier.

To encourage convergence it was necessary to introduce a damping factor to the pressures before reapplying them to find the new distortions. Instead of replacing the previous distribution it was altered by a proportion of the new. Reiteration gave a pressure curve which satisfied the elasto-hydrodynamic requirements of the bearing. The next solution of the set took the initial estimated pressure distribution equal to that found for the previous case. A problem that would not converge from an initial pressure of zero could still be studied by considering it as one of a set. The detailed steps for the above procedure are given in Appendix II.

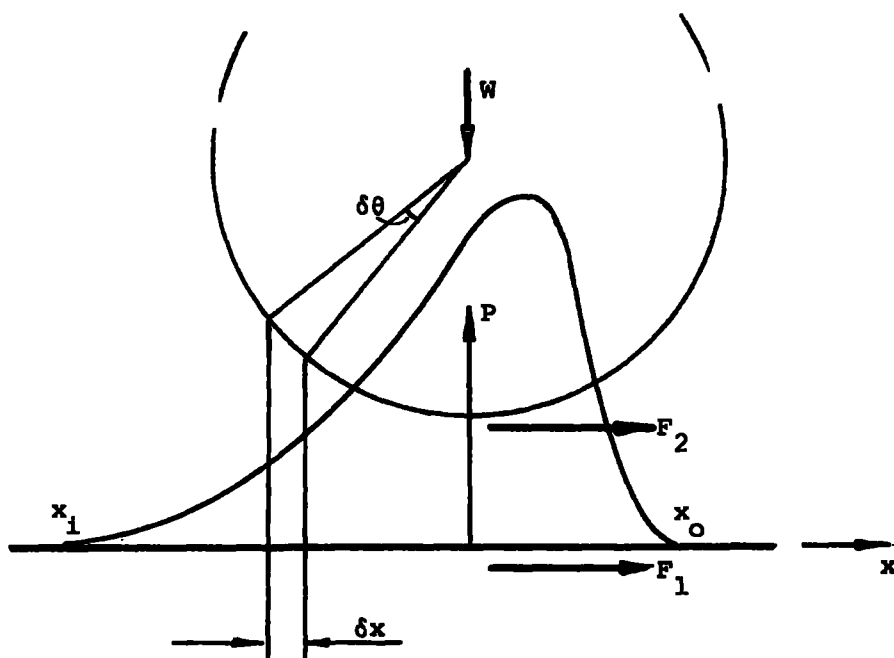### 3.4 Theory; Load and Friction Forces

Fig. 3.2 Forces on Roller and Plane

For the cylinder and plane the width of the contact zone is small compared to the radius of the cylinder. The length of an element on the surface of the cylinder at angle θ is Rδθ; Fig. 3.2. Near the contact zone

$$R\delta\theta \simeq \delta x$$

On this length the incremental load/unit width

$$\delta w = p\delta x$$

hence from inlet to outlet of the pressure curve the total load/unit width

$$w = \int_{x_i}^{x_o} p\,dx$$

or in non-dimensional terms

$$W = \int_{X_i}^{X_o} P\,dX$$

The inlet point for the pressure curve is chosen significantly far from the "contact" zone to ensure that the pressures are not affected by its position. The tangential "friction" forces f_1 and f_2 acting on the plane and cylinder are still appreciable in the pre-inlet region. However, the same equation for the surface shear forces may be used in the pre-inlet and pressure zones. It is convenient to separate the two in the computation as the deformation is negligible compared to the film thickness in the pre-inlet zone.

In the post-outlet region the lubricant forms thin streams separated by air bubbles. Only a small proportion of the solid surfaces experiences shear stresses. At any point in the cavitated region, if $\bar{z}$ is the fraction of the clearance occupied by the lubricant streams in the axial direction, then from flow continuity

$$\bar{z} = h'/h$$

The end of the cavitation is unpredictable occurring somewhere between outlet, x_o and $x = R$. The contribution to the friction forces at large values of x from this region is small. For convenience the tangential shear forces are computed over the region $-R \leqslant x \leqslant R$. Only the force f_1 on the plane is required, the general expression being

$$f_1 = \int_{-R}^{x_o} \tau \, dx + \int_{x_o}^{R} \bar{z} \, \tau \, dx$$

The shear stress at the stationary plane is

$$\tau = \frac{\eta u}{h} - \frac{h}{2} \frac{dp}{dx}$$

For $-R \leqslant x \leqslant x_o$, from Eq. (3.1)

$$\tau = \frac{\eta u}{h^2}(3h' - 2h)$$

For $x_o \leqslant x \leqslant R$, $\dfrac{dp}{dx} = 0$ and

$$\tau = \frac{\eta u}{h}$$

Hence

$$f_1 = \int_{-R}^{x_o} \frac{\eta u}{h^2}(3h' - 2h) \, dx + \int_{x_o}^{R} \frac{\eta u}{h^2} h' \, dx$$

or in non-dimensional terms

$$F_1 = U \int_{-1}^{X_o} \frac{1}{H^2}(3H' - 2H) \, dX + U \int_{X_o}^{1} \frac{H'}{H^2} \, dX$$

Simpson's rule was used for the integrations to find load W and friction force F_1.

CHAPTER 4

FINITE ELEMENT ANALYSIS OF ELASTIC LAYERS

4.1 Introduction

The finite-element model of a continuum consists of values of the function at a discrete number of points or nodes in the domain, with piecewise approximations of the function over a finite number of subdomains or elements interconnected appropriately at nodes on their boundaries. The approximating functions over each element are uniquely defined in terms of the values of the function at the nodal points.

In the problems under investigation the strain distribution in an elastic continuum is required. The displacements at the nodal points become the basic unknown parameters. The state of strain within an element is defined in terms of these nodal displacements. The stress throughout the element is found from these strains, the initial strains and the elastic properties of the material. The boundary stresses and any distributed loads on the element are represented by a system of forces concentrated at the nodes. These forces for all elements are equated to the external loading. A stiffness relationship results linking external loading, distributed loads and initial strain to nodal displacements.

As the problem under consideration is the prediction of displacements in an elastic layer of rectangular cross-section; finite elements of rectangular form are developed below.

4.2 Basic Formulation
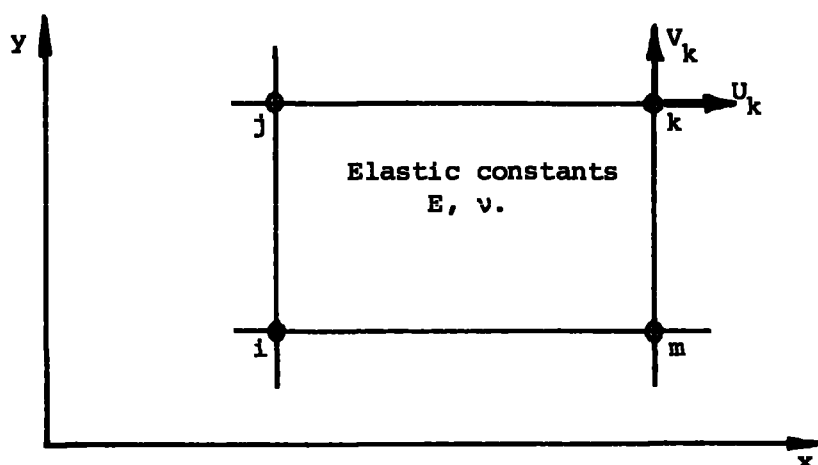
Fig. 4.1 Quadrilateral Element in a Two-Dimensional
Elastic Domain.

The finite element technique is well documentated, Ref. 51-56.
The important relationships are summarised below with regard to
quadrilateral element idealizations of the elastic domain, Fig. 4.1.

Let the displacements at any point within an element be
defined by $\{f(x,y)\}$

$$\{f\} = [N]\{\delta\} \tag{4.1}$$

The components of $[N]$ are functions of position; $\{\delta\}$ is a listing
of nodal displacements for the element. The horizontal u and the
vertical v movements of the node i are given by

$$\{\delta_i\} = \begin{Bmatrix} u_i \\ v_i \end{Bmatrix}$$

and of a point within the element by

$$\{f\} = \begin{Bmatrix} u(x,y) \\ v(x,y) \end{Bmatrix} \tag{4.2}$$

where for example the horizontal component

$$u = \alpha_1 + \alpha_2 x + \alpha_3 y + \alpha_4 xy + \ldots$$

Hence the nodal displacements may be written as

$$\{\delta\} = [C]\{\alpha\} \qquad (4.3)$$

and Eq. (4.2) in the form

$$\{f\} = [P]\{\alpha\} \qquad (4.4)$$

Hence

$$\{f\} = [P][C]^{-1}\{\delta\} \quad \text{and} \quad [N] = [P][C]^{-1}$$

The strains may be represented by

$$\{\epsilon\} = \begin{Bmatrix} \epsilon_x \\ \epsilon_y \\ \gamma_{xy} \end{Bmatrix} = \begin{bmatrix} \partial/\partial x & 0 \\ 0 & \partial/\partial y \\ \partial/\partial y & \partial/\partial x \end{bmatrix} \begin{Bmatrix} u \\ v \end{Bmatrix}$$

$$= [Q]\{\alpha\} \qquad (4.5)$$

then

$$\{\epsilon\} = [Q][C]^{-1}\{\delta\} = [B]\{\delta\} \qquad (4.6)$$

If there are no initial strains before loading then the

stresses

$$\{\sigma\} = [D]\{\epsilon\}$$

assuming general elastic behaviour. The elasticity matrix $[D]$ is

obtained from stress-strain relationships.

Let the nodal forces equivalent statically to the element

boundary stress be defined by

$$\{F_i\} = \begin{Bmatrix} U_i \\ V_i \end{Bmatrix}$$

By virtual work methods it can be shown that

$$\{F\} = \left(\int [B]^T [D] [B] \; d(vol) \right) \{\delta\}$$

if there are no distributed loads acting across the element.

Recognising this as a stiffness relationship the element

stiffness matrix becomes

$$[k] = \int [B]^T [D] [B] \, d(vol) \qquad (4.7)$$

If the boundary of the continuum is subject to a distributed external loading say {g} per unit area, it can be represented as loads at the appropriate nodes by

$$\{R\}_b = \int [N]^T \{g\} \, d(area) \qquad (4.8)$$

For equilibrium at node i

$$\{R_i\} = \Sigma \{F_i\}$$

the summation being over all elements. Another stiffness relationship can now be formed;

$$\{R\} = [K]\{\delta\}$$

where {δ} now represents the nodal displacements for the whole system and [K] the overall stiffness matrix formed from the individual element stiffness matrices. The simultaneous equations may be solved to find the nodal displacements. Convergence to the correct solution with increased subdivision of the continuum is ensured if certain criteria are followed, Ref. 52, 56.

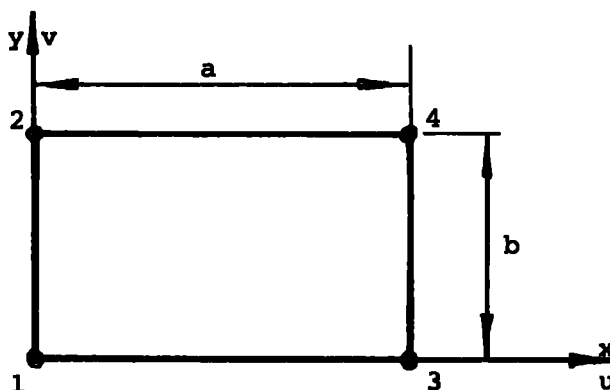## 4.3   Rectangular Element with Four Nodes

Fig. 4.2 Linear Element

As previously stated rectangular elements were chosen as the elastic body could be easily divided into a mesh of such elements. By imposing a cartesian coordinate system parallel to the sides of the rectangle, coordinate transformations may be avoided. Consider the rectangular element with four nodes each having two degrees of freedom, Fig. 4.2. For continuity of displacement along the boundaries it is necessary for the components of displacement u and v of Eq. (4.2) to vary linearly along the rectangle's edges; for example

$$u = \alpha_1 + \alpha_2 x + \alpha_3 y + \alpha_4 xy$$

which can be written as

$$\{f\} = [P]\{\alpha\} \tag{4.4}$$

Substituting the nodal coordinates yields four equations each in u and v, which may be represented in the form of Eq. (4.3).

The strains are defined by Eq. (4.6) as

$$\{\varepsilon\} = [Q][C]^{-1}\{\delta\} = [B]\{\delta\}$$

The element stiffness matrix is

$$[k] = \int [B]^T[D][B] \, d(\text{vol}) \tag{4.7}$$

or taking the element thickness as constant throughout the continuum

$$[k] = \{[C]^{-1}\}^T \left(\int \int [Q]^T[D][Q] \, dx \, dy \right) [C]^{-1}$$

The term within the integration sign may be multiplied out and integrated explicitly. The relevant matrices are given in Appendix I.

Although the concentrated nodal loads representing a distributed external load on the element's boundary may be found using Eq. (4.8), it is simpler to calculate these by direct static procedures. The results will be identical for this particular element.

4.4 Rectangular Element with Twelve Nodes
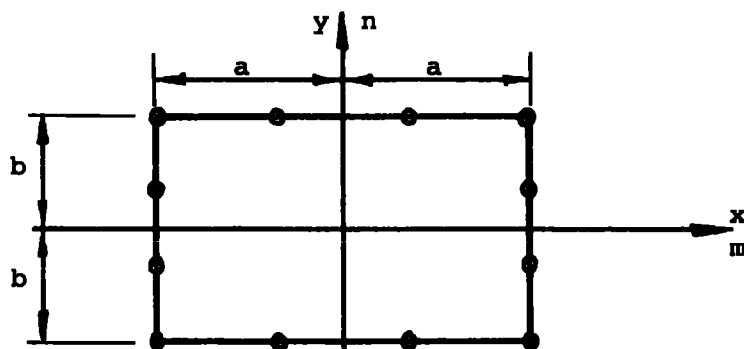
Fig. 4.3 Cubic Element

Generally by using elements having several nodes along their edges a better representation of the stress and displacement fields may be obtained than would be given with the same number of nodes using a finer mesh of simpler elements. The rectangular element, Fig. 4.3 having four nodes and hence a cubic variation along each side was developed. It is a special case of the more complex curved isoparametric element, Ref. 53.

Using normalised coordinates (m,n) so that their values are ±1 on the faces of the rectangle, the displacement component u, for example, may be expressed as

$$u = \alpha_1 + \alpha_2 m + \alpha_3 n + \alpha_4 mn + \alpha_5 m^2 + \alpha_6 n^2 + \alpha_7 m^2 n +$$
$$\alpha_8 mn^2 + \alpha_9 m^3 + \alpha_{10} n^3 + \alpha_{11} m^3 n + \alpha_{12} mn^3 \qquad (4.9)$$

where $m = x/a$, $n = y/b$.

Placing nodes at 1/3 and 2/3 along each side, the shape function for a corner node is

$$N_i = \frac{1}{32} (1 + m_o)(1 + n_o) \left[-10 + 9(m^2 + n^2) \right]$$

where $m_o = mm_i$ and $n_o = nn_i$; m_i and n_i being both ±1.

For a node along the sides $m_i = \pm 1$ with $n_i = \pm \frac{1}{3}$ the shape function is

$$N_i = \frac{9}{32} (1 + m_o)(1 - n^2)(1 + n_o)$$

and along the sides $n_i = \pm 1$, with $m_i = \pm \frac{1}{3}$ is

$$N_i = \frac{9}{32} (1 - m^2)(1 + m_o)(1 + n_o)$$

From Eqs. (4.5) and (4.6)

$$\{\varepsilon\} = \left\{ \begin{array}{c} \frac{\partial u}{\partial x} \\ \frac{\partial v}{\partial y} \\ \frac{\partial u}{\partial y} + \frac{\partial v}{\partial x} \end{array} \right\} = [B]\{\delta\}$$

in which $[B] = [B_1, B_2, B_3, \ldots]$

with

$$[B_i] = \left[\begin{array}{cc} \frac{\partial N_i}{\partial x} & 0 \\ 0 & \frac{\partial N_i}{\partial y} \\ \frac{\partial N_i}{\partial y} & \frac{\partial N_i}{\partial x} \end{array} \right]$$

The 24 x 24 stiffness matrix of Eq. (4.7) may be partioned so that the 2 x 2 submatrices are represented by

$$[k_{i,j}] = \iint [B_i]^T [D] [B_j] \, dx \, dy = ab \, I([B_i]^T [D] [B_j])$$

with $I(h) = \int_{-1}^{+1} \int_{-1}^{+1} h(m,n) \, dm \, dn$

As the elasticity matrix for plane stress or strain may be written in the form

$$[D] = \left[\begin{array}{ccc} d_1 & d_2 & 0 \\ d_2 & d_1 & 0 \\ 0 & 0 & d_3 \end{array} \right]$$

then $[k_{i,j}] = \left[\begin{array}{cc} L_{11} & L_{12} \\ L_{21} & L_{22} \end{array} \right]$

where

$$L_{11} = \frac{b}{a} d_1 I\left(\frac{\partial N_i}{\partial m} \frac{\partial N_j}{\partial m} \right) + \frac{a}{b} d_3 I\left(\frac{\partial N_i}{\partial n} \frac{\partial N_j}{\partial n} \right)$$

$$L_{12} = d_2 I \left(\frac{\partial N_i}{\partial m} \frac{\partial N_j}{\partial n} \right) + d_3 I \left(\frac{\partial N_i}{\partial n} \frac{\partial N_j}{\partial m} \right)$$

$$L_{21} = d_2 I \left(\frac{\partial N_i}{\partial n} \frac{\partial N_j}{\partial m} \right) + d_3 I \left(\frac{\partial N_i}{\partial m} \frac{\partial N_j}{\partial n} \right)$$

$$L_{22} = \frac{b}{a} d_3 I \left(\frac{\partial N_i}{\partial m} \frac{\partial N_j}{\partial m} \right) + \frac{a}{b} d_1 I \left(\frac{\partial N_i}{\partial n} \frac{\partial N_j}{\partial n} \right)$$

The three integrations represented in the stiffness matrix are carried out numerically by applying the Gaussian quadrature formulae. They are stored to be used for every element. Half of the matrix $[k_{i,j}]$ is independent of the dimensions of the element. This is calculated once for all elements. Further reduction in computation is obtained by noting that the matrix is symmetrical.

If the boundary of an element is subjected to a distributed pressure p which may be approximated by

$$p = q + rx + sx^2 + tx^3$$

then the equivalent nodal forces on that boundary are given by Eq. (4.8) so that

$$R_i = \int_{-a}^{+a} N_i p \, dx = a \int_{-1}^{+1} N_i p \, dm$$

For the corner nodes $x_i = \pm a$

$$R_i = \frac{a}{4} \left[q + \frac{11}{15} x_i r + \frac{11}{15} x_i^2 s + \frac{19}{35} x_i^3 t \right] \qquad (4.10)$$

and for the intermediate nodes $x_i = \pm \frac{a}{3}$

$$R_i = \frac{9a}{4} \left[\frac{1}{3} q + \frac{3}{5} x_i r + \frac{3}{5} x_i^2 s + \frac{27}{35} x_i^3 t \right] \qquad (4.11)$$

Similar equations may be obtained for other boundaries.

4.5 Supporting Programmes and Element Testing

The elasticity problems involved their description as a mesh of elements with appropriate constrained and loaded nodes. A set of simultaneous equations relating nodal displacements to external loads was established from the element stiffness matrices and solved.

The entire programme and its working store were held in the computer's core storage. Both elements were treated in the following way. The parts of the element stiffness matrix common to all elements and common matrices required to evaluate the remainder, were calculated and stored. The mesh nodal numbering was automatically generated. The assemblage of elements to form the global stiffness matrix was written specifically for each type of element. Constraints were applied by setting the appropriate row and column of the matrix to zero and the diagonal to unity. On introducing the loads solution to the simultaneous equations was by a "Choleski" method due to Bettess, Ref. 57.

Even though the matrix was symmetrical and banded, storage was a limiting factor. However, the "Irons Frontal Solution" technique, Ref. 54, 57 became available. Reduction of stored data was achieved by holding only "active" terms in the solution, in the core storage. Much larger element meshes could be solved allowing finer subdivision of a problem.

Only the "cubic" element was adapted for this solution routine. A supporting programme created data such as nodal numbering, loading, constraints and element dimensions. Constraints were applied through Lagrange multipliers, Ref. 55. Flow charts for the linear and cubic element are given in Appendix II.

In order to test the elements they were used to solve for the displacements in simple problems. The deformations of the plane surface of a semi-infinite elastic body under a pressure, semi-elliptical in cross-section were predicted. The mesh was systematically altered in size and number of elements. The finite element solution compares favourably with that predicted by the Hertz equations, graphs G4.1 and G4.2. It was at this point that the simple linear element was abandoned in favour of the more versatile cubic element.

4.6 Influence Coefficients from Cubic Element

The cubic element was used to provide influence coefficients for the surface deformations of a rigidly backed soft layer under a pressure distribution of constant cross-section. Pressures of uniform, linear and quadratic cross-section were applied to a layer, whose dimensions, except for thickness, were semi-infinite compared to the width of the pressure zone. Solutions for the ratio layer thickness to pressure zone width of 1:10, 1:1 and 10:1 were obtained.

For the finite element analysis, the layers were represented by the two dimensional plane strain problem of an infinitely long elastic body of rectangular cross-section, whose height was much smaller than the width, Fig. 4.5. On dividing the body into a mesh of elements all nodes on the base were constrained to form the rigid boundary. The normalised pressures were applied as equivalent nodal forces, Eqs.(4.10) and(4.11) to the top surface. The axes of the global coordinate system were taken along and perpendicular to the top surface, the origin at the centre of pressure. Due to symmetry about the vertical axis only half of the elastic body was considered. Nodes

(a)

Pressure Curve — Elements

P y

b

Thickness t

Soft Layer

Nodes on Base Fully Constrained   Rigid Base

(b)

P y   P = constant   −b ⩽ x ⩽ b

x

Nodes on Y Axis Con-
strained Horizontally

Soft Layer

Nodes on Base Fully Constrained   Rigid Base

(c)

Nodes on Y Axis Con-
strained Vertically

P y   P = kx   −b ⩽ x ⩽ b

x

Soft Layer

Nodes on Base Fully Constrained   Rigid Base

(d)

P y $P = k(x^2 - b^2/3)$
for −b ⩽ x ⩽ b

x

Nodes on Y Axis Con-
strained Horizontally

Soft Layer

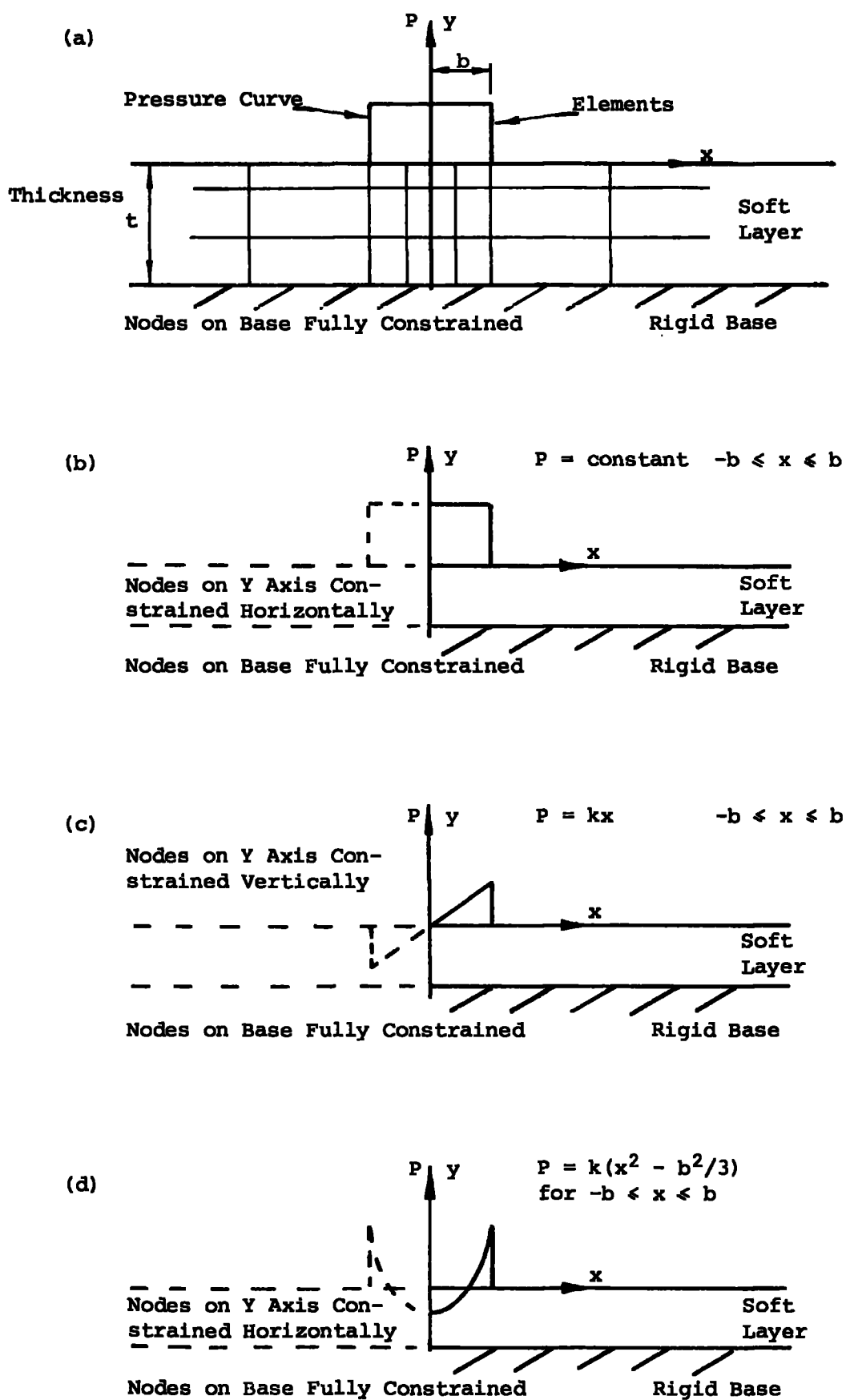Nodes on Base Fully Constrained   Rigid Base

Fig. 4.5   Finite Element Representation of Soft Layer Under

(a) General, (b) Uniform, (c) Linear, (d) Quadratic Loads

on the axis of symmetry were constrained ~~vertically~~ *horizontally* in the uniform

and quadratic load cases and ~~horizontally~~ *vertically* in the linear case, in

order to represent the full problem, Fig. 4.5. Number and size of

elements were altered to ensure convergence to a solution.

Applying the three pressure curves each to the three soft

layers the graphs G4.3 to G4.11 show the surface shape for one

Poisson's ratio, 0.3. For the same pressure curve of unit width

the maximum deformation and the deflection remote from the pressure

zone decrease with decreasing layer thickness. For the thinnest

layer, surface deformation is almost proportional to pressure, graphs

G4.5, G4.8 and G4.11.

Graphs G4.12 to G4.14 show the effect of Poisson's ratio for

the uniform load only. For the thinnest layer the centre deformation

remains constant, being far enough from the edge of the pressure

curve to be unaffected by it. For this reason, taking axes parallel

to the global axes, origin at the point on the surface directly under

the edge of the pressure curve, the surface shape may be described

as an uneven function, i.e. $f(-x) = - f(x)$. The graph G4.14

illustrates this feature.

To compare their compatability the three sets of influence

coefficients, corresponding to the ratios of layer thickness to

width of pressure curve of 10:1, 1:1 and 1:10, were used on one

problem. The surface shape for the 1:10 ratio for a uniform load

was plotted using one hundred of the first, ten of the second, or

one of the last set of influence coefficients for a uniform load.

As shown by graph G4.15 the three sets are in good agreement.

The influence coefficients for the ratio 1:1 were required in

the lubrication problem. Elastomers with a Poisson's ratio between

0.45 and 0.5 were used in the experiments. Graph G4.4 shows the

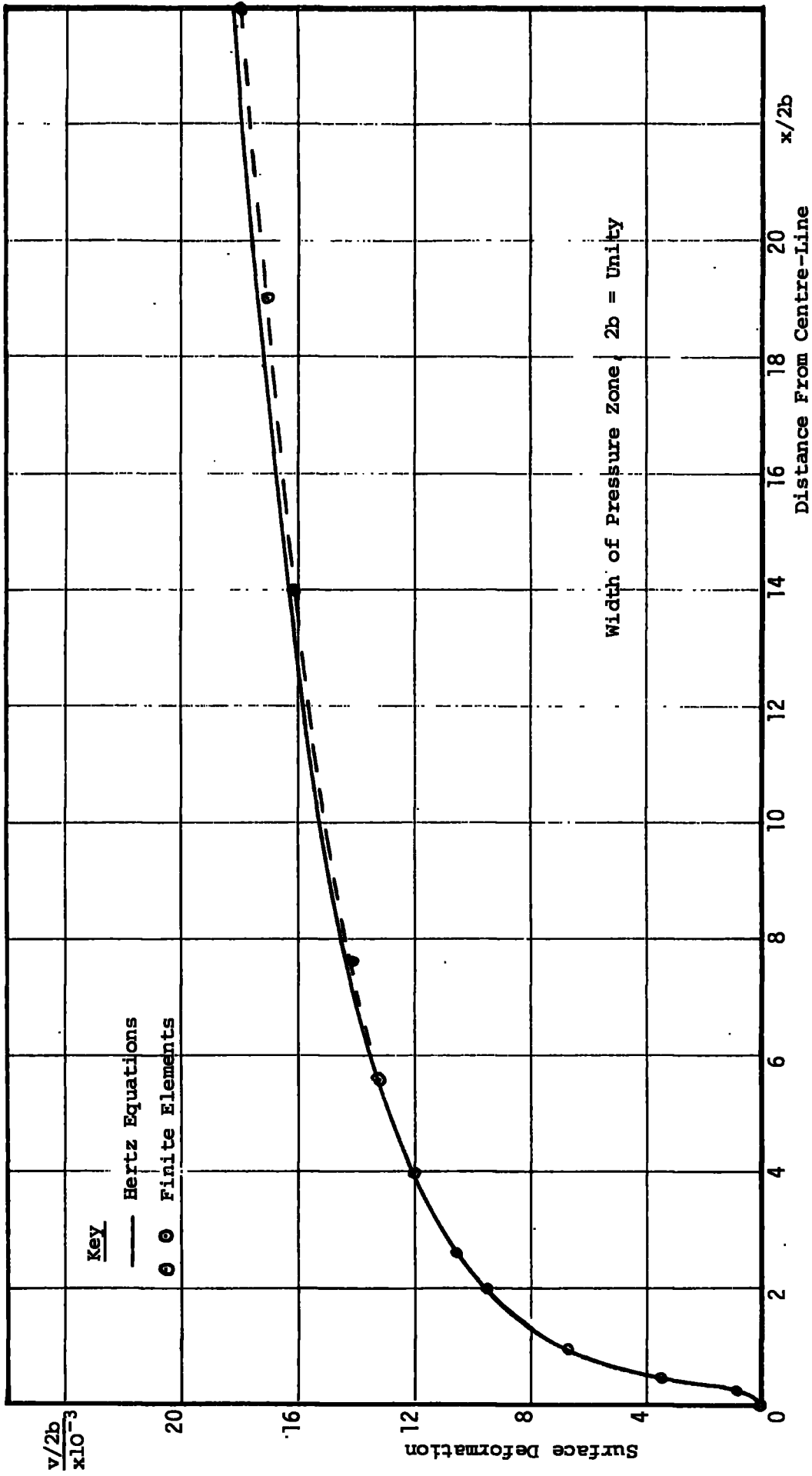surface shapes for Poisson's ratios up to 0.495; at higher values the elasticity equations were ill-conditioned. A Poisson's ratio of 0.48 was used for the soft layers in the lubrication problem as a compromise between the two materials employed.

With the relevant influence coefficients the deformation and pressure curves could be obtained from the lubrication computer programme for a particular bearing. Such a pressure curve was applied to a finite element programme to predict the surface shape of the bearing's soft layer. Comparison of the two deformation curves, graph G4.16, enabled both the influence coefficients and part of the lubrication programme to be checked.

Graphs G4.4, G4.7 and G4.10 represent the influence co-efficients as obtained from the cubic, quadrilateral finite element programme applied to a rigidly backed, elastic layer. The surface deformations for pressure curves of uniform, linear and quadratic cross-section are shown. The influence coefficients were used in the lubrication programme as described elsewhere, in the form of data as given in Appendix III.
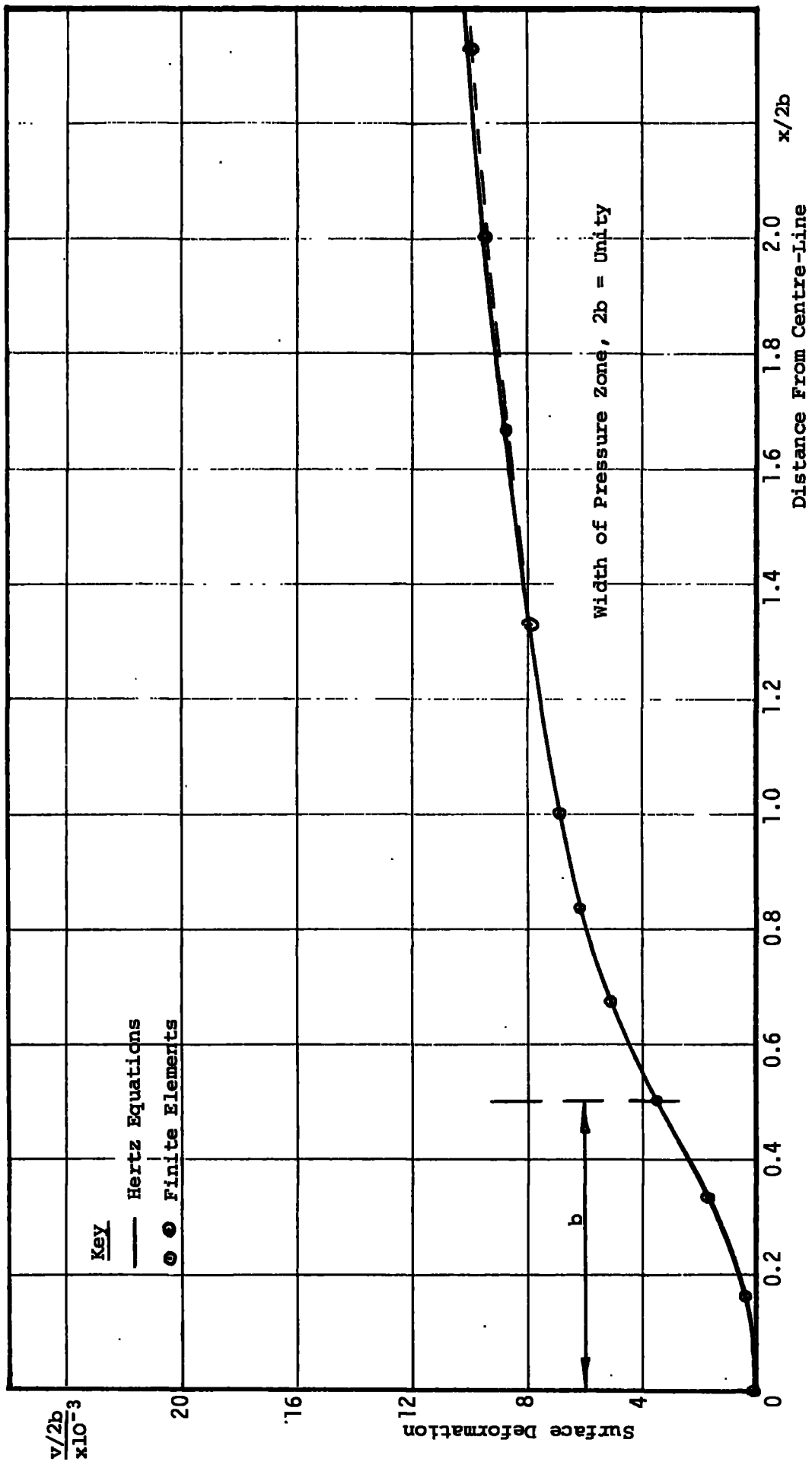
GRAPH G4.1 SURFACE SHAPE OF AN ELASTIC BODY UNDER A HERTZIAN PRESSURE

GRAPH G4.2 SURFACE SHAPE OF AN ELASTIC BODY UNDER A HERTZIAN PRESSURE

Distance From Centre-Line

x/2b

$\frac{P}{E} = 10^{-3}$

b

Total Width of Load, 2b = Unity

Poissons Ratio = 0.3

b

Surface Deformation

$\frac{v/2b}{x10^{-5}}$
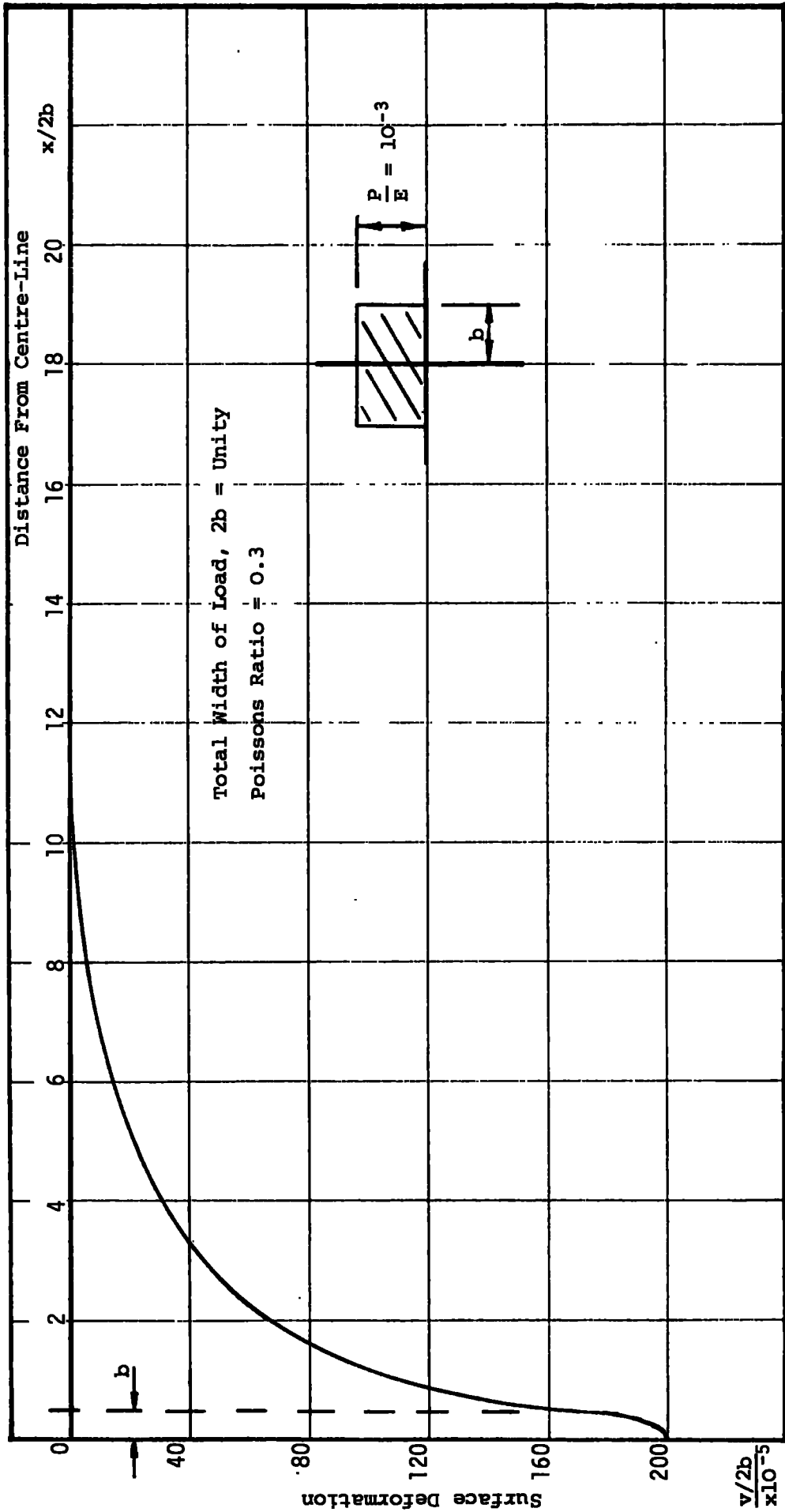
GRAPH G4.3   SURFACE DEFORMATION OF SOFT LAYER UNDER UNIFORM LOAD: WIDTH OF LOAD : LAYER THICKNESS = 1 : 10
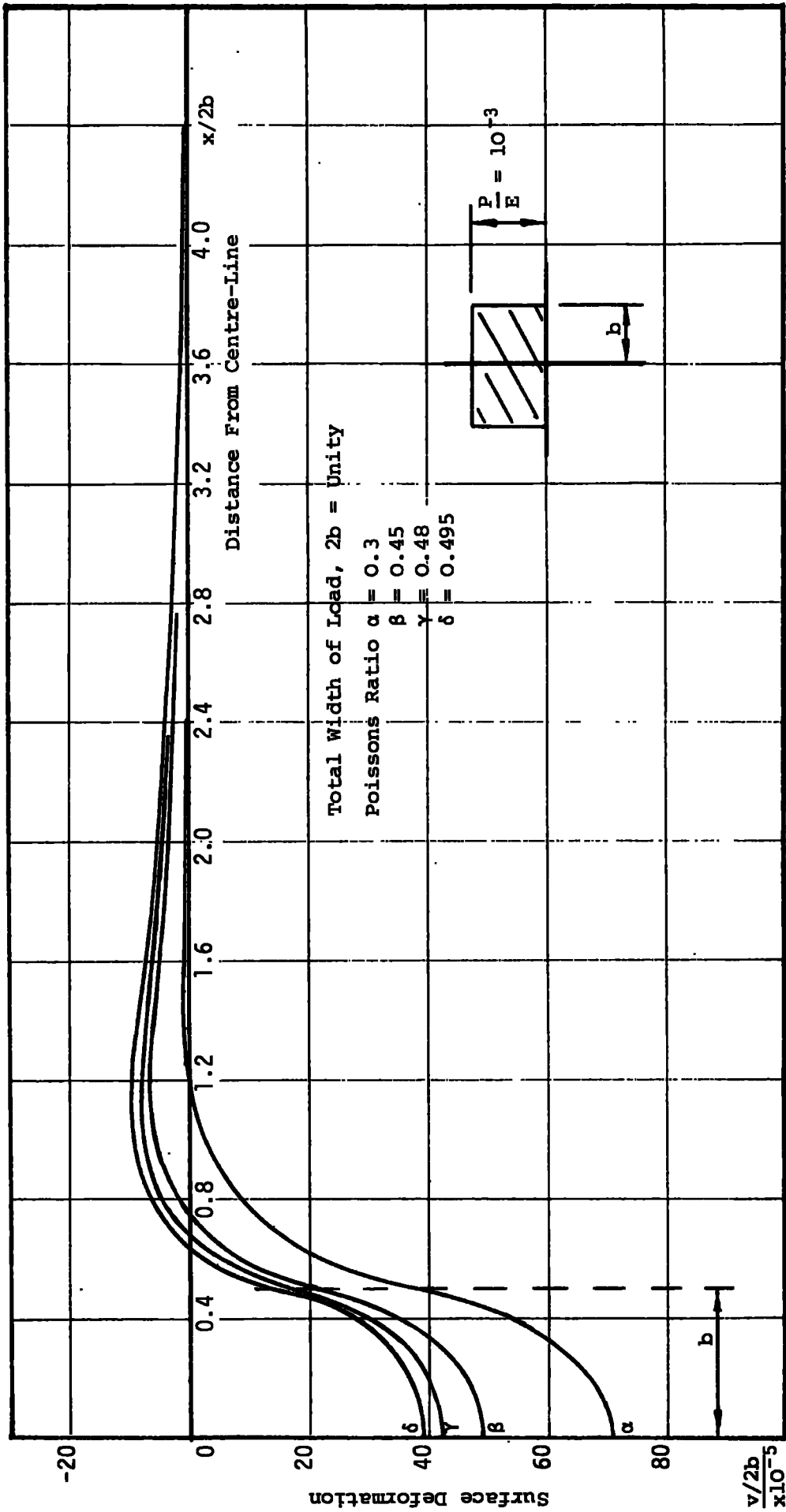
GRAPH G4.4 SURFACE DEFORMATION OF SOFT LAYER UNDER UNIFORM LOAD; WIDTH OF LOAD : LAYER THICKNESS = 1 : 1
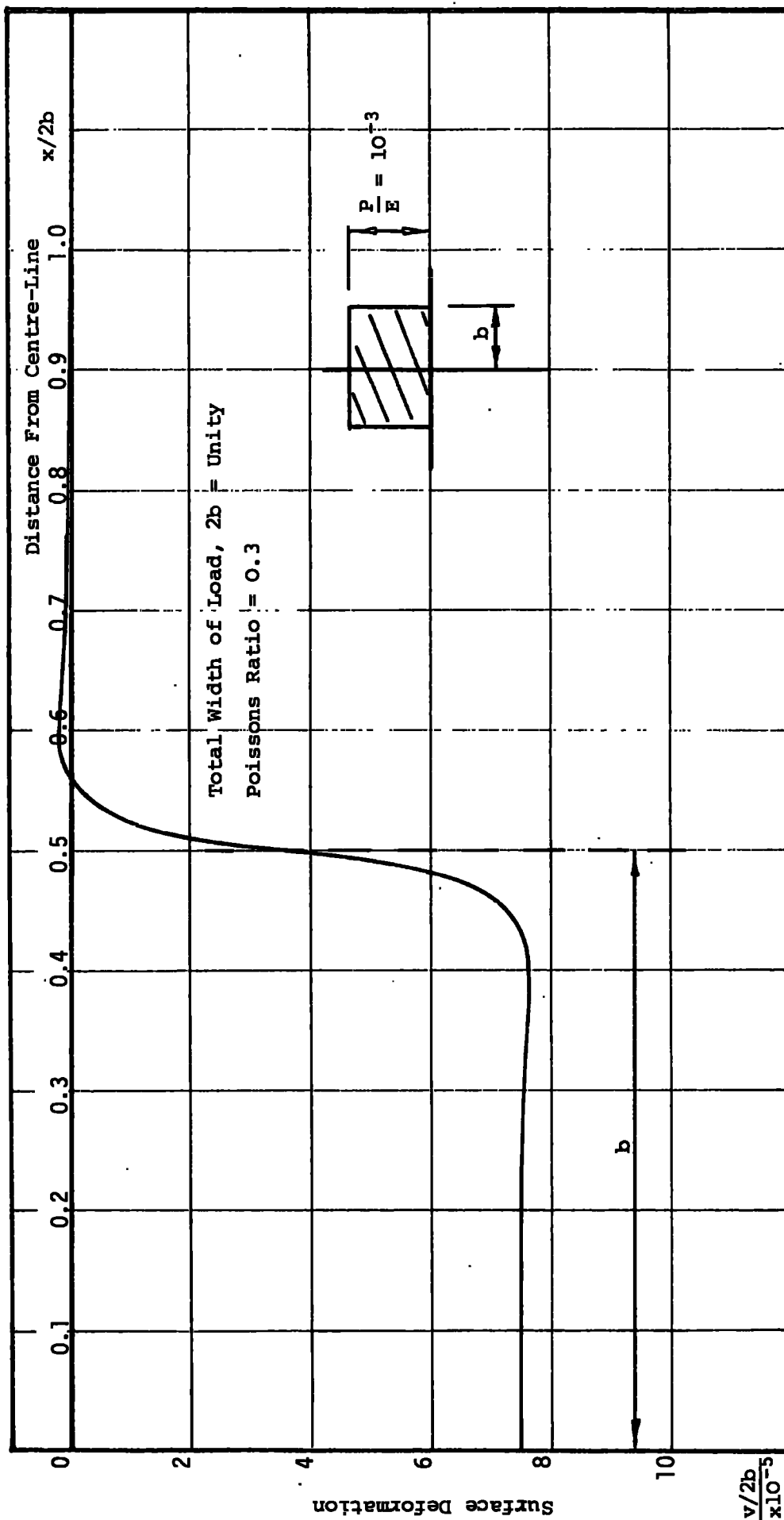
GRAPH G4.5 SURFACE DEFORMATION OF SOFT LAYER UNDER UNIFORM LOAD; WIDTH OF LOAD : LAYER THICKNESS = 10 : 1

GRAPH G4.6   SURFACE DEFORMATION OF SOFT LAYER UNDER LINEAR LOAD; WIDTH OF LOAD : LAYER THICKNESS = 1 : 10

42

GRAPH G 4.7 SURFACE DEFORMATION OF SOFT LAYER UNDER LINEAR LOAD; WIDTH OF LOAD : LAYER THICKNESS = 1 : 1

Distance From Centre-Line

x/2b

Total Width of Load, 2b = Unity

Poissons Ratio α = 0.3
β = 0.48

Surface Deformation

$\frac{v/2b}{\times 10^{-6}}$

P = 10⁻³

GRAPH G4.8 **SURFACE DEFORMATION OF SOFT LAYER UNDER LINEAR LOAD: WIDTH OF LOAD : LAYER THICKNESS = 10 : 1**

The graph shows Surface Deformation ($\frac{v/2b}{\times 10^{-6}}$) versus Distance From Centre-Line ($x/2b$).

Total Width of Load, 2b = Unity

Poissons Ratio = 0.3

$\frac{P}{E} = 10^{-3}$

GRAPH G4.9 SURFACE DEFORMATION OF SOFT LAYER UNDER QUADRATIC LOAD; WIDTH OF LOAD : LAYER THICKNESS = 1 : 10
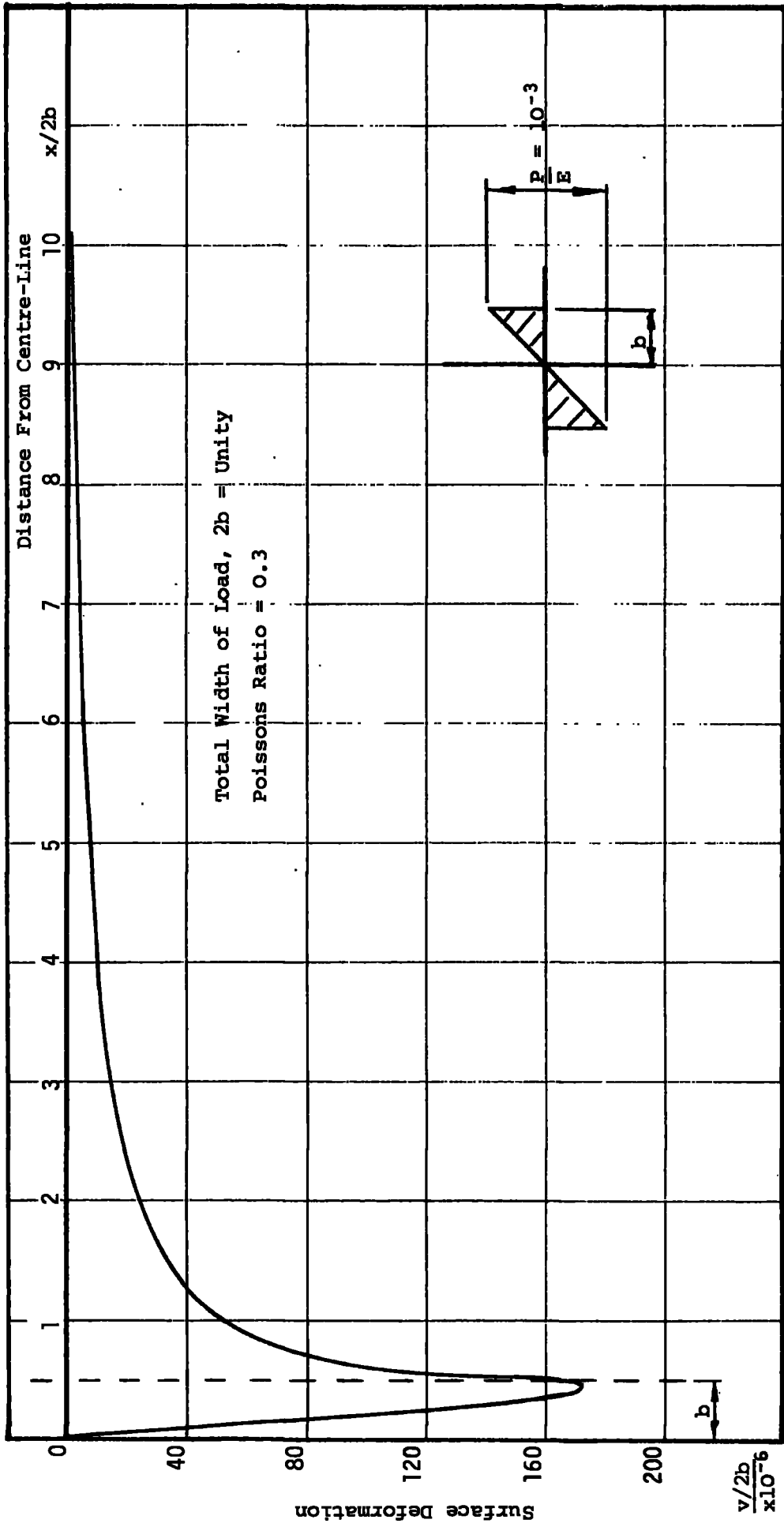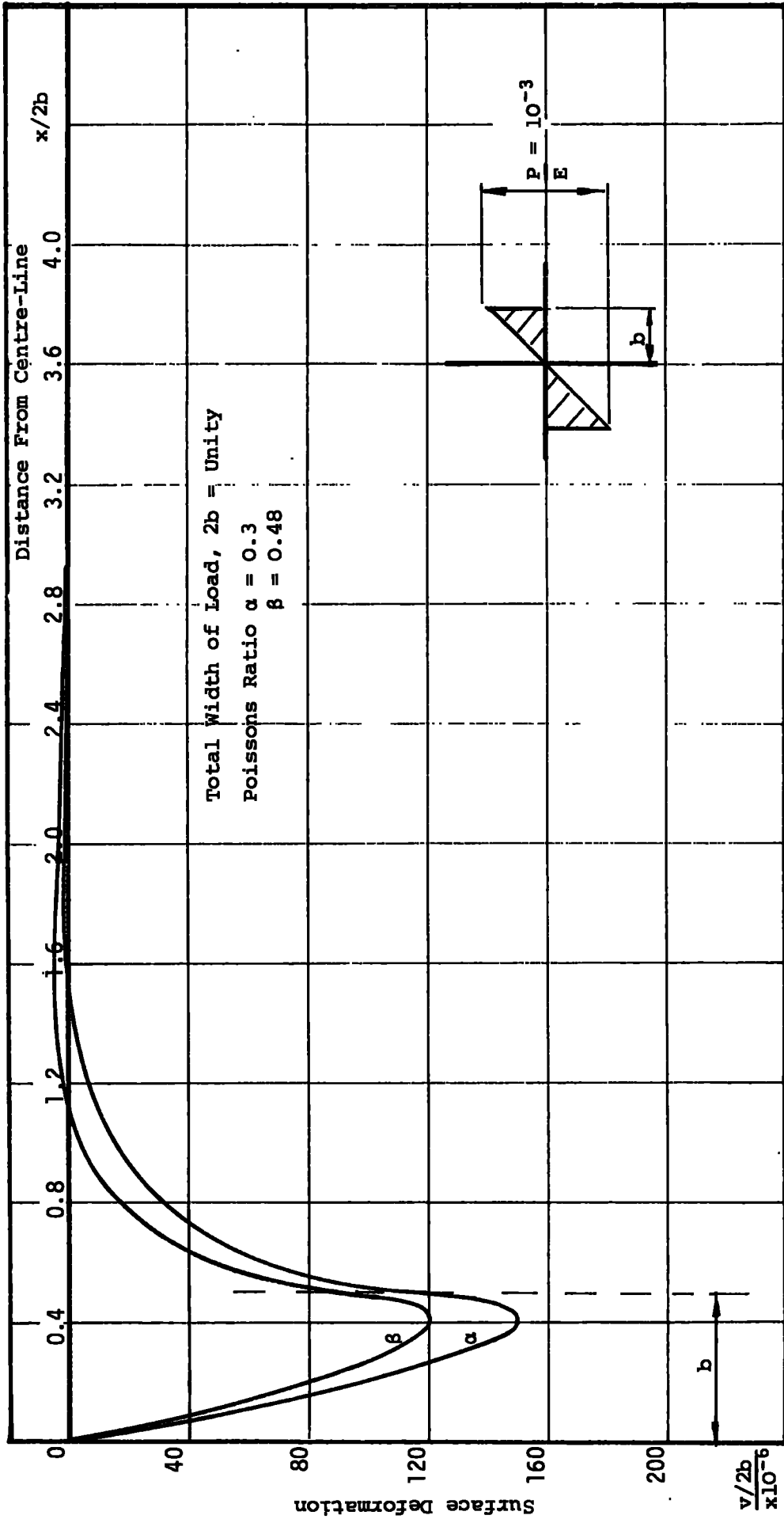
GRAPH G4.10 SURFACE DEFORMATION OF SOFT LAYER UNDER QUADRATIC LOAD; WIDTH OF LOAD : LAYER THICKNESS = 1 : 1

The graph plots Surface Deformation ($\frac{v/2b}{\times 10^{-6}}$) against Distance From Centre-Line ($x/2b$).

Axis labels:
- Vertical axis (Surface Deformation): -12, -8, -4, 0, 4, 8, $\frac{v/2b}{\times 10^{-6}}$
- Horizontal axis (Distance From Centre-Line, $x/2b$): 0.1, 0.2, 0.3, 0.4, 0.5, 0.6, 0.7, 0.8, 0.9, 1.0

Inset annotations:
- $\frac{P}{E} = 10^{-3}$
- b
- Total Width of Load, $2b$ = Unity
- Poissons Ratio = 0.3
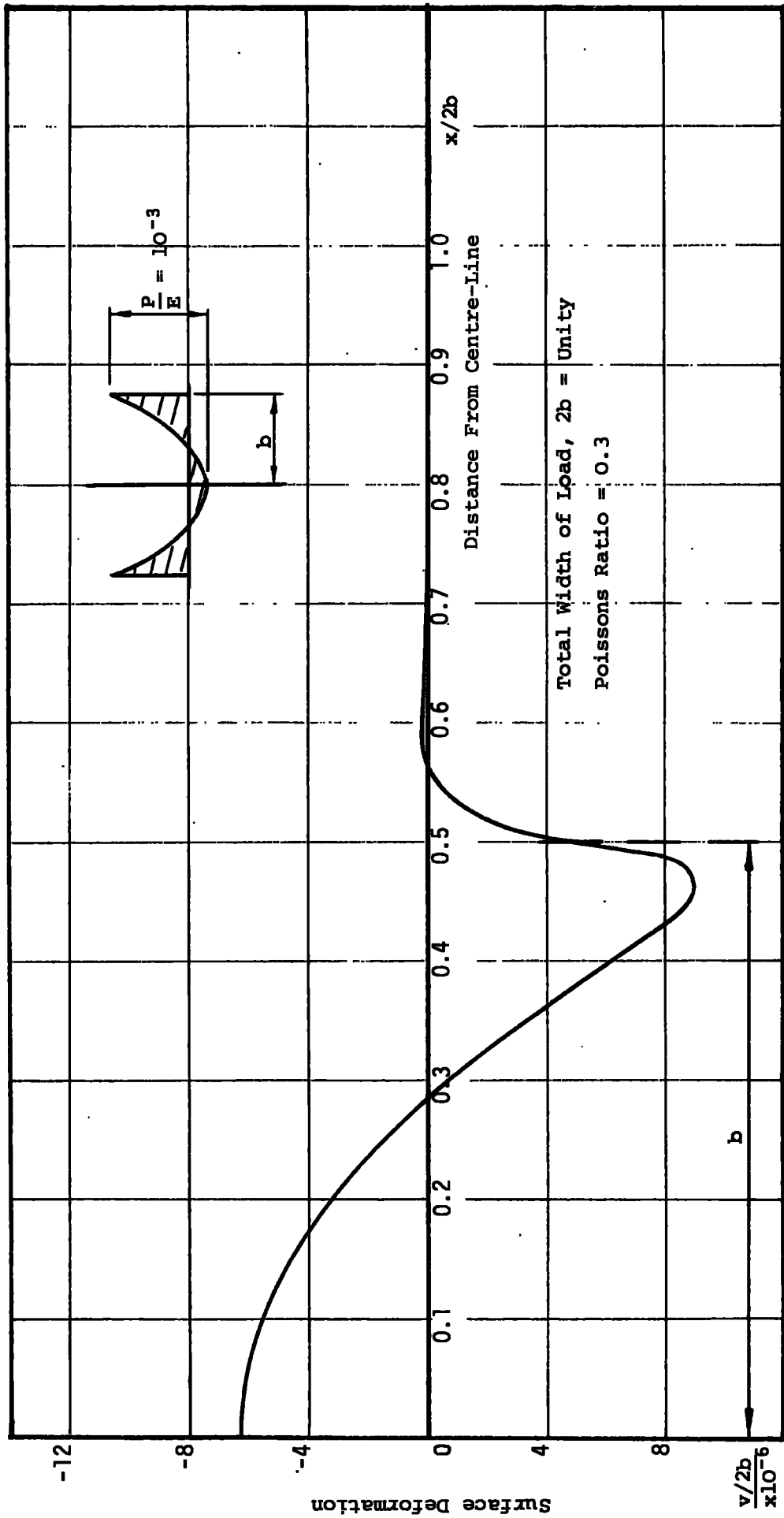
GRAPH G4.11   SURFACE DEFORMATION OF SOFT LAYER UNDER QUADRATIC LOAD;   WIDTH OF LOAD : LAYER THICKNESS = 10 : 1

47
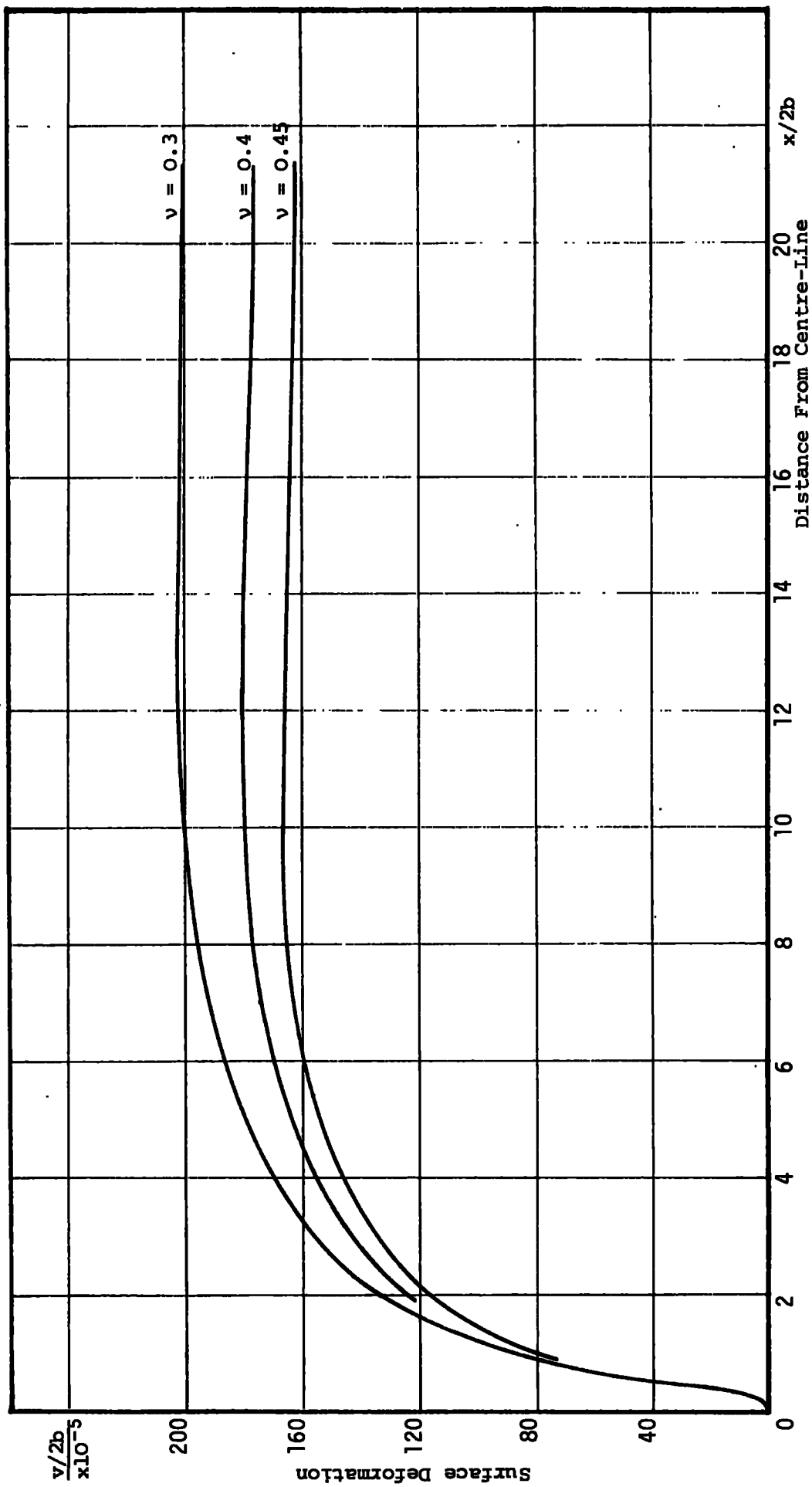
GRAPH G4.12 SURFACE SHAPE OF SOFT LAYER UNDER UNIFORM LOAD; WIDTH OF LOAD : LAYER THICKNESS = 1 : 10
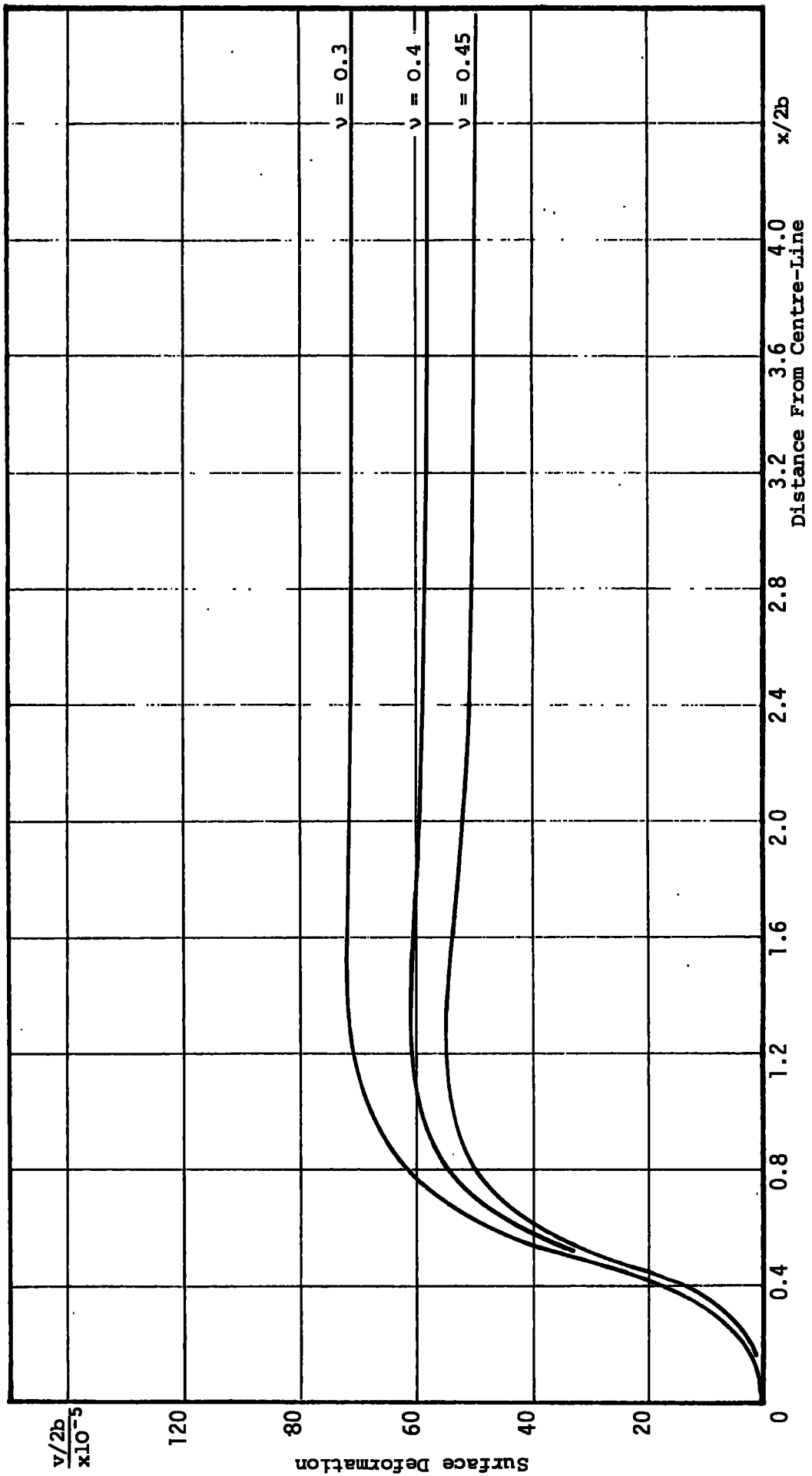
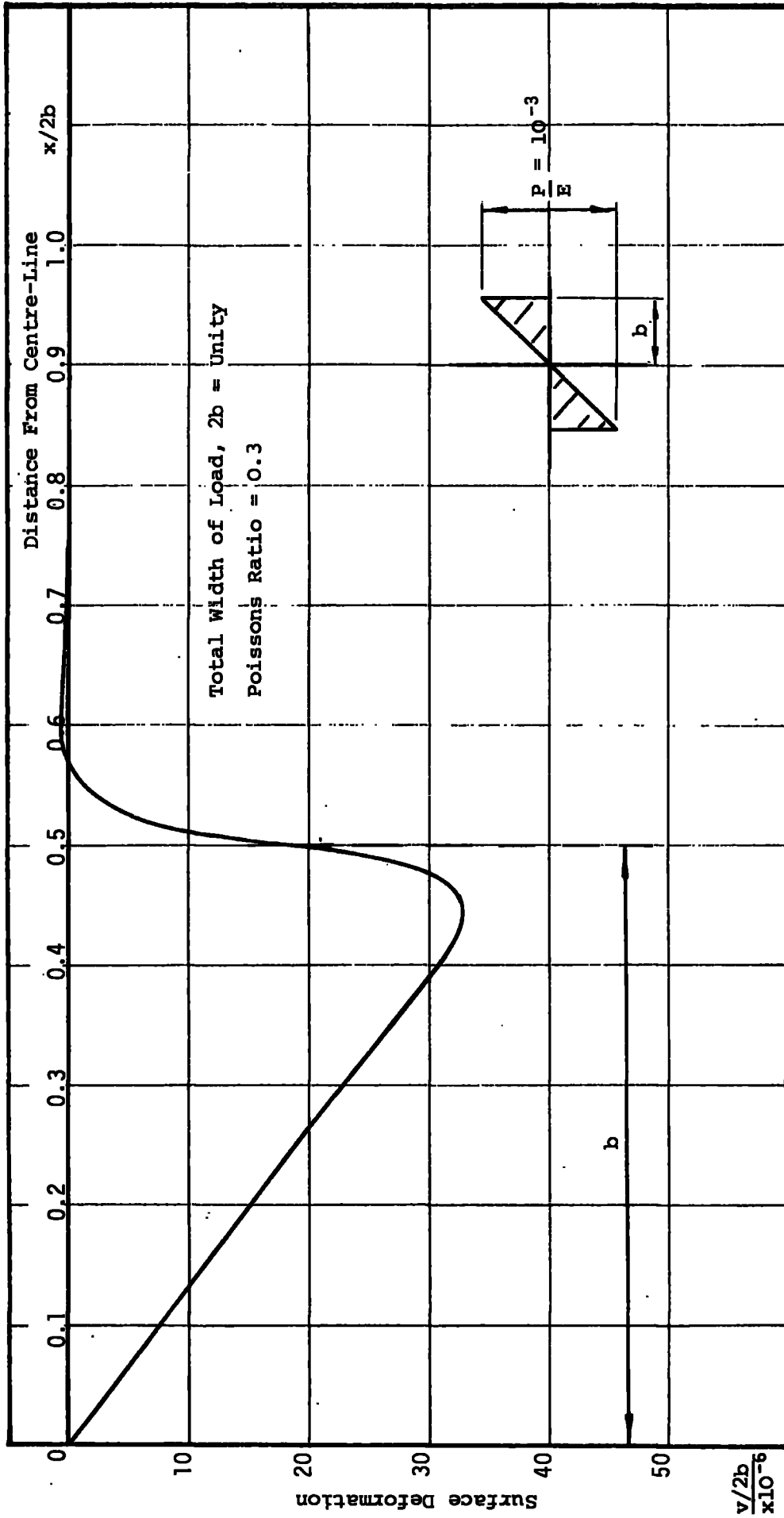GRAPH G4.13 SURFACE SHAPE OF SOFT LAYER UNDER UNIFORM LOAD; WIDTH OF LOAD : LAYER THICKNESS = 1 : 1

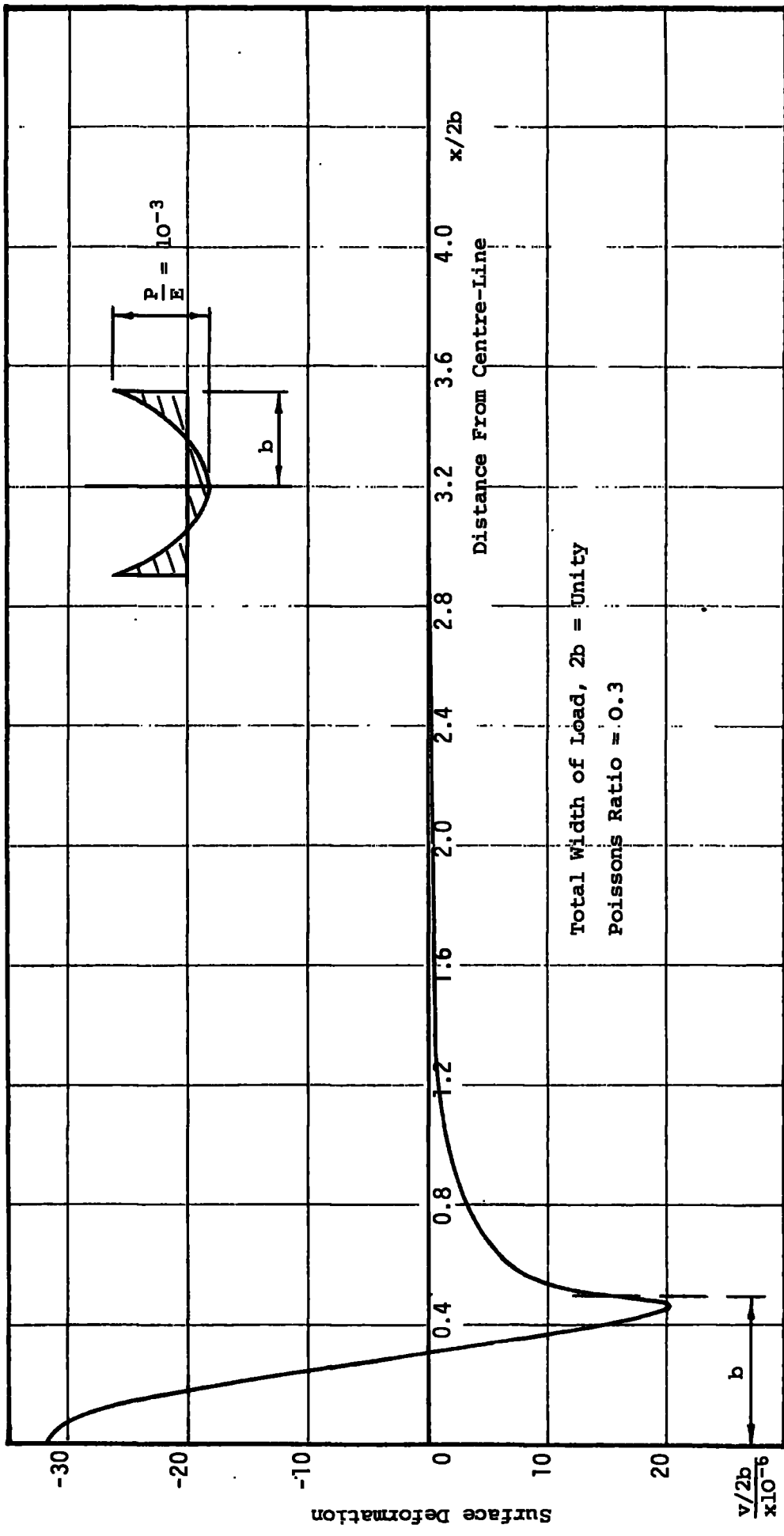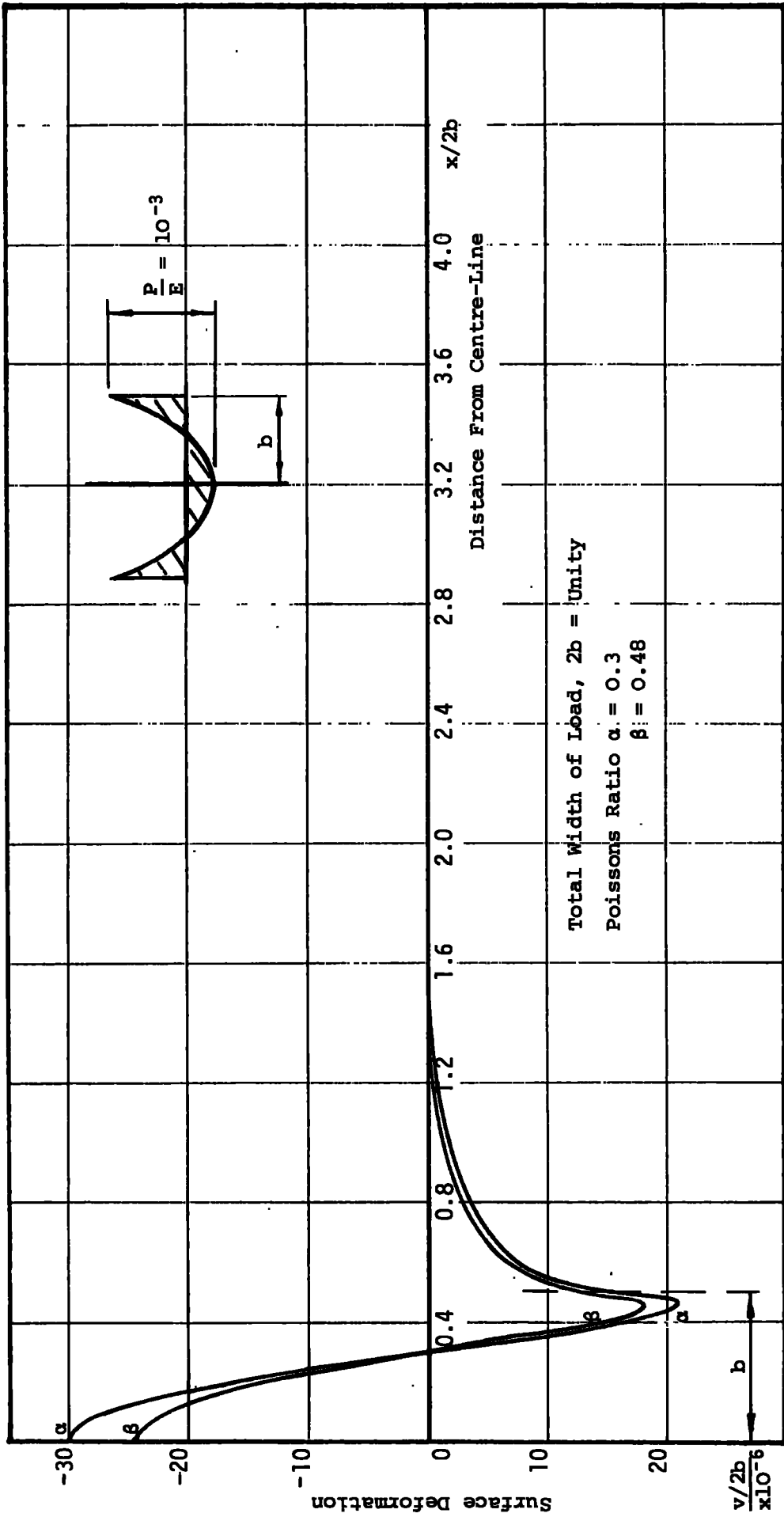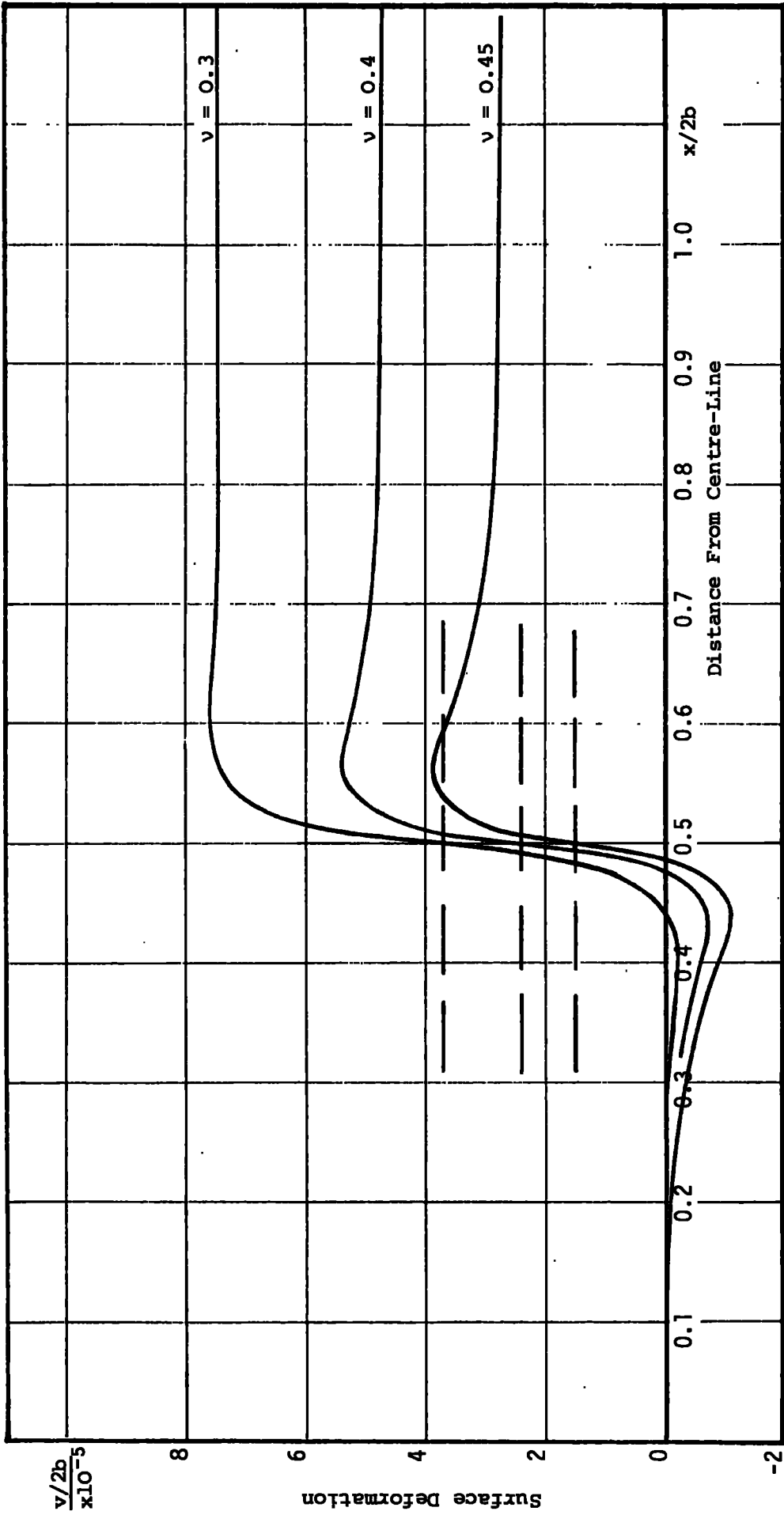GRAPH G4.14 SURFACE SHAPE OF SOFT LAYER UNDER UNIFORM LOAD: WIDTH OF LOAD : LAYER THICKNESS = 10 : 1

$\frac{v/2b}{\times 10^{-5}}$

8

6

4

2

0

-2

0.1   0.2   0.3   0.4   0.5   0.6   0.7   0.8   0.9   1.0

x/2b

Distance From Centre-Line

Width of Load : Layer Thickness

$= 2b:t = 10:1$

Poissons Ratio $= 0.3$

Key

——— Finite Element Solution
(Width of Load, 2b : Layer Thickness t = 10:1)

o o Influence Displacements Solution
(Using Coeffs. for 2b:t = 1:1)

– – Influence Displacements Solution
(Using Coeffs. for 2b:t = 1:10)
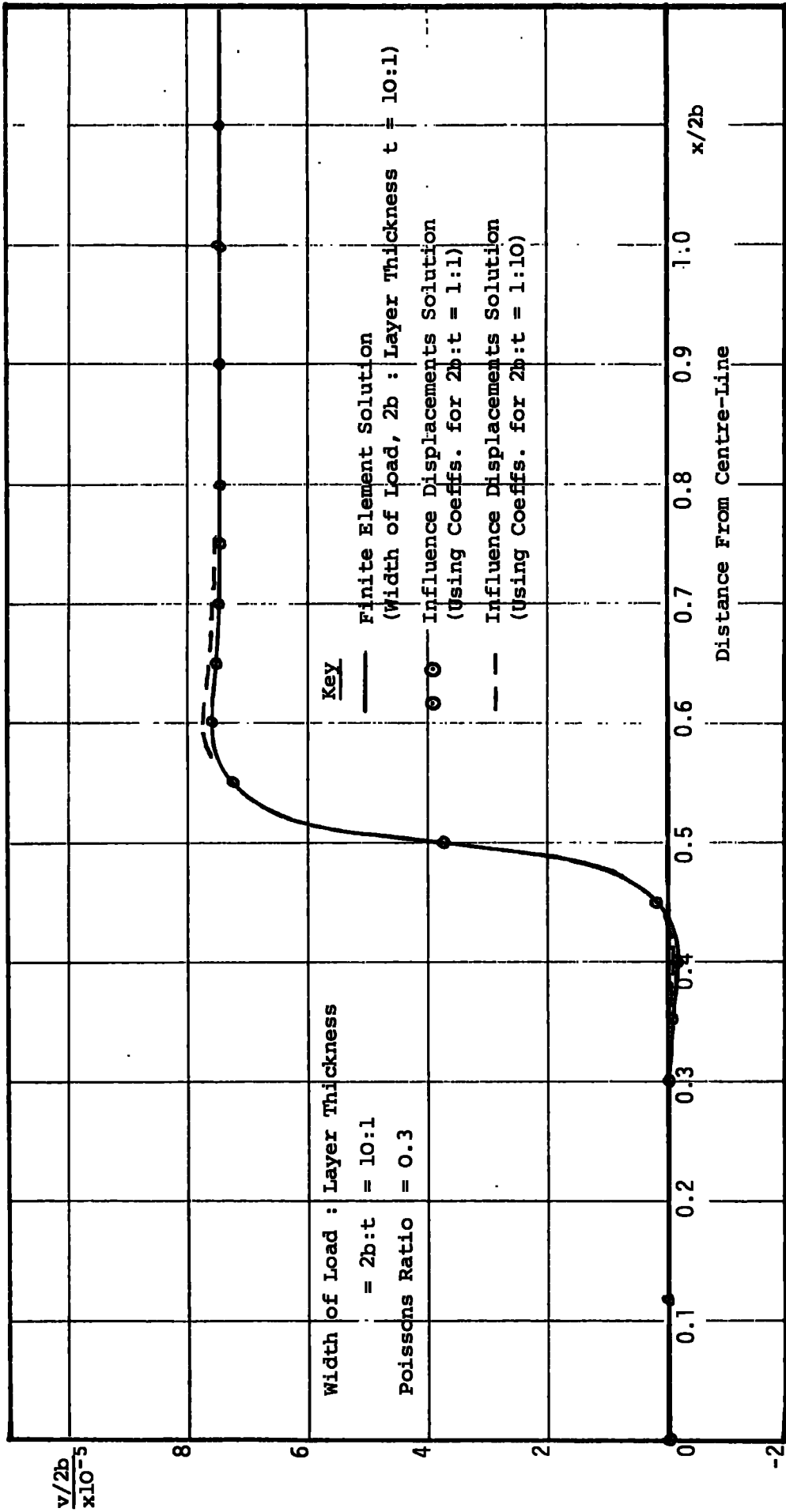
GRAPH G4.15 SURFACE SHAPE OF SOFT LAYER UNDER UNIFORM LOAD, SOLUTIONS FROM DIFFERENT INFLUENCE DISPLACEMENTS.
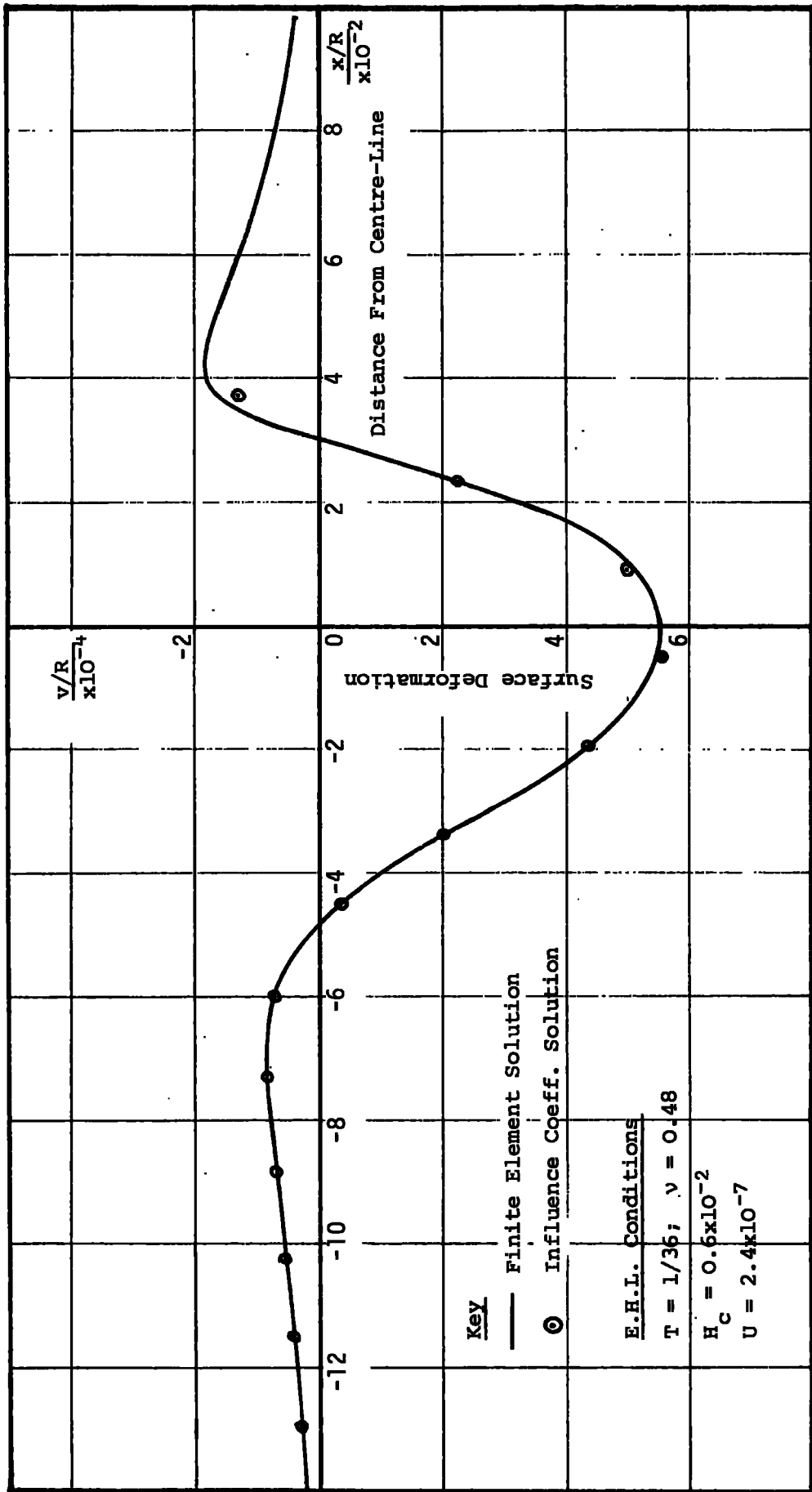
GRAPH G4.16 SURFACE SHAPE OF "SOFT LAYER BEARING" UNDER E.H.L. CONDITIONS

CHAPTER 5

DISCUSSION OF RESULTS

5.1   INTRODUCTION

Several characteristics of the performance of the soft layer

bearing were measured and/or predicted. It was possible to compare

the theoretical and experimental tangential forces and pressures

for various conditions of speed-viscosity, gometry and load. The

lubricant film shape and elastic deformations of the bearing were

forecast by the computer programme. The relationship between the

minimum film thickness and the load for several bearing conditions

was also plotted.

5.2   Friction

Two lubricants were used in the experiments providing a wide

range of the speed-viscosity parameter. The tangential friction

force on the plane was plotted against the speed-viscosity for a

series of loads. The limited number of results for the higher

viscosity lubricant compare favourably with the identical

experiments of Bennett, (1969), Ref. 38,39. Curves for the rigid

plane and a representative soft layer, 2.5 mm thick, are shown,

graphs G5.1 and G5.2. The slightly higher values of friction

obtained could be due to the poor surface finish of the planes.

It was hoped that an extrapolation of the soft layer curves

for low values of the non-dimensional speed would coincide with the

experiments using the low viscosity lubricant. For the 2.5 mm soft

layer, comparing graphs G5.2 and G5.3, the non-dimensional friction

in the experiment is higher than anticipated from extrapolation, a

result common to the 1.25 mm layer. Graph G5.4 for the 5.1 mm

soft layer does indicate values of friction compatible with the

curve for the higher viscosity lubricant. It is possible that the

conditions of surface finish load and low viscosity lubricant were

not conducive to full film lubrication of the thinner layers.

The tangential forces for the rigid plane show a sharp

increase on decreasing sliding speed as "dry" contact occurs. Much

lower speeds were obtainable in the presence of a soft layer. In

terms of friction at low speeds, the benefit in using a thin soft

layer is shown to be considerable.

The computer programme results provided curves of load against

tangential force for various speeds, e.g. graphs G5.5 and G5.6.

From these were plotted friction force and coefficient of friction

against speed. The friction measured in the experiments for full

film lubrication was 5 to 10% higher than that predicted, G5.1 and

G5.2. This was possibly due to surface roughness and "side-leakage"

effects in the bearing. The coefficient of friction, e.g. G5.7 and

G5.8, is found to be slightly higher with a thin elastic layer

than without.

The non-dimensional friction force on a fixed rigid plane

loaded against a rotating cylinder is given by (Ref. 48)

$$F = 0.79(UW)^{\frac{1}{2}}$$

Graph G5.9 of the computer results indicates 0.80 as the coefficient.

A single curve is therefore obtained for the coefficient of friction

F/W against U/W for all loads. This is not true of the soft layers;

graphs G5.10 and G5.11 for 0.75 mm and 2.5 mm layer thickness may

be represented approximately by

$$F = 0.75(UW)^{\frac{1}{2}} + f(T,W)$$

Plots of coefficient of friction against U/W for a soft layer show

several curves dependent upon the load W. As would be expected the thinner the layer the closer the friction is to the rigid case.

5.3 Pressure

The pressure distributions for a rigid plane and soft layers (Young's modulus 1.0 MN/m^2) of non-dimensional thicknesses 0.028, 0.056 and 0.111 under various loads were found experimentally. Neither load nor peak pressure could be controlled in the computer programme. Hence a series of curves were obtained covering the load ranges for identical values of layer thickness and speed in the experiments.

On comparing theory and experiment discrepancies were evident at the "run-out" (outlet) point for all conditions. The cavitation boundary condition in the theory was altered from zero to the average empirical negative pressure, e.g. graph G5.12. A new set of pressures were computed. Due to the large number of curves only a selection is shown, G5.13 to G5.17. All show good agreement for the shape of the pressure distribution between theory and experiment. Divergence of theory and experiment mainly occurs at the run-out point, if the experimental cavitation pressure still differs from the chosen theoretical value.

As expected, increasing sliding speed, G5.12 to G5.14, encourages a wider flatter curve for the same load and reduces the influence of the layer thickness. All the graphs indicate the effect of increased load. For a fully elastic plane there is a gradual transition from a pressure distribution representative of rigid solids to a near Hertzian curve at higher loads (P.126, Ref. 48). There is a similar tendency shown by the soft layers, graphs G5.12 to G5.17, most prominent in the thick layer, although the Hertzian

curve is not evident for the load range used. Reducing the layer thickness delays the transition. The effect of the layer thickness can be seen by comparing graphs G5.14 to G5.17. Graph G5.18, obtained by interpolating from the theoretical curves for one load and speed, shows the increasing influence of the rigid backing as the layer thickness is reduced.

5.4 Film Shape

The lubricant film shape as well as the pressure distribution was predicted by the computer programme. A selection of curves is shown, G5.19 to G5.22, for the same variables as in the pressure experiments. It can be seen that the rigid backing influences the layer's surface deformation. For the loads at which this occurs a small change in cavitation pressure has a minimal effect, G5.12 and G5.19. All film shapes therefore refer to a cavitation pressure of zero.

The change in form of the film shape as the layer thickness is increased is shown in G5.20 and G5.21. There is an obvious movement away from the "rigid" curve to one representative of an elastic body.

Typical curves are obtained for increasing load for a particular layer thickness, e.g. G5.22. The effect of load is more evident, however, in the plots of centre-line and minimum film thickness for various speeds, G5.23 to G5.25. The "rigid" curves are derived directly from the Martin formula for rigid solids $(H = 2.45U/W)$. The "elastic" curves are plotted from the results of Weber and Saalfield as presented by Koets (Ref. 48) for elastic solids. Both are for cylinders lubricated by an isoviscous lubricant. They represent the bounds within which the minimum film thickness for a soft layer should fall.

At low loads the Martin formula is applicable to all. At higher loads the film thickness for the soft layer diverges from both "rigid" and "elastic" curves; the layer thickness determines which it follows more closely. The difference between computed centre-line and minimum film thickness is least for the thinnest layer. For a given layer the minimum film thickness is greater in magnitude and less dependent upon load than the "rigid" theory indicates.
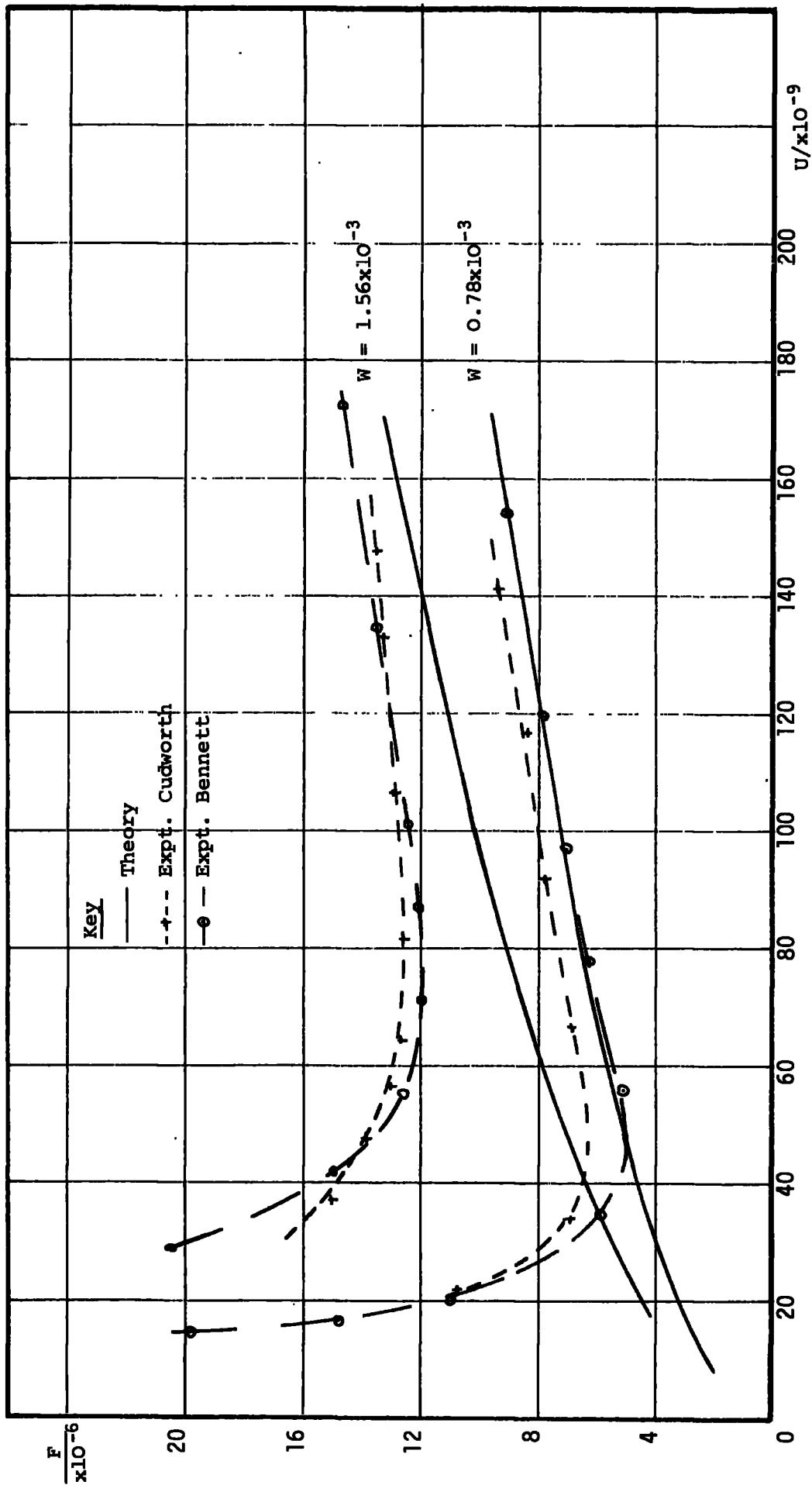
GRAPH G5.1 FRICTION AGAINST SPEED FOR RIGID PLANE
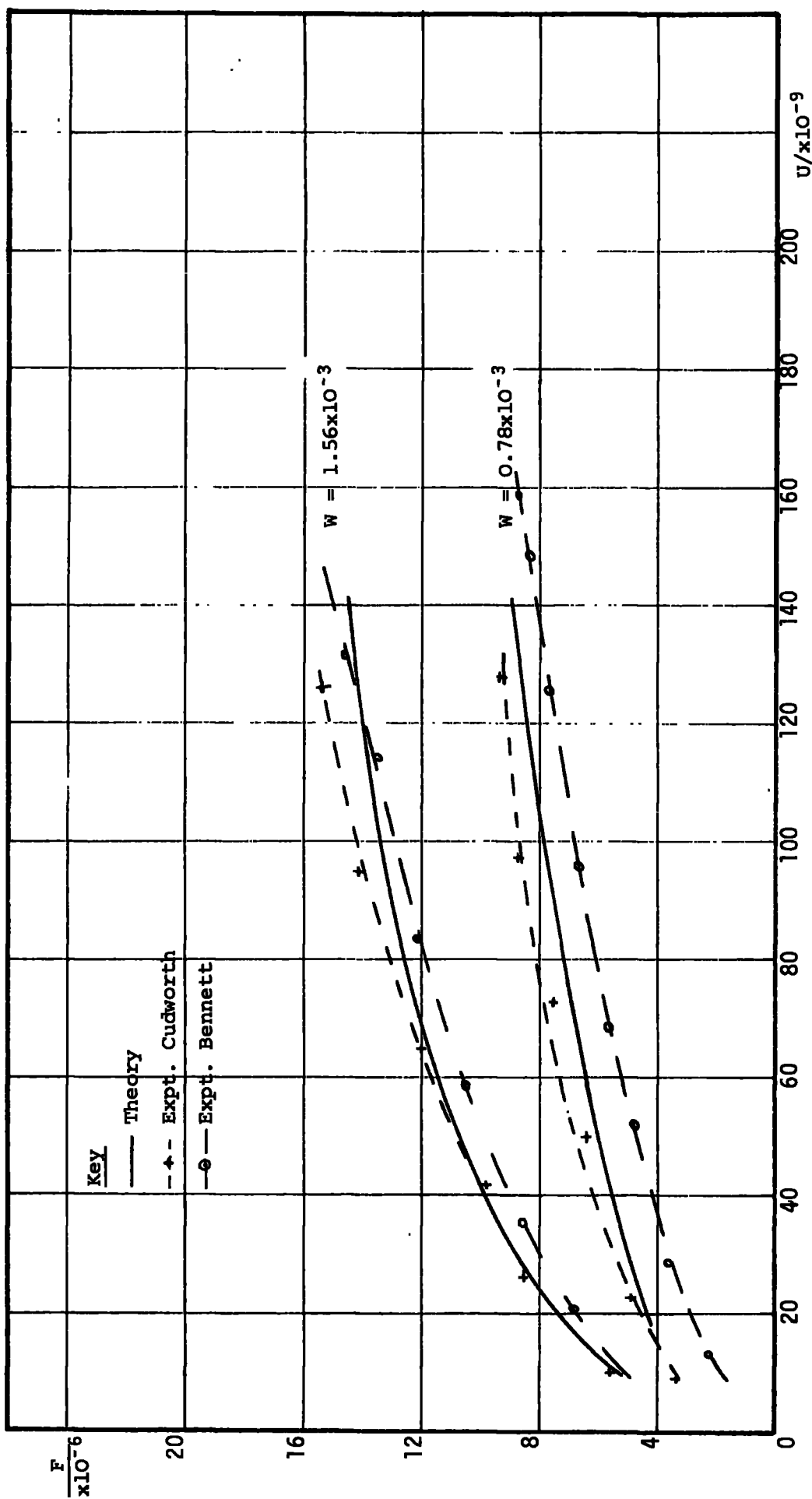
GRAPH G5.2 FRICTION AGAINST SPEED FOR 2.5 mm SOFT LAYER
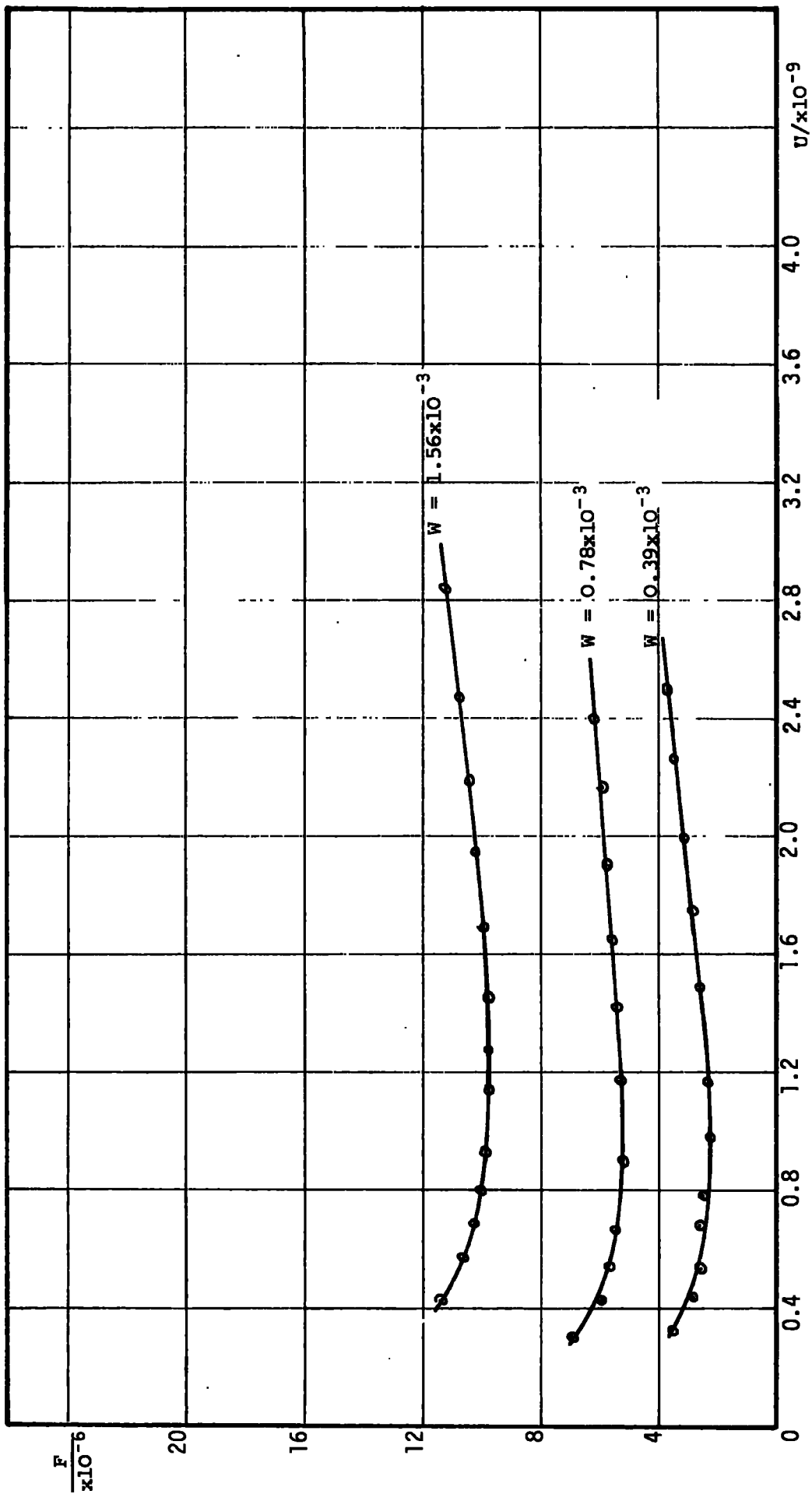
GRAPH G5.3 FRICTION AGAINST SPEED FOR 2.5 mm SOFT LAYER
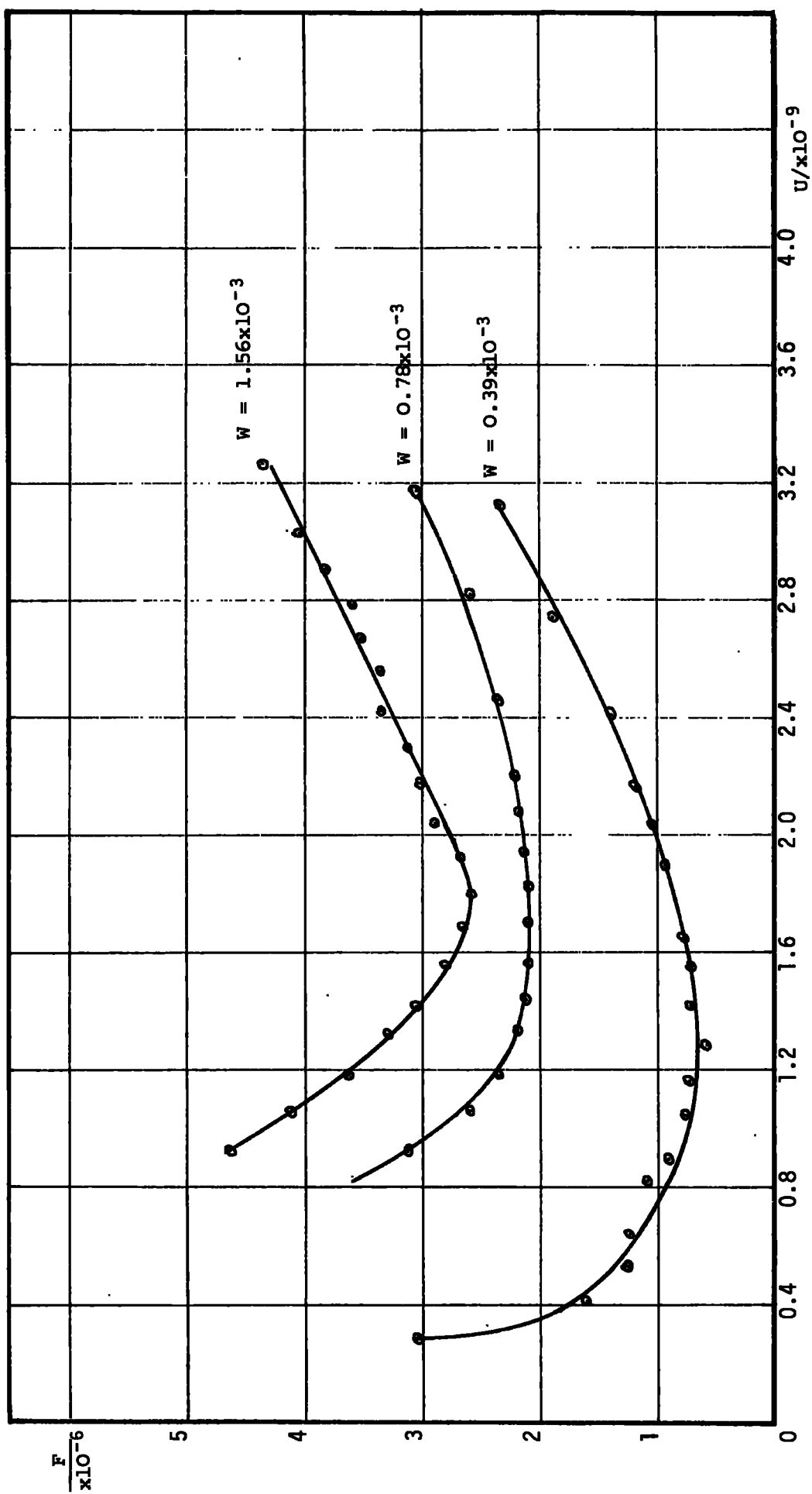
GRAPH G5.4 FRICTION AGAINST SPEED FOR 5.1 mm SOFT LAYER
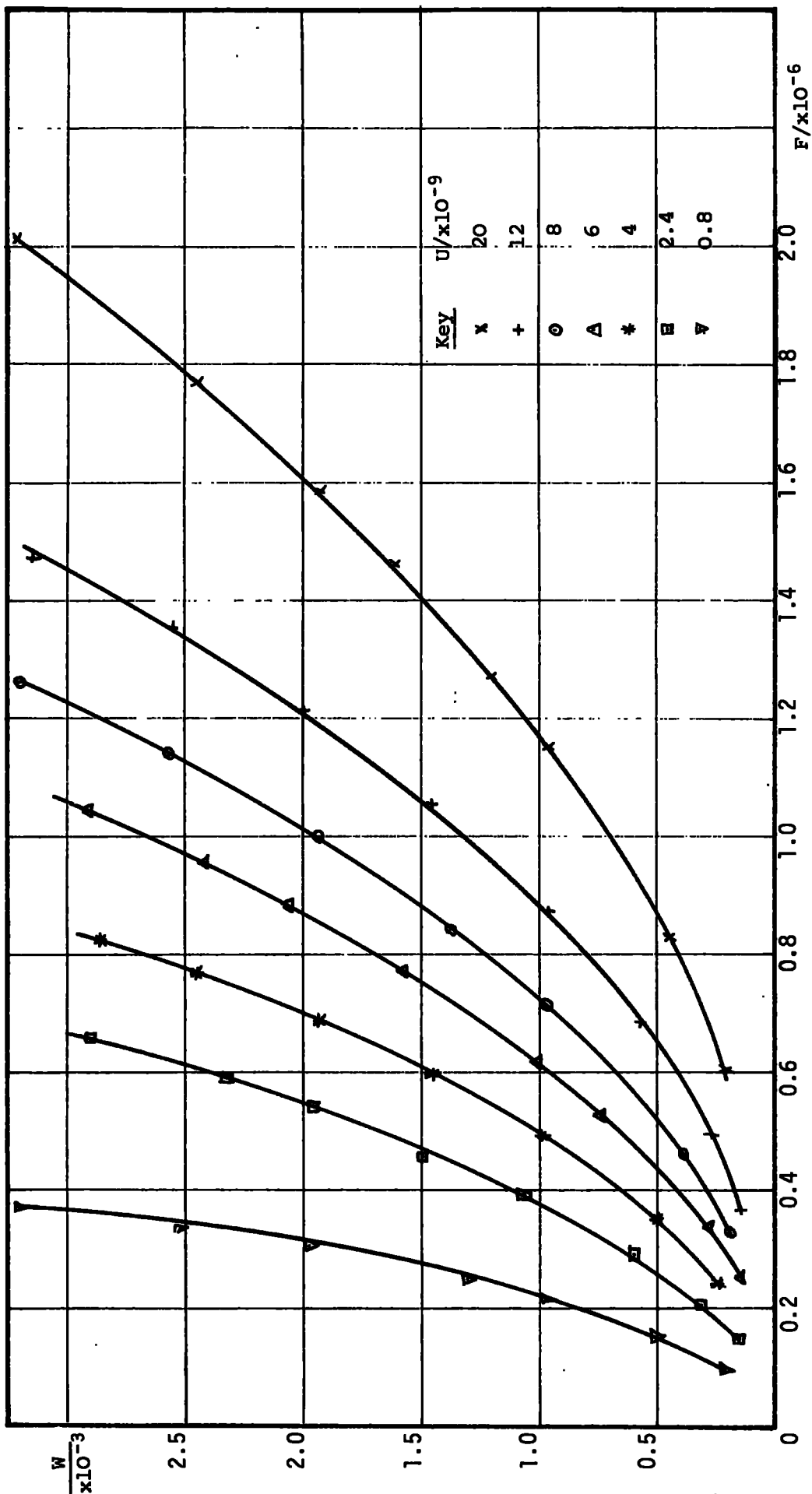
GRAPH G5.5 LOAD AGAINST FRICTION FORCE FOR RIGID PLANE
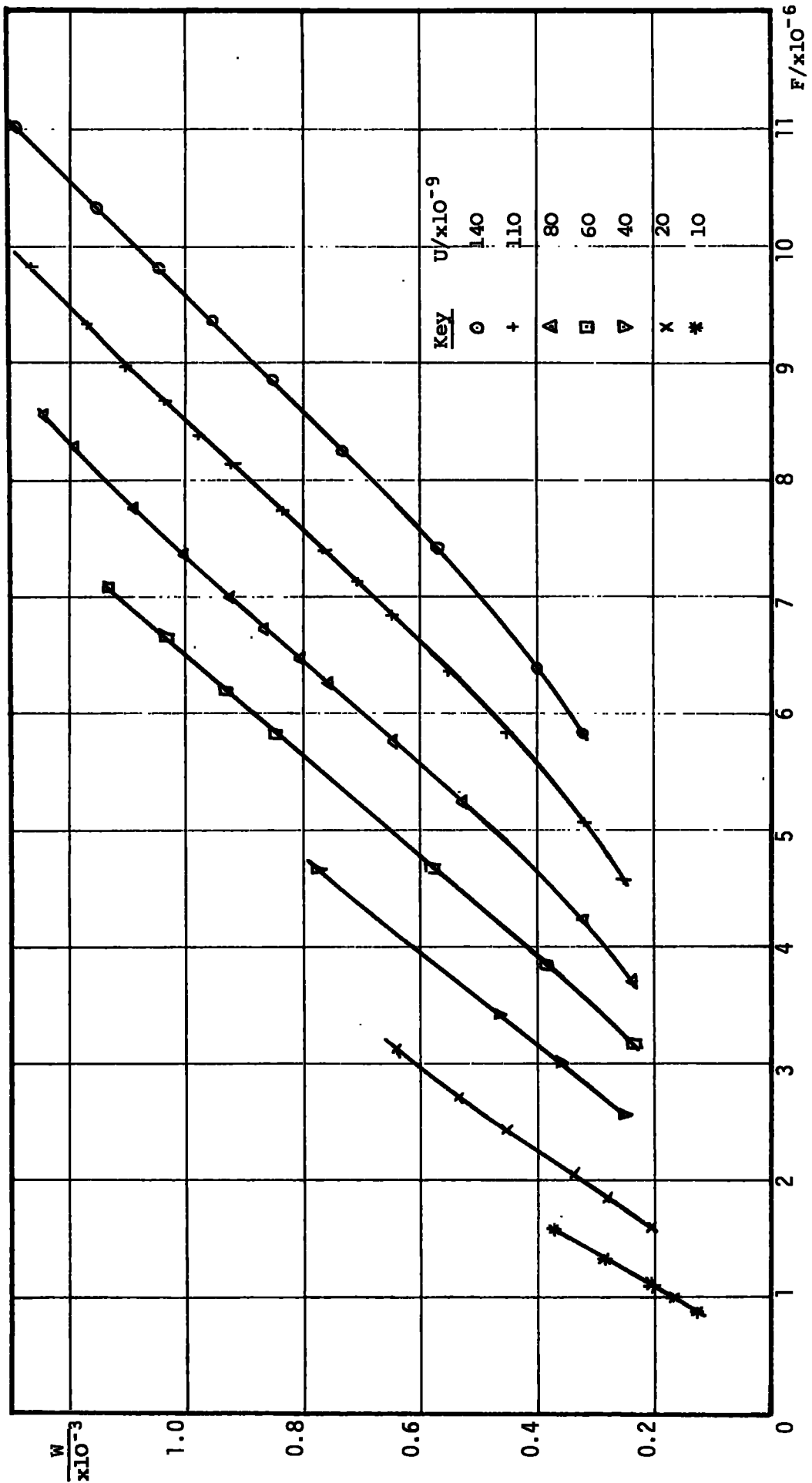
GRAPH G5.6 LOAD AGAINST FRICTION FOR 0.75 mm SOFT LAYER
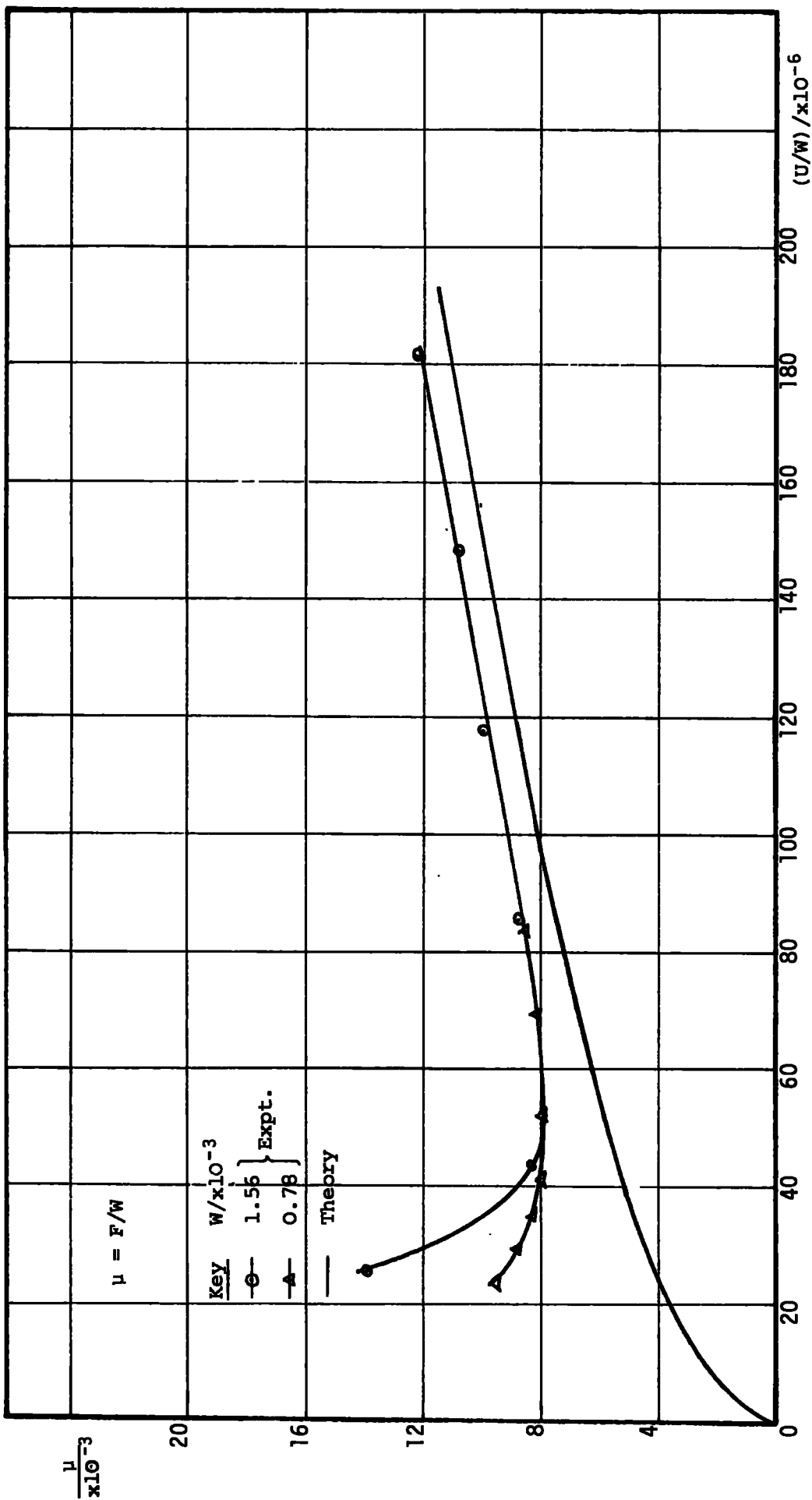
GRAPH G5.7 COEFFICIENT OF FRICTION AGAINST U/W FOR RIGID PLANE
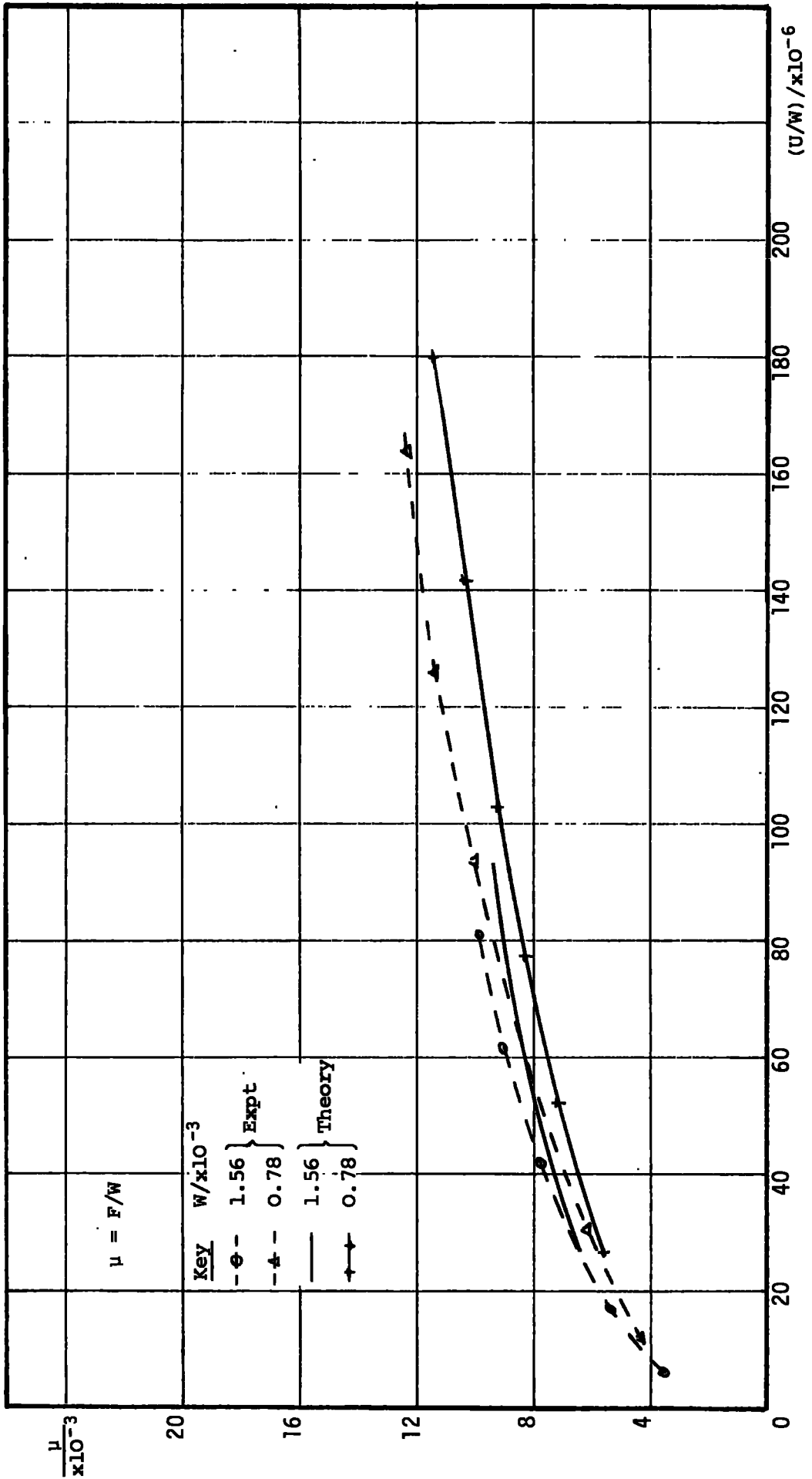
GRAPH G5.8   COEFFICIENT OF FRICTION AGAINST U/W FOR 2.5 mm SOFT LAYER
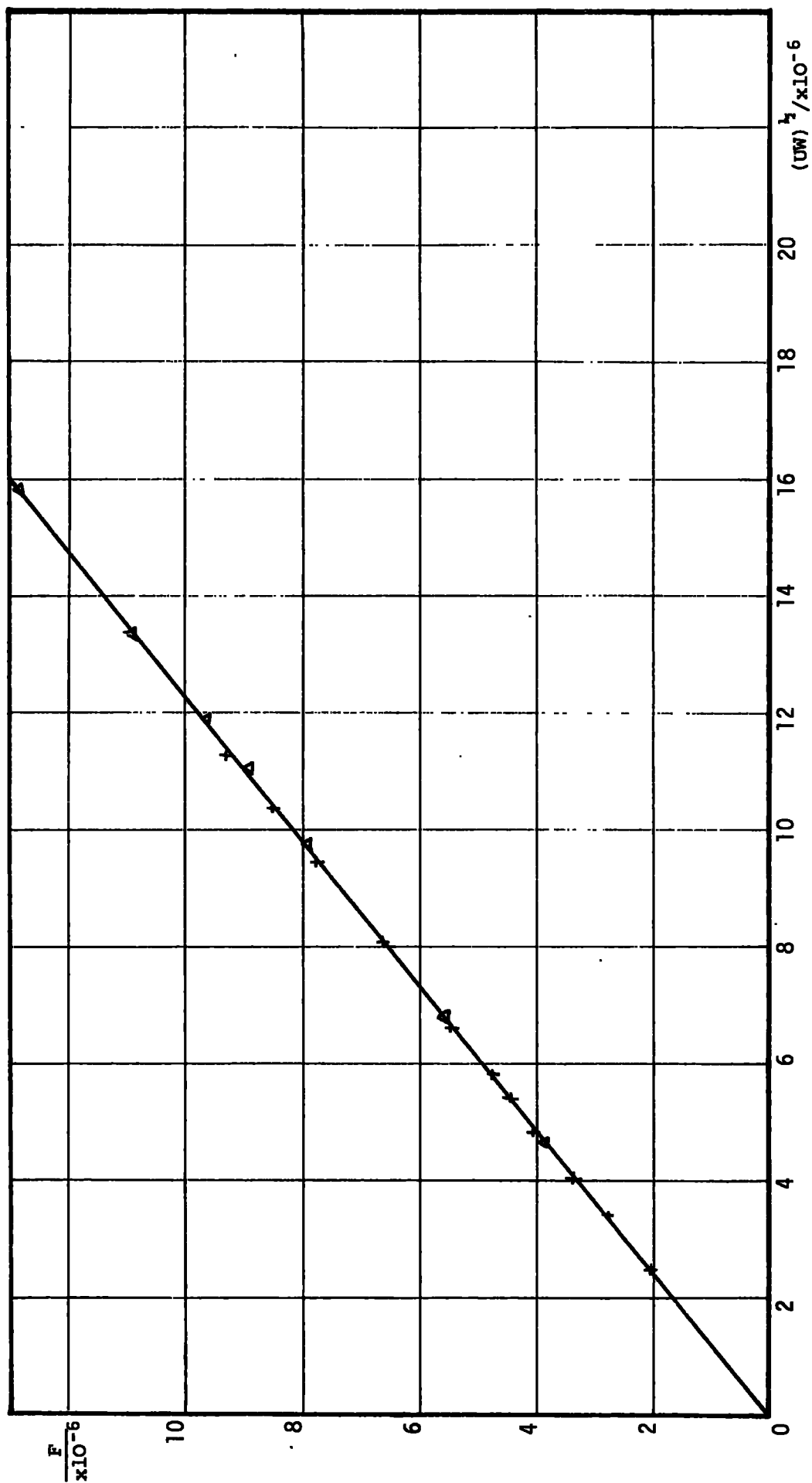
GRAPH G5.9 FRICTION (F) AGAINST $(UW)^{\frac{1}{2}}$ FOR RIGID PLANE
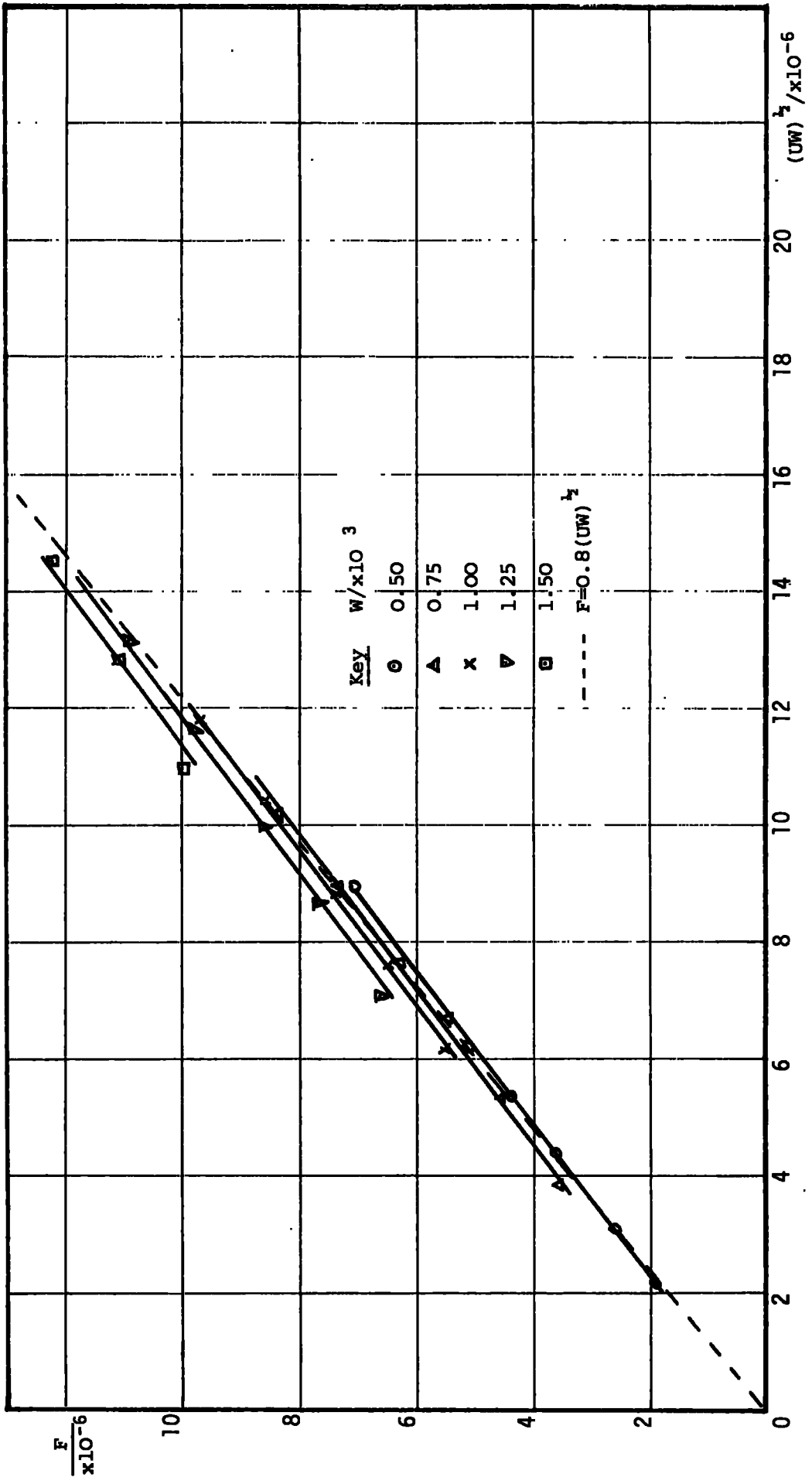
GRAPH G5.10 FRICTION (F) AGAINST $(UW)^{\frac{1}{2}}$ FOR 0.75 mm SOFT LAYER

Key $W/\times 10^{3}$

⊖	0.50
▲	0.75
✕	1.00
▼	1.25
▣	1.50

$--- F = 0.8(UW)^{\frac{1}{2}}$

$\dfrac{F}{\times 10^{-6}}$

$(UW)^{\frac{1}{2}}/\times 10^{-6}$
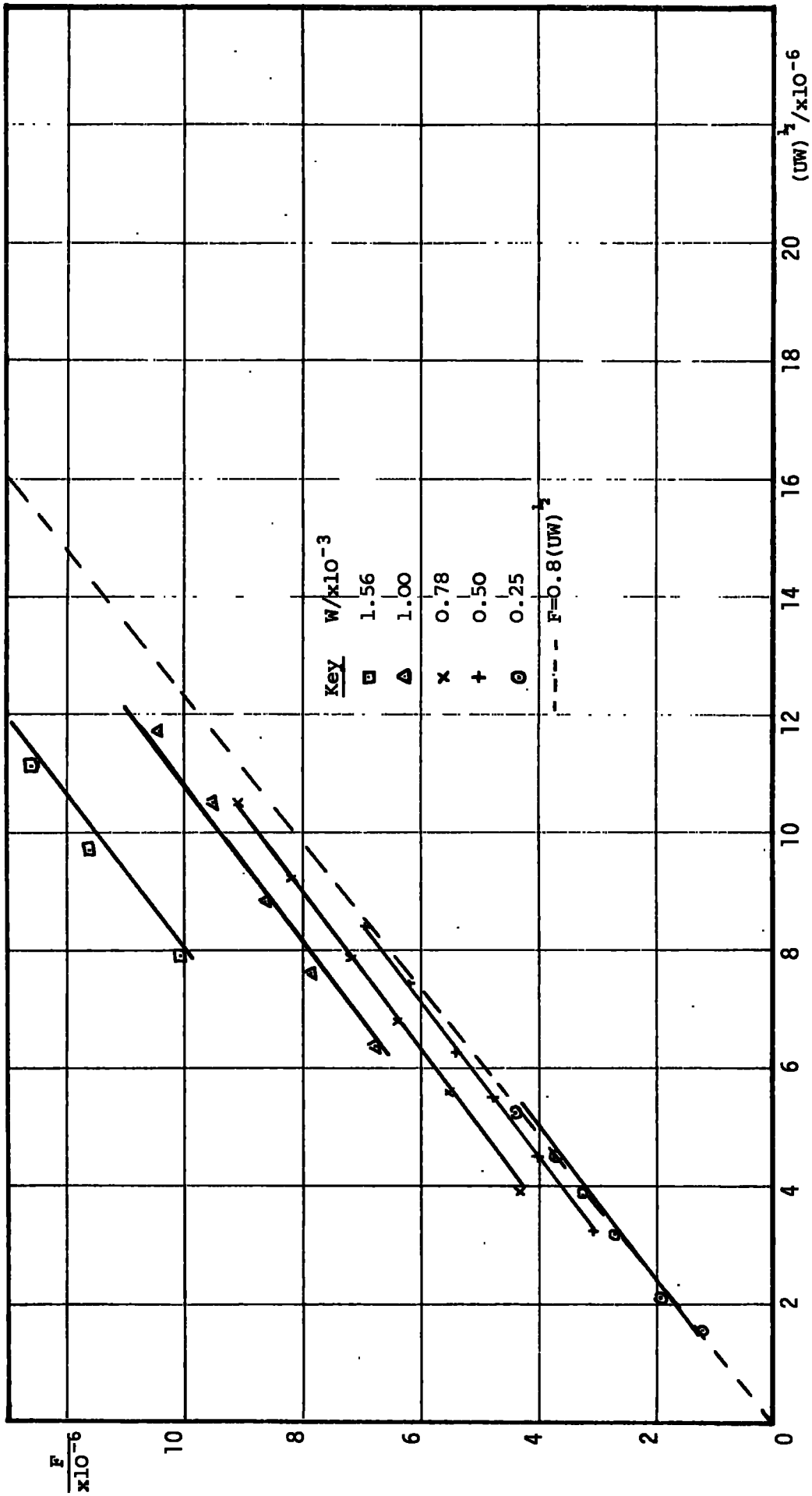
GRAPH G5.11 FRICTION (F) AGAINST $(UW)^{\frac{1}{2}}$ FOR 2.50 mm SOFT LAYER

GRAPH G5.12 PRESSURE DISTRIBUTIONS AND FILM SHAPES: EFFECT OF CAVITATION PRESSURE; $T = 27.8 \times 10^{-3}$, $U = 1.0 \times 10^{-6}$
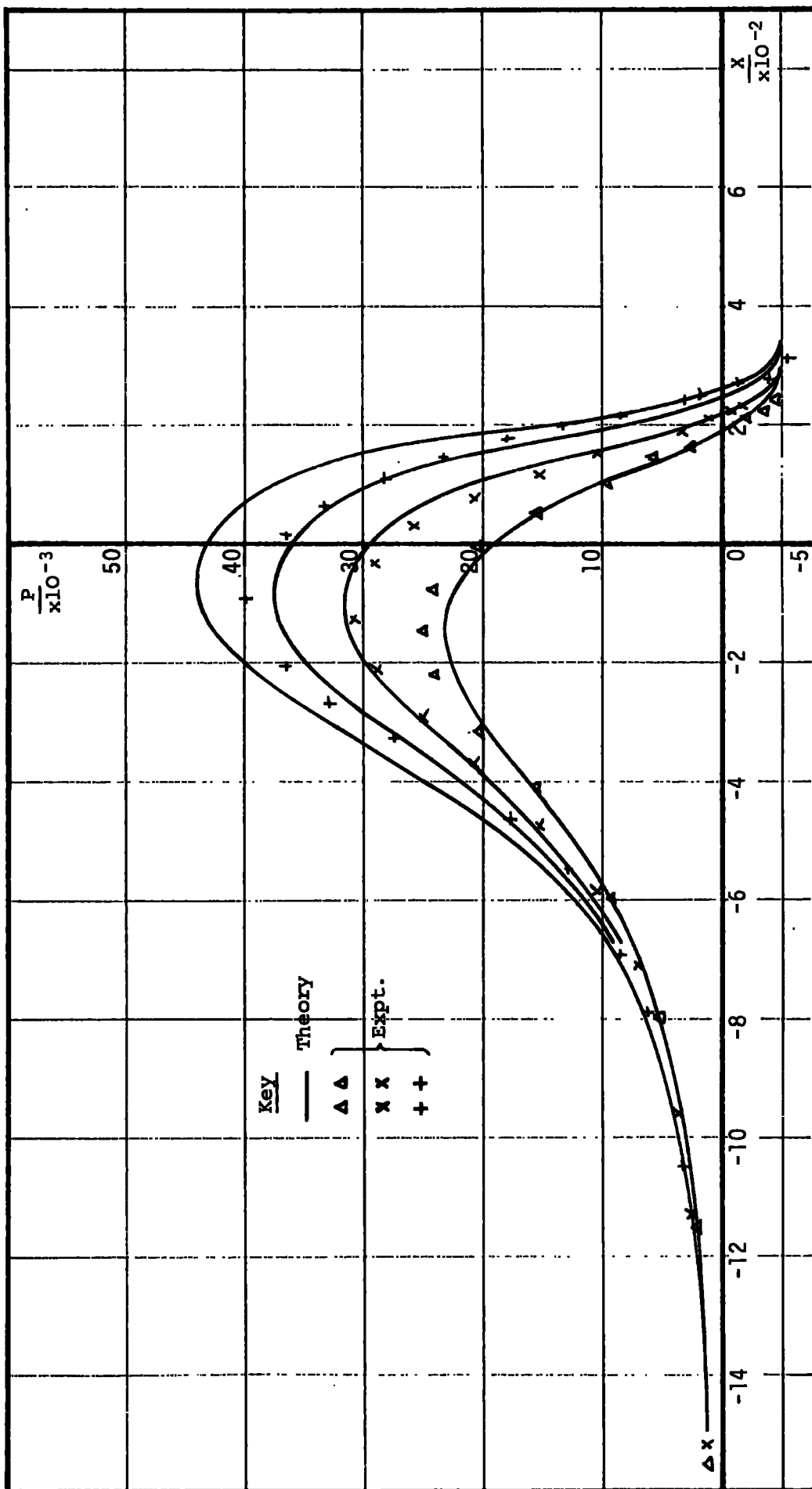
GRAPH G5.13   PRESSURE DISTRIBUTIONS FOR VARIOUS LOADS; T = 27.8x10^{-3} U = 0.5x10^{-6}
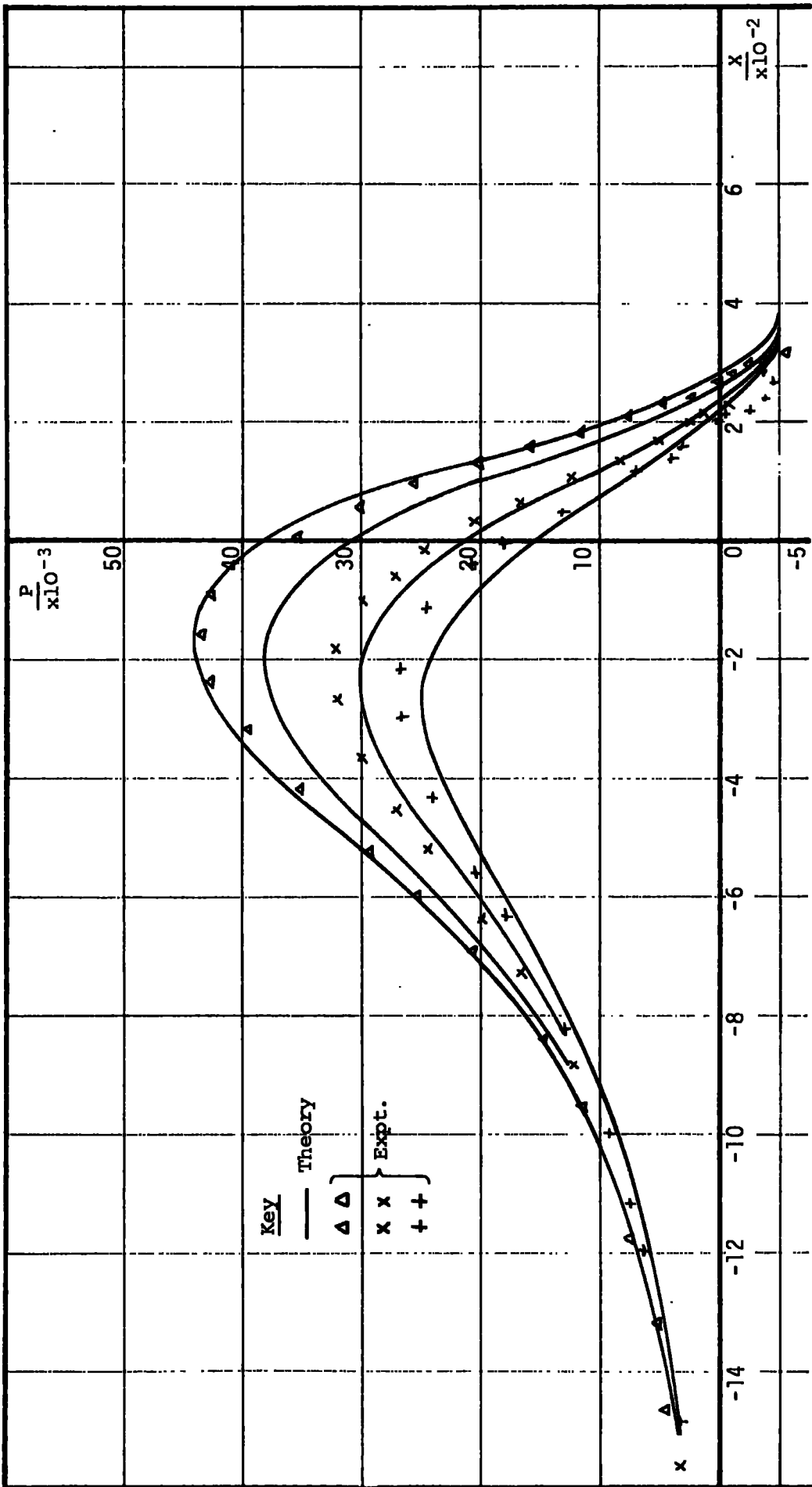
GRAPH G5.14 PRESSURE DISTRIBUTIONS FOR VARIOUS LOADS; T = 27.8x10^{-3} U = 2x10^{-6}
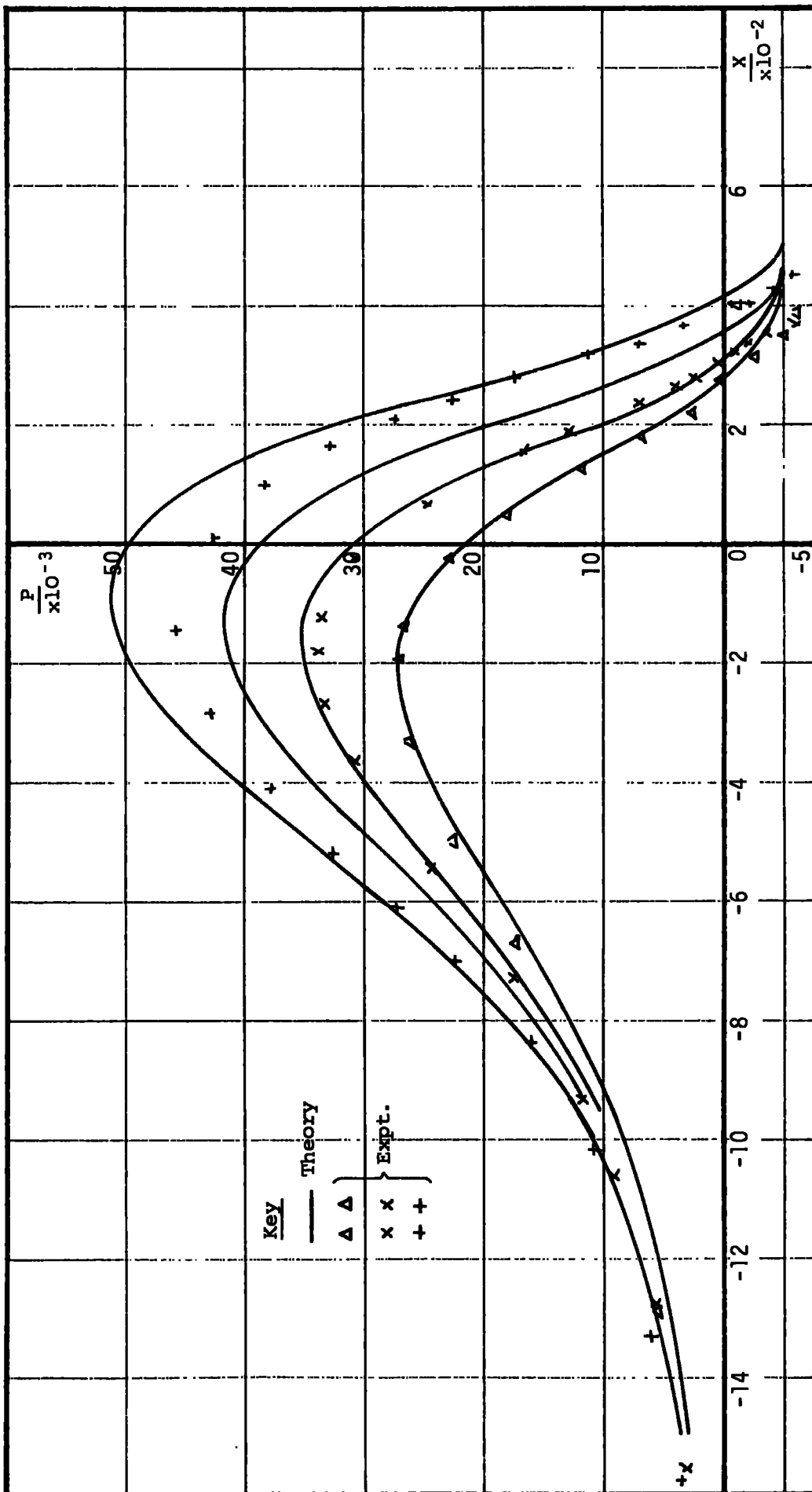
GRAPH G5.15 PRESSURE DISTRIBUTIONS FOR VARIOUS LOADS: T = 55.6x10⁻³ U = 2x10⁻⁶
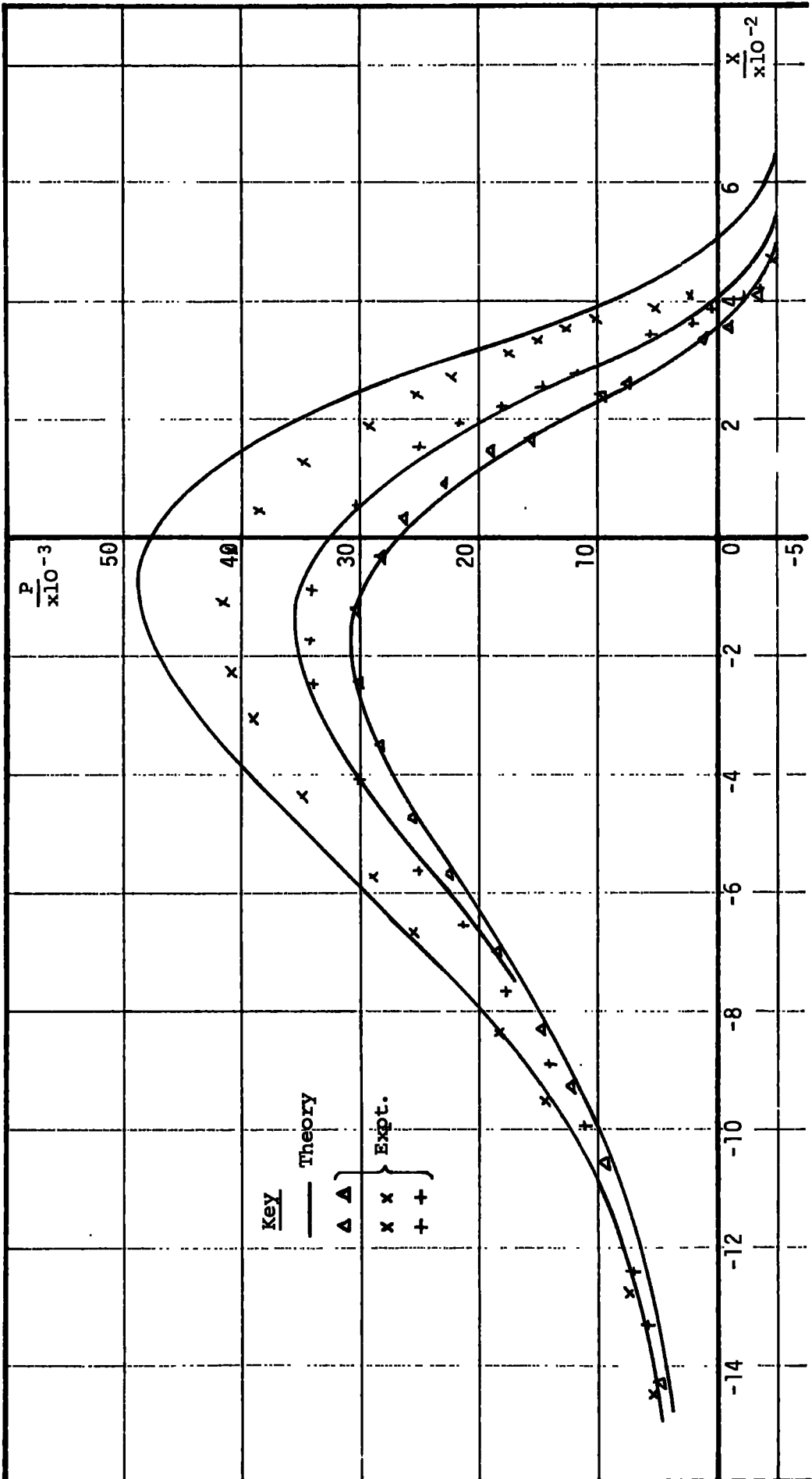
GRAPH G5.16 PRESSURE DISTRIBUTIONS FOR VARIOUS LOADS; $T = 111.1 \times 10^{-3}$ $U = 2 \times 10^{-6}$
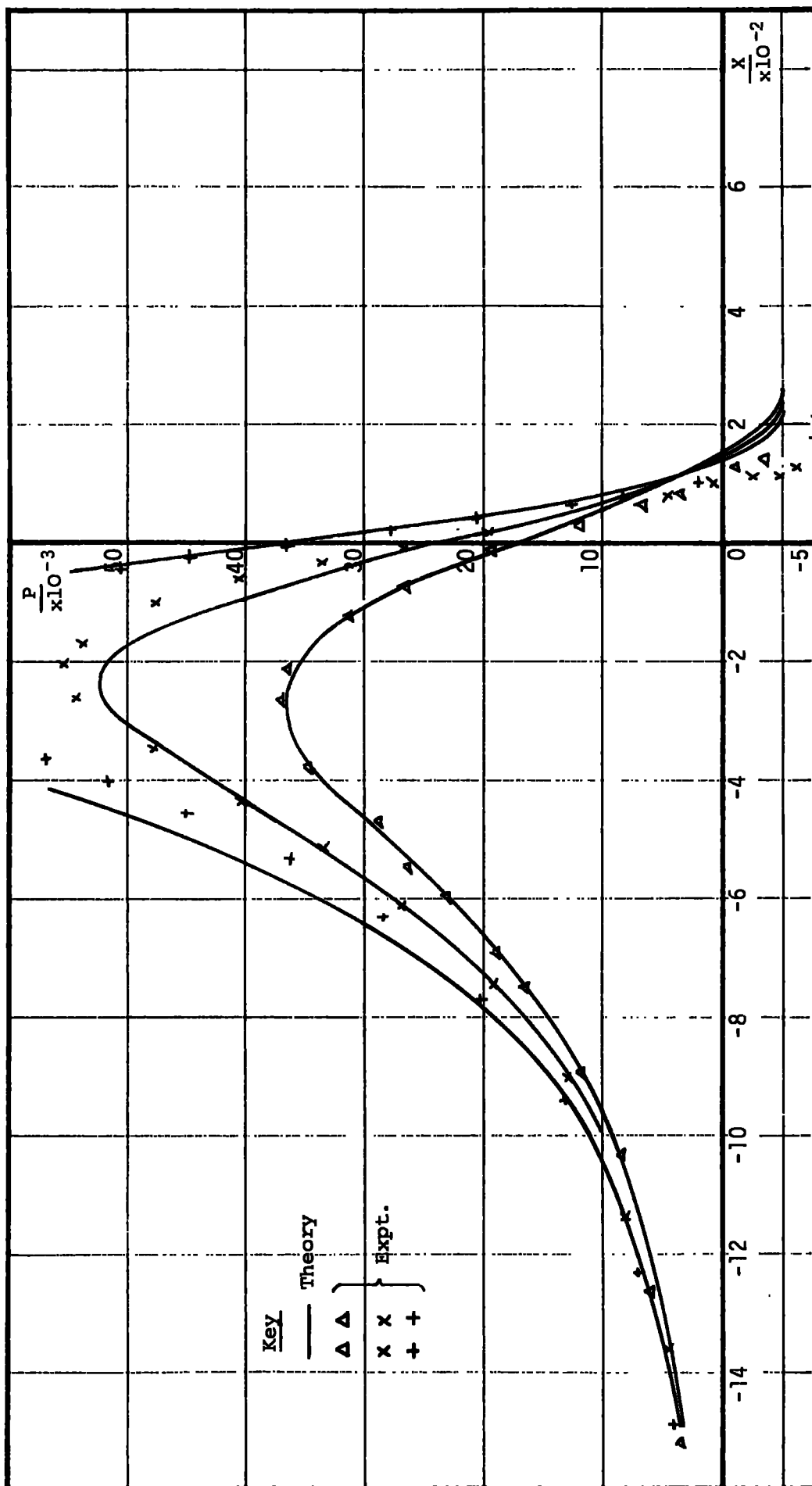
GRAPH G5.17 PRESSURE DISTRIBUTIONS FOR VARIOUS LOADS; RIGID PLANE, U = 2x10⁻⁶
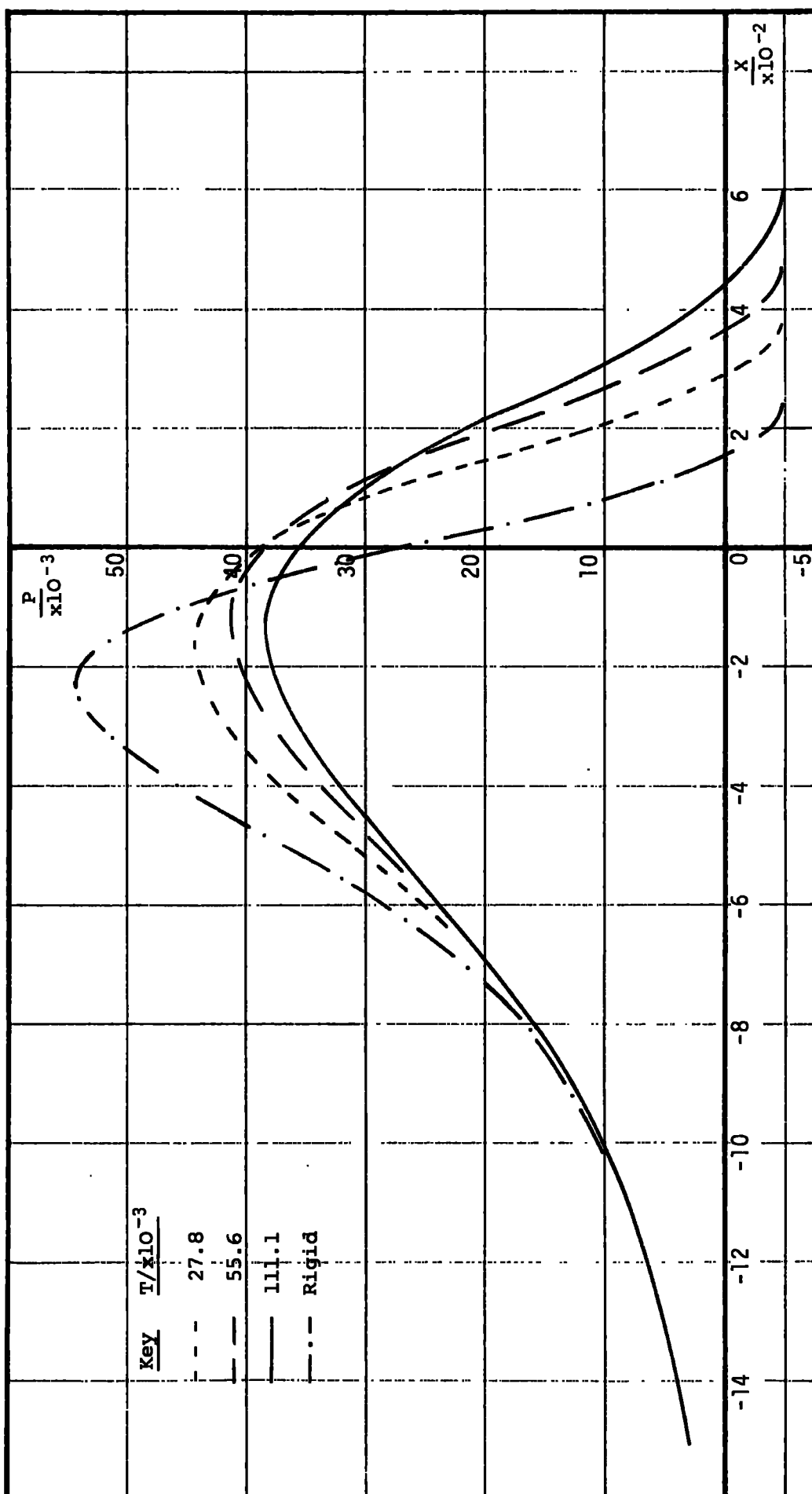
GRAPH G5.18 INTERPOLATED THEORETICAL PRESSURE DISTRIBUTIONS FOR $W = 4\times10^{-3}$; $U = 2\times10^{-6}$
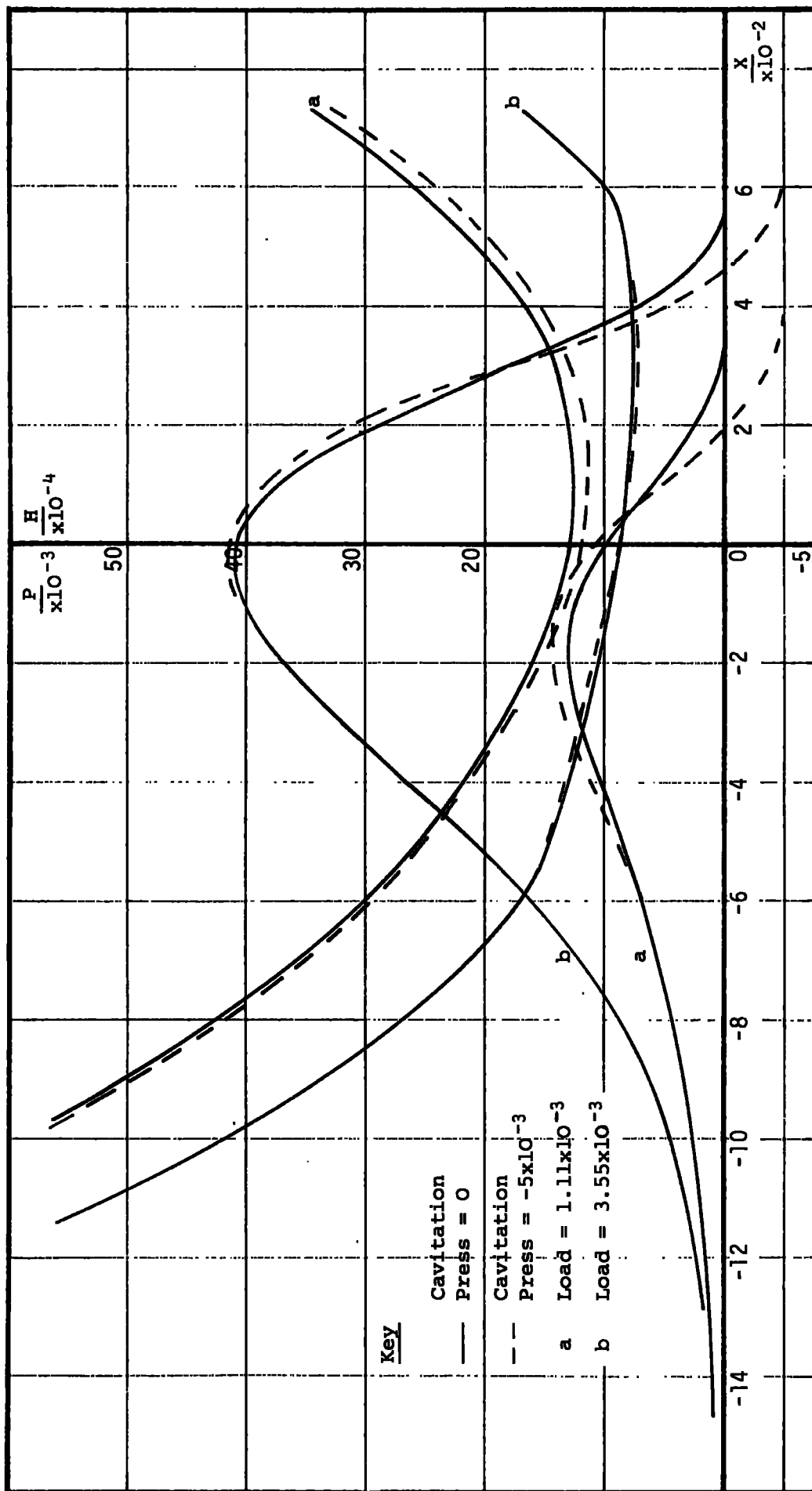
GRAPH G5.19 PRESSURE DISTRIBUTIONS AND FILM SHAPES: EFFECT OF CAVITATION PRESSURE; $T = 111.1 \times 10^{-3}$, $U = 0.5 \times 10^{-6}$

Key

Cavitation
—— Press = 0

Cavitation
- - - Press = -5×10^{-3}

a   Load = 1.11×10^{-3}
b   Load = 3.55×10^{-3}
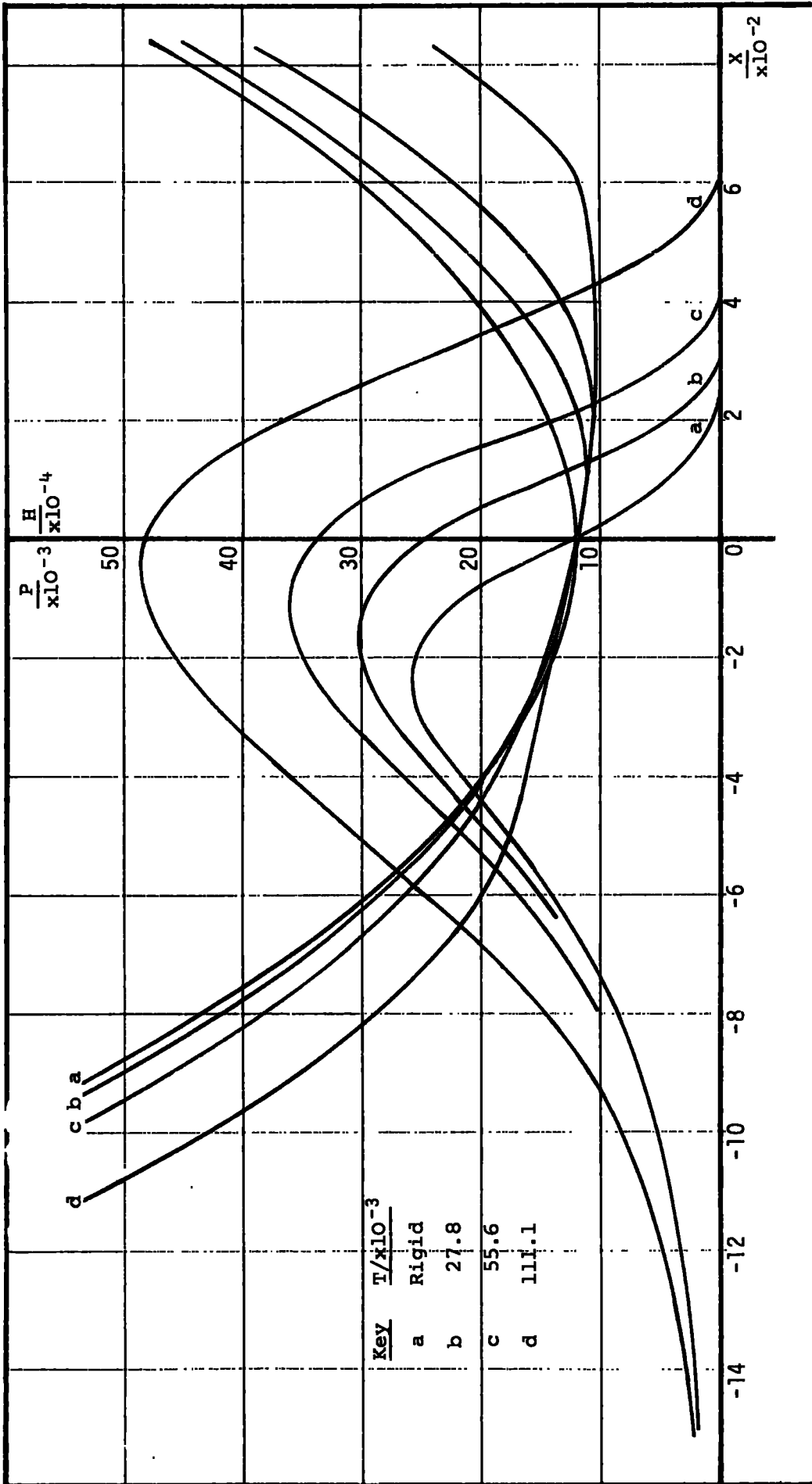
GRAPH G5.20 PRESSURE DISTRIBUTIONS AND FILM SHAPES FOR THE SAME CENTRE-LINE FILM THICKNESS; U = 1.0x10⁻⁶

Key	T/x10⁻³
a	Rigid
b	27.8
c	55.6
d	111.1

Key	T/x10⁻³
a	Rigid
b	27.8
c	55.6
d	111.1
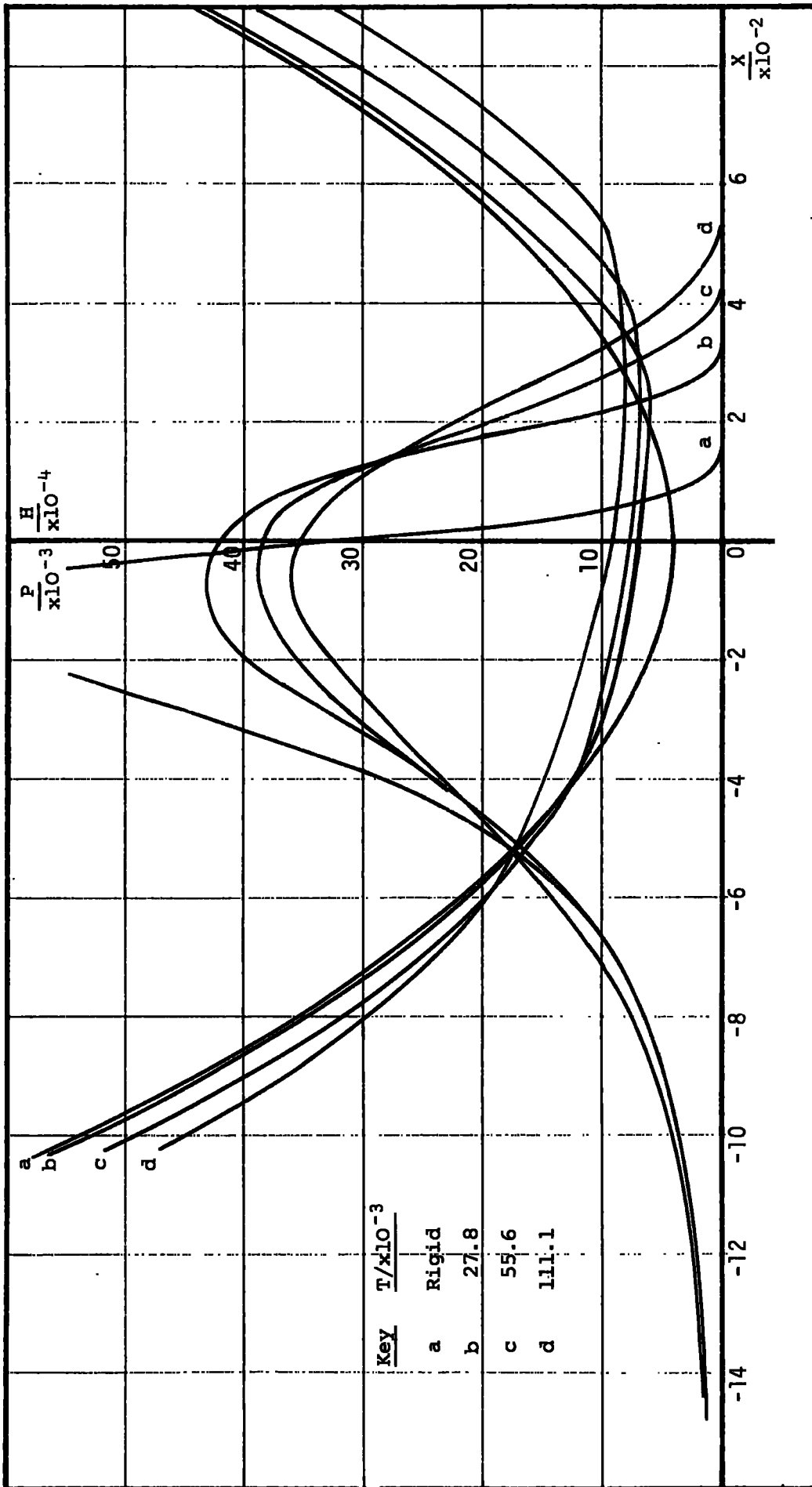
GRAPH G5.21 PRESSURE DISTRIBUTIONS AND FILM SHAPES FOR THE SAME LOAD, W = 3x10⁻³; U = 0.5x10⁻⁶
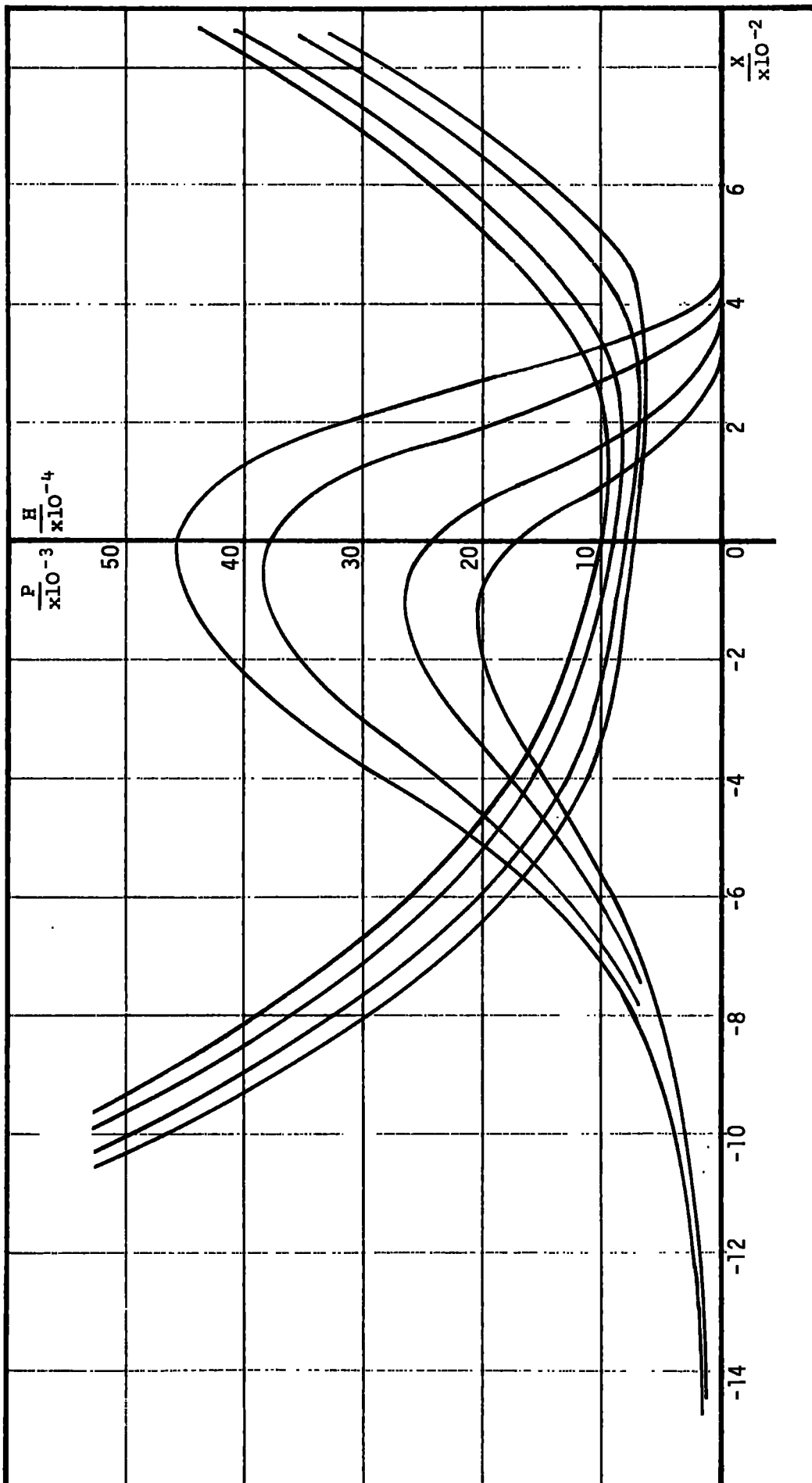
GRAPH G5.22 PRESSURE DISTRIBUTIONS AND FILM SHAPES FOR LAYER THICKNESS, T = 55.6x10^{-3}; U = 0.5x10^{-6}
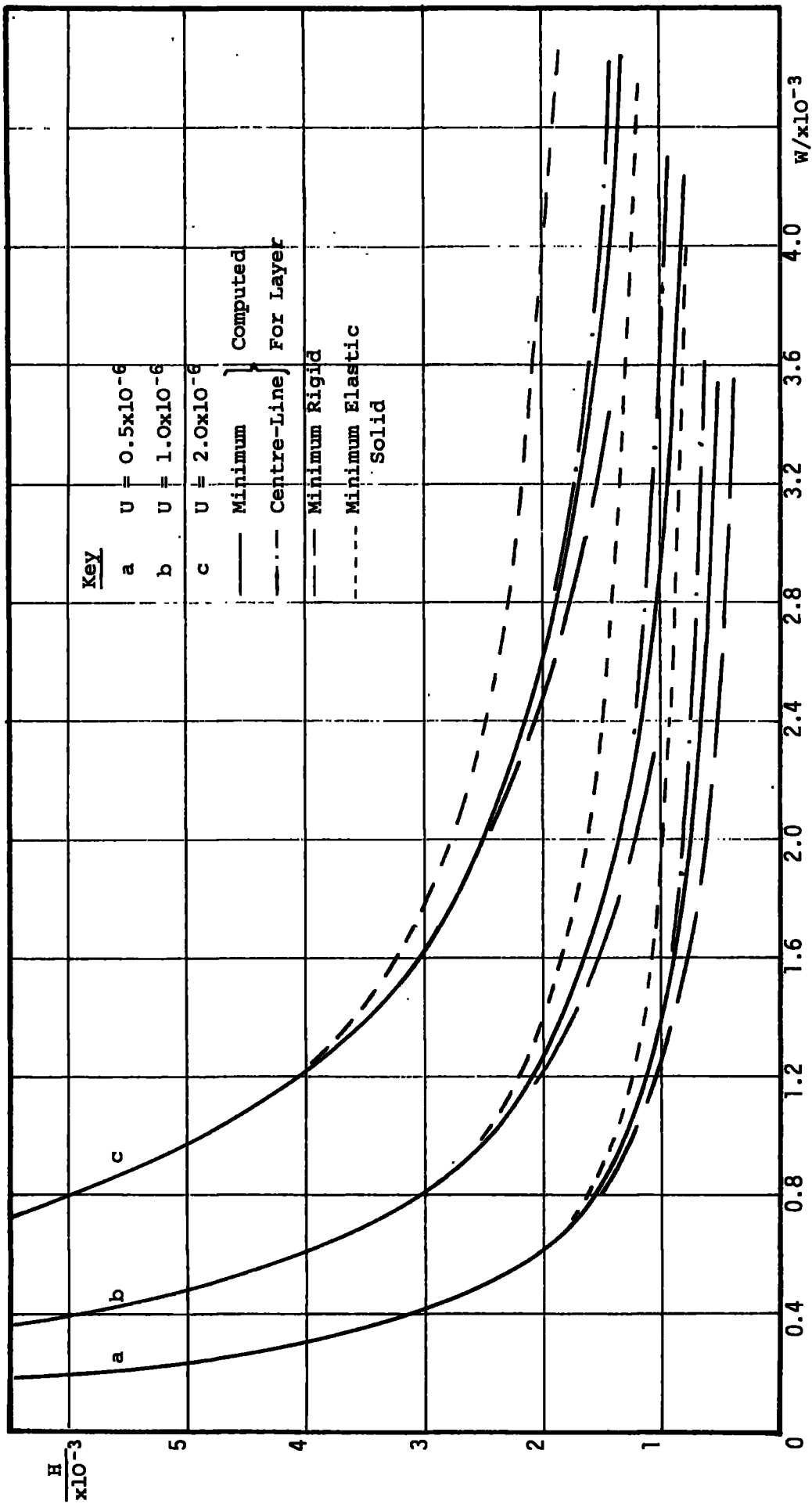
GRAPH G5.23   VARIATION OF FILM THICKNESS WITH LOAD FOR T = 27.8x10⁻³
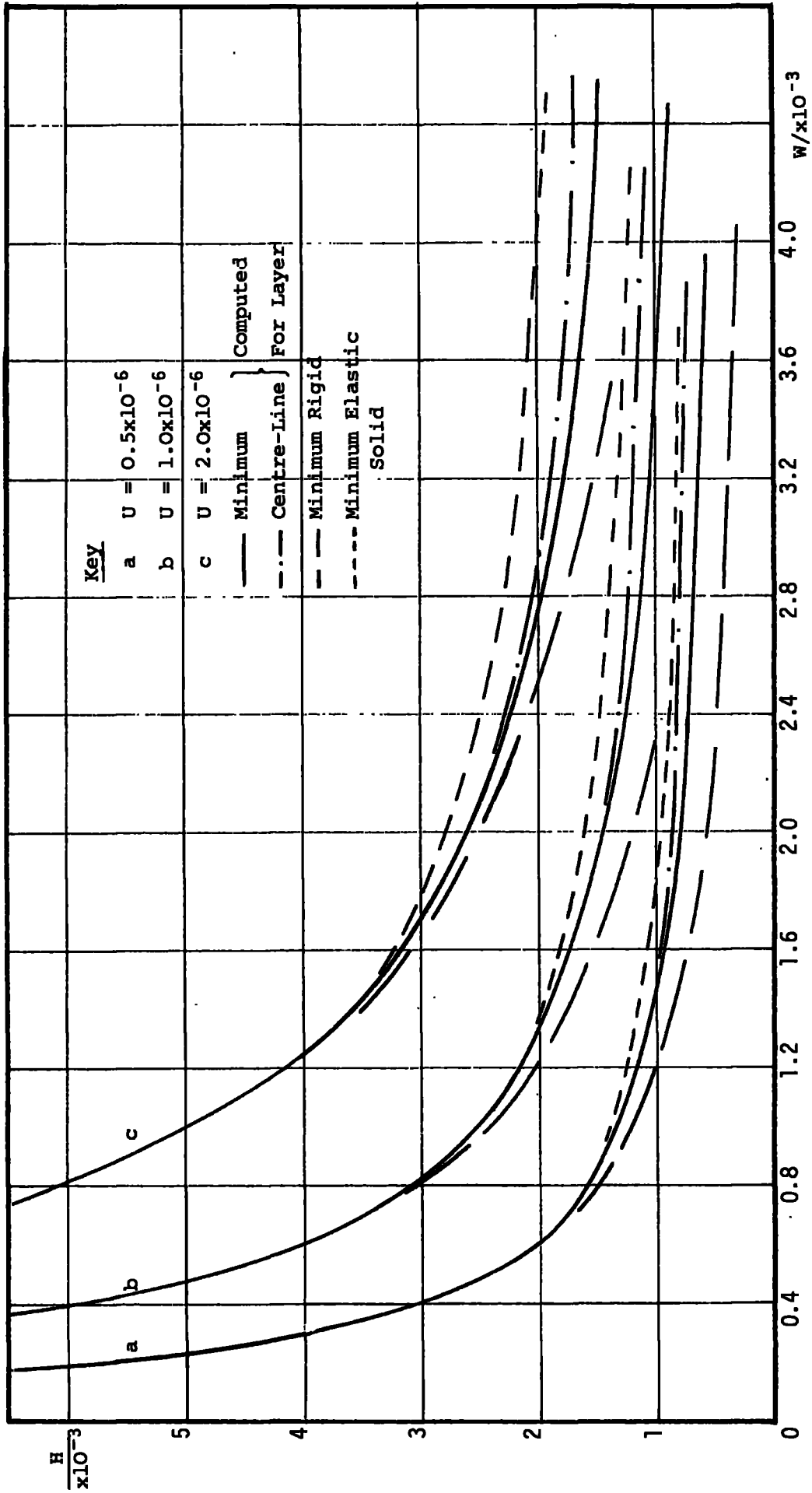
GRAPH G5.24 VARIATION OF FILM THICKNESS WITH LOAD FOR T = 55.6x10⁻³

Key

a	U = 0.5x10⁻⁶
b	U = 1.0x10⁻⁶
c	U = 2.0x10⁻⁶

Minimum } Computed
Centre-Line } For Layer
Minimum Rigid
Minimum Elastic Solid

$\dfrac{H}{x10^{-3}}$

5

4

3

2

1

0

c

b

a

0.4 0.8 1.2 1.6 2.0 2.4 2.8 3.2 3.6 4.0

$W/x10^{-3}$

Key

a $U = 0.5 \times 10^{-6}$

b $U = 1.0 \times 10^{-6}$

c $U = 2.0 \times 10^{-6}$

——— Minimum } Computed

—·— Centre-Line } For Layer

—— Minimum Rigid

––– Minimum Elastic Solid
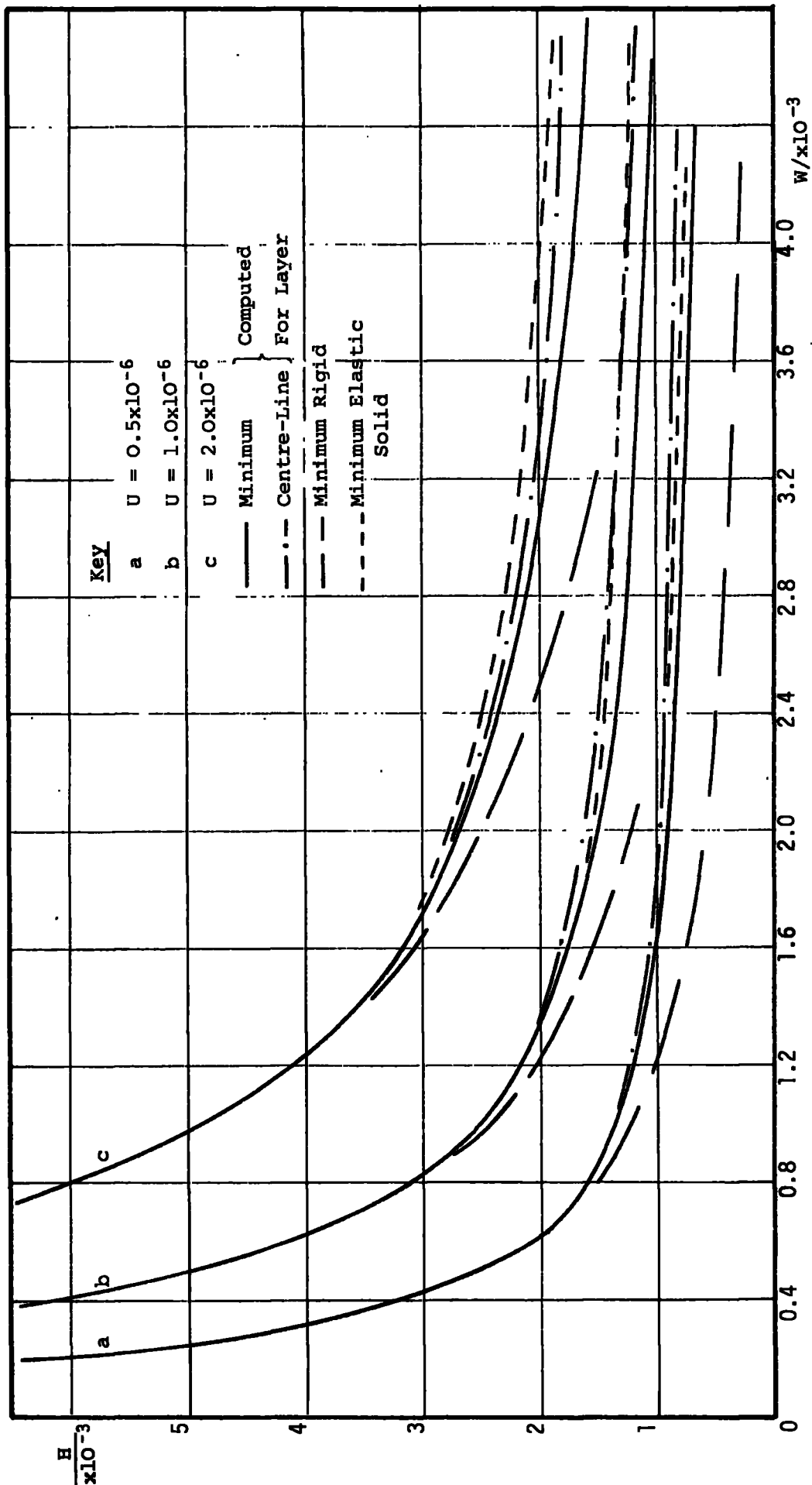
GRAPH G5.25   VARIATION OF FILM THICKNESS WITH LOAD FOR T = 111.1×10^{-3}

CHAPTER 6

SUMMARY

6.1   Conclusions

One objective of the analysis was to obtain the surface deformations of a rigidly backed, plane, elastomer layer under any pressure distribution. The finite element technique has been applied effectively to calculate influence coefficients for three ratios of width of load: layer thickness and two Poisson's ratios, 0.30 and 0.48.

The elastohydrodynamic lubrication problem of a loaded rigid cylinder sliding against a rigid plane, covered with an elastic layer, has been studied. Friction, pressures and film shapes have been predicted. The effect of the layer thickness on the film shape is clearly illustrated. The variation of minimum film thickness with load for different speeds and layers has been compared with results for rigid and elastic bodies. The transition from the hydrodynamic (rigid) regime to elastohydrodynamic is delayed with reduction of layer thickness.

It should be noted that with decreasing film thickness and increasing load, the main iteration in the computation to find the pressure (steps d. to p., Appendix II.4) eventually becomes very sensitive to changes in film shape. Even with a large damping factor the problem then fails to converge. Although it was not attempted, it is possible to obtain solutions for high loads, by assuming that the deformation and pressure curves are identical to the static loaded condition, except at inlet and outlet. The influence coefficients could be used to predict both the static dry

contact pressures for a given indentation and the deformations under the modified curve.

The theoretical results have been supported by experimental friction and pressure measurements. For the thinner layers the coefficient of friction varies in a similar manner to the rigid case, i.e. $\mu \simeq 0.8 \ (U/W)^{\frac{1}{2}}$. The thicker layers show a further dependence upon the load. In the experiments, the addition of an elastic layer allows much lower speeds or a lower viscosity lubricant to be used in the bearing, before dry contact occurs. Coefficients of friction as low as 0.002 were obtained at speeds well below the breakdown for the rigid plane.

All aspects of the variations of the experimental pressure curves with speed, load and layer thickness were predicted by the theory. A comparison of the distributions for the same load shows the tendency towards the "rigid" pressure curve with reduction of layer thickness. It has been shown that the influence displacements presented in the current work can provide an accurate representation of the deformations of soft layers in lubricated bearings.

6.2   Suggestions for Future Work

The theoretical work has been limited to establishing the computational technique for finding the influence coefficients and using them in a single lubrication case. The problems solved were dictated by the parameters in the verifying experiments. The finite element method could be employed alone in a comprehensive study of the effect of Poisson's ratio on the deformation of soft layers. Axisymmetric influence coefficients could also be developed. Small additional computation would allow the sub-surface stresses to be

calculated.

Any change in the type of influence coefficient derived would be reflected in further possible solutions in the lubrication problem. The analysis of several other bearing configurations could be attempted, with a view to obtaining non-dimensionals to describe minimum film thickness, friction, etc.

On the experimental side film thickness remains to be measured. The materials are suitable for optical interference techniques to be used. A new rig might be developed explicitly for this purpose. The friction experiments could be extended to the regime of boundary lubrication with the use of low viscosity lubricants, although a careful study of the materials would be needed. The range of the pressure measurements also could be enlarged by altering the lubricant or layer properties.

APPENDIX I

Matrices for the calculation of the stiffness matrix of the rectangular element with four nodes (from Chapter 4).
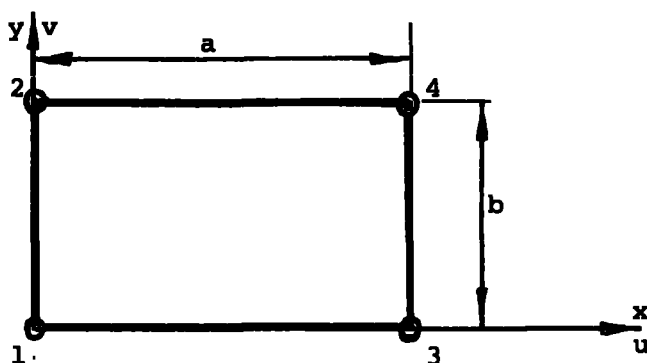
Fig. 4.2 Linear Element

NB. $\{\delta\} = [c]\{\alpha\}$, $\{\varepsilon\} = [Q]\{\alpha\}$

$$[k] = \{[c]^{-1}\}^T (\iint [Q]^T [D] [Q] \ dx \ dy) [c]^{-1}$$

For plane stress, let $s = (1 - \nu)/2$ then

$$[k] = \frac{E}{(1 - \nu^2)} \begin{bmatrix} k_{11} & k_{12} & k_{13} & k_{14} & k_{15} & k_{16} & k_{17} & k_{18} \\ & k_{11} & k_{14} & k_{13} & k_{17} & k_{18} & k_{15} & k_{16} \\ & & k_{11} & k_{12} & k_{16} & k_{15} & k_{18} & k_{17} \\ & & & k_{11} & k_{18} & k_{17} & k_{16} & k_{15} \\ & & & & k_{55} & k_{56} & k_{57} & k_{58} \\ & & & & & k_{55} & k_{58} & k_{57} \\ & & & & & & k_{55} & k_{56} \\ & & & & & & & k_{55} \end{bmatrix}$$

$k_{11} = \dfrac{1}{3} \left(\dfrac{b}{a} + \dfrac{sa}{b} \right)$; $k_{12} = \dfrac{1}{6} \left(\dfrac{b}{a} - \dfrac{2sa}{b} \right)$; $k_{13} = \dfrac{1}{6} \left(\dfrac{sa}{b} - \dfrac{2b}{a} \right)$;

$k_{14} = \dfrac{-1}{6} \left(\dfrac{b}{a} + \dfrac{sa}{b} \right)$; $k_{15} = \dfrac{1}{4} \left(\nu + s \right)$; $k_{16} = \dfrac{1}{4} \left(s - a \right)$;

$k_{17} = \dfrac{1}{4} \left(\nu - s \right)$; $k_{18} = \dfrac{-1}{4} \left(\nu + s \right)$; $k_{55} = \dfrac{1}{3} \left(\dfrac{sb}{a} + \dfrac{a}{b} \right)$;

$k_{56} = \dfrac{1}{6} \left(\dfrac{sb}{a} - \dfrac{2a}{b} \right)$; $k_{57} = \dfrac{1}{6} \left(\dfrac{a}{b} - \dfrac{2sb}{a} \right)$; $k_{58} = \dfrac{-1}{6} \left(\dfrac{sb}{a} + \dfrac{a}{b} \right)$:

APPENDIX II

Computer Programmes

1. Linear Rectangular Plane Stress Element.

2. Cubic "Serendipity" Rectangular Element.

3. Data creation programme for cubic element and the "Irons" solving routine.

4. Lubrication programme.

1. **Detailed Steps in Linear Rectangular Plane Stress Element Programme**

   (a) Element and mesh sizes, elastic constants and nodal numbers for constraints and loads read in.

   (b) Element stiffness matrix generated.

   (c) Nodes in the mesh automatically numbered and the band-width of the main stiffness matrix found.

   (d) For each element, the position in the main matrix of the coefficients for each node in the element was located. Relevant coefficients posted into the main stiffness matrix.

   (e) Information on nodal loads and constraints collected.

   (f) For each constrained node, row and column of the main stiffness matrix set to zero and the diagonal to unity.

   (g) Load vector generated from data.

   (h) Main stiffness matrix and load vector applied to solving routine; nodal displacements as output.

2. Cubic "Serendipity" Rectangular Element

The programme was used as a sub-routine in conjunction with the "Irons" assembly and solving routine, Ref. 54,57. Those matrices common to all elements were calculated for the first element only and stored for further use.

Flow chart

```
┌─────────────────────────────────────┐
│ READ:- Dimensions                    │
└─────────────────────────────────────┘
┌─────────────────────────────────┐
│ Is this the first element?    ── │
└─────────────────────────────────┘
                  +

┌────────────────────────────────────────┐
│ Plane stress or plane strain?  Generate │
│ appropriate elasticity matrix, [D].     │
└────────────────────────────────────────┘

┌────────────────────────────────────────┐
│ Calculate coords. of Gaussian Integration│
│ points and weighting factors.           │
└────────────────────────────────────────┘

┌────────────────────────────────────────┐
│ Calculate Partial Derivatives of Shape  │
│ Functions for each node, at Gauss Points│
└────────────────────────────────────────┘

┌────────────────────────────────────────┐
│ Gaussian Integration of products of     │
│ Differentiated Shape Functions, stored. │
└────────────────────────────────────────┘

┌────────────────────────────────────────┐
│ Formation of invariable part of stiffness│
│ matrix; stored permanently.             │
└────────────────────────────────────────┘

        ┌──────────────────────────────────────┐
        │ Transfer stored invariable part of   │
        │ stiffness matrix to place in element │
        │ stiffness matrix.  Transfer stored   │
        │ Integrated products of differentiated│
        │ shape functions.                     │
        └──────────────────────────────────────┘

┌────────────────────────────────────────┐
│ Generate remainder of stiffness         │
│ matrix from element dimensions,         │
│ elasticity matrix, and integrated       │
│ products of differentiated shape        │
│ functions.                              │
└────────────────────────────────────────┘

┌────────────────────────────────────────┐
│ Return to Irons programme with          │
│ element stiffness matrix.               │
└────────────────────────────────────────┘
```

3. <u>Data creation programme for cubic element in conjunction with</u>

   <u>"Irons" programme.</u>

   The "Irons" assembly and solving programme was written for
use with many different elements. The data input was of general
form making no allowances for order in either the mesh or element.
To facilitate input and checking a programme was developed to create
the "Irons" data for the cubic element. It relied upon the ordered
nature of the mesh to predict element and nodal numbers, element
dimensions, loads and constraints from the minimum of input. A 100%
reduction in data requirement was achieved.

   <u>Flow Chart</u>

   ```
   ┌─────────────────────────────────────────────────┐
   │ READ:- Type of problem, mesh size and loaded     │
   │        element details; Dimensions of each row   │
   │        and column of elements.                   │
   └─────────────────────────────────────────────────┘
   ┌─────────────────────────────────────────────────┐
   │ Generate half-dimensions of each element         │
   └─────────────────────────────────────────────────┘
   ┌─────────────────────────────────────────────────┐
   │ OUTPUT:- Standard data for IRONS                 │
   └─────────────────────────────────────────────────┘
   ┌─────────────────────────────────────────────────┐
   │ Generate nodal nicknames in mesh for each        │
   │ element from mesh size data.  Generate           │
   │ Lagrange multipliers' nicknames for each         │
   │ element with constraints.                        │
   └─────────────────────────────────────────────────┘
   ┌─────────────────────────────────────────────────┐
   │ OUTPUT:- Nodal and Lagrange multipliers' nick-   │
   │          names for each element                  │
   └─────────────────────────────────────────────────┘
   ┌─────────────────────────────────────────────────┐
   │ Generate nodal numbers in standard element       │
   │ which may be constrained.                        │
   └─────────────────────────────────────────────────┘
   ┌─────────────────────────────────────────────────┐
   │ OUTPUT:- Indicators for IRONS                    │
   └─────────────────────────────────────────────────┘
   ┌─────────────────────────────────────────────────┐
   │ READ:- Type of load (General, Uniform, Linear    │
   │        or Quadratic).  Generate nodal numbers    │
   │        in standard element which may be          │
   │        constrained.                              │
   └─────────────────────────────────────────────────┘
   ```

   Check For Type of Loading

   General   Uniform, Linear or Quadratic.

   ```
   ┌──────────────────────────────┐   ┌──────────────────────────┐
   │ READ:- Pressure and coords.  │   │ READ:- Maximum Press.    │
   │        at intervals on curve │   └──────────────────────────┘
   └──────────────────────────────┘   ┌──────────────────────────┐
                                       │ Generate nodal Loads.    │
                                       └──────────────────────────┘
   ┌─────────────────────────────────────────────────────────────────┐
   │ OUTPUT:- Each element:- Indicators, Dimensions, Loads, Constraints│
   └─────────────────────────────────────────────────────────────────┘
   ```

4.   Elasto-Hydrodynamic Programme.

The influence displacements from the finite element solutions were used to provide the deformed surface shape of the plane elastic layer under e.h.l. conditions. The dimensions, elastic constants and oil viscosity were specified; speed and/or centre line film thickness were varied; pressures, surface deformations, film shape, load and friction force within the bearing were calculated.
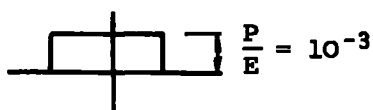
Detailed Steps

(a)   Input of Finite Element Data for Influence Displacements.

(b)   Conversion to non-dimensional influence displacements at equally spaced points along surface.

(c)   Input of initial pressure curve as magnitudes at equally spaced points (Simpson points).

(d)   Description of pressure curve as several quadratics. Co-efficients and coordinates of quadratics stored for reference.

(e)   Calculation of pressure at "loading points" appropriately spaced for the influence displacements.

(f)   Description of pressures as several quadratics between "loading points".

(g)   Application of quadratics as summation of multiples of the influence coefficients to give displacement at points spaced similarly to (b).

(h)   Description of displacements as several cubics.

(j)   Use of cubics to give lubricant film thickness at "Simpson points"; Simpson integration of Reynolds equation to find inlet pressure.

(k)   Iteration to satisfy boundary conditions involving movement of pressure outlet point and recalculation of (j).

(m)   Final integration to find new pressures at new "Simpson
      points".

(n)   Comparison with old pressure curve using stored coefficients
      of (d).

(p)   Update of pressure curve and re-application at (d) unless
      limits satisfied.

(q)   Integration of pressure to find load.

(r)   Calculation of displacements outside pressure zone (in post-
      outlet); description as several cubics.

(s)   Film thickness after outlet point at equally spaced points for
      integration to find friction.

(t)   Integration for friction in pre-inlet, pressure, deformed post-
      outlet and undeformed post-outlet regions, to find total
      tangential force on place.

APPENDIX III

Influence Displacements for Soft Layer Under a

Uniform Load

Poisson's Ratio = 0.48

Width of Load : Layer Thickness = 1 : 1

$$\frac{P}{E} = 10^{-3}$$

Distance from centre line	Influence displace- ment	Distance from centre line	Influence displace- ment
$\times 10^{-2}$	$\times 10^{-6}$	$\times 10^{-2}$	$\times 10^{-6}$
0.0	425.5	66.7	7.0
4.1	424.3	70.8	- 12.8
8.3	421.3	75.0	- 28.2
12.4	416.2	87.5	- 62.1
16.6	408.5	100.0	- 77.9
20.8	398.0	112.5	- 81.8
25.0	384.7	125.0	- 80.6
29.1	369.3	137.5	- 76.0
33.3	349.6	150.0	- 71.0
37.4	324.2	216.7	- 38.2
41.6	291.2	283.3	- 20.1
45.8	245.3	350.0	- 11.3
50.0	177.9	550.0	- 3.2
54.2	110.8	750.0	- 0.1
58.3	65.2	950.0	- 1.0
62.5	32.5		

Influence Displacements for Soft Layer Under a Linear Load

Poisson's Ratio = 0.48

Width of Load : Layer Thickness = 1 : 1

$$\frac{P}{E} = 10^{-3}$$
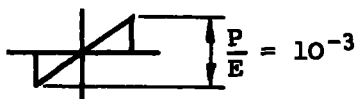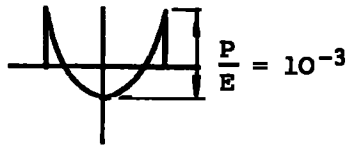
Distance from Centre-line $\times 10^{-2}$	Influence Displacement $\times 10^{-6}$	Distance from Centre-line $\times 10^{-2}$	Influence Displacement $\times 10^{-6}$
0.0	0.0	50.0	91.9
2.0	8.4	51.0	83.4
4.0	16.7	52.0	77.0
6.0	25.0	53.0	71.8
8.0	33.2	54.0	67.3
10.0	41.3	55.0	63.3
12.0	49.2	56.0	60.0
14.0	57.0	57.3	55.7
16.0	64.5	58.7	51.8
18.0	71.8	60.0	48.4
20.0	78.7	62.0	43.9
22.0	85.8	64.0	39.8
24.0	91.6	66.0	36.1
26.6	98.9	70.0	29.6
29.1	105.5	74.0	24.2
31.6	111.0	78.0	19.8
33.6	114.7	84.0	14.1
35.6	117.6	90.0	9.5
37.6	119.6	96.0	6.0
39.6	120.7	108.0	0.8
41.6	120.3	120.0	- 2.3
43.6	118.3	132.0	- 3.8
45.0	116.1	150.0	- 4.7
46.4	112.4	168.0	- 4.5
47.8	106.9	186.0	- 3.8
48.6	103.2	222.0	- 2.1
49.3	98.4	258.0	- 0.4
		294.0	1.7

Influence Displacements for Soft Layer Under a Quadratic Load

Poisson's Ratio = 0.48

Width of Load : Layer Thickness = 1 : 1

$$\frac{P}{E} = 10^{-3}$$

Distance from centre-line $\times 10^{-2}$	Influence Displace-ments $\times 10^{-6}$	Distance from centre-line $\times 10^{-2}$	Influence Displace-ments $\times 10^{-6}$
0.0	− 24.7	48.5	17.2
4.2	− 24.2	49.3	16.3
8.3	− 22.5	50.0	14.8
12.5	− 19.8	52.1	11.5
16.7	− 16.1	54.2	9.6
20.8	− 11.6	56.3	8.3
25.0	− 6.4	58.3	7.3
27.1	− 3.7	60.4	6.6
29.2	− 0.8	62.5	6.0
31.3	2.1	66.7	5.0
33.3	5.0	70.8	4.2
35.4	7.8	75.0	3.6
37.5	10.5	83.3	2.6
40.0	13.1	91.7	1.9
41.7	15.2	100.0	1.5
43.8	16.9	133.3	0.2
44.4	17.3	166.7	− 0.1
45.1	17.6	200.0	− 0.1
45.8	17.8	266.7	− 0.1
46.4	18.0	333.3	− 0.0
47.1	18.0	400.0	− 0.0
47.8	17.8		

<u>APPENDIX IV</u>

<u>REFERENCES</u>

1. REYNOLDS, O., "On the Theory of Lubrication and its Application
    to Mr. B. Tower's Experiments", Phil. Trans. R. Soc., 1886,
    177 (pt.1), pp.157.

2. JONES, E. S., "Joint Lubrication", The Lancet, 1934, 226,
    pp.1426-27.

3. MacCONAILL, M. A., "The Function of Intra-Articular Fibro-
    cartilages", J. of Anatomy, 1931-32, 66, pp.210-27.

4. CHARNLEY, J., "The Lubrication of Animal Joints", Proc. Symp.
    Biomechanics, Instn. Mech. Engrs., 1959, pp.12-22.

5. LEWIS, P. R. and McCUTCHEN, C. W., "Mechanism of Animal Joints",
    Nature, 1959, 184, pp.1284-85.

6. McCUTCHEN, C. W., "Frictional Properties of Animal Joints",
    Wear, 1962, 5, pp.1-17.

7. McCUTCHEN, C. W., "Animal Joints and Weeping Lubrication", New
    Scientist, 1962, 301, pp.412-413.

8. DINTENFASS, L., "Lubrication in Synovial Joints", J. Bone Joint
    Surgery, 1963, 45(a), pp.1241.

9. TANNER, R. I., "Alternative Mechanism for the Lubrication of
    Synovial Joints", Phys. Med. Biol., 1966, 11, pp.119-127.

10. FEIN, R. S., "Are Synovial Joints Squeeze Film Lubricated",
    Proc. Instn. Mech. Engrs., 1967, 181 (3J), pp.125-128.

11. DOWSON, D., "Modes of Lubrication in Human Joints", Symp.
    Lubrication and Wear in Living and Artificial Human Joints,
    Instn. Mech. Engrs., 1966, 181, pp.45-54.

12. DOWSON, D., LONGFIELD, M. D., WALKER, P. S., WRIGHT, V.,
     "Investigation of the friction and lubrication in Human Joints",
     Proc. Instn. Mech. Engrs., 1967-68, 182 (3N), pp.68-76.

13. LINN, F. C., "Lubrication of Animal Joints", J. Lubrication
     Technology, Trans. A.S.M.E., 1969, pp.329-341.

14. WALKER, P. S., DOWSON, D., LONGFIELD, M. D. and WRIGHT, V.,

15. McCUTCHEN, C. W., "Boundary Lubrication by Synovial Fluid,
     Demonstration and Possible Osmotic Explanation", Ref. Proc.,
     1966, 25, pp.1061.

16. DOWSON, D., UNSWORTH, A. and WRIGHT, V., "Analysis of Boosted
     Lubrication in Human Joints", J. Mech. Eng. Sci., 1970, 12 (5),
     pp.364-9.

17. HIGGINSON, G. R. and NORMAN, R., "A Model Investigation of
     Squeeze-Film Lubrication in Animal Joints", J. Mech. Eng. Sci.,
     1974, 16 (No. 4).

18. BOWDEN, F. P. "Friction and Surface Damage of Non-Metallic
     Solids", Proc. Intl. Con. Abrasion Wear, "Engineering, 1951,
     172, pp. 694 and 724.

19. DENNY, D. F., "Influence of Load and Surface Roughness on the
     Friction of Rubber-like Materials", Proc. Phys. Soc., 1953,
     66 (9B), pp.721-27.

20. PASCOE, M. W. and TABOR, D., "Friction and Deformation of
     Polymers", Proc. Phys. Soc., 1956, 235(a), pp.210.

21. McLAREN, K. G. and TABOR, D., "Friction of Polymers at
     Engineering Speeds: Influence of Speed, Temperature and
     Lubricants", Lubrication and Wear, Proc. Inst. Mech. Engrs.,
     1963, pp.210-15.

22. COHEN, S. C. and TABOR, D., "Friction and Lubrication of
     Polymers", Proc. Roy. Soc., 1965, 291(a), 186-207.

23. ANON, "More about Rubber Bearings for Marine Propeller Shafts",
India-Rubber J., 1927, 73, pp.1044-46.

24. ANON, "Rubber Bearings", ibid, pp.592.

25. HAUSMALTER, F. L. and MOFFITT, L. Q., "Water Lubricated Rubber
Bearings", The Machinist, Lond., 1933, 79, pp.342e-44e.

26. BRAZIER, S. A. and HOLLAND-BOWYER, W. "Rubber as a material for
Bearings", Proc. Gen. Disc. Lubrication and Lubricants, Instn.
Mech. Engrs., 1937, 1, pp.30-37.

27. BUSSE, W. F. and DENTON, W. H., "Water Lubricated Soft-Rubber
Bearings, India-Rubber J., 1932, 84, pp.347-53.

28. FOGG, A. and HUNWICKS, S. A., "Some experiments with Water
Lubricated Rubber Bearings", Proc. Gen. Disc. Lubrication and
Lubricants, Instn. Mech. Engrs., 1937, 1, pp.95-100.

29. HOTHER-LUSHINGTON, S. and SELLORS, P. "Water-Lubricated Bearings:
Initial Studies and Future Prospects in the Power Generation
Industry", Lubrication and Wear, Proc. Inst. Mech. Engrs., 1963,
pp.139-46.

30. HIGGINSON, G. R., "A Model Experiment in Elasto-Hydrodynamic
Lubrication", Int. J. Mech. Sci., 1962, 4, pp.205-10.

31. KIRK, M. T., "Hydrodynamic Lubrication of Perspex", Nature,
1962, 194, pp.965-6.

32. ARCHARD, J. F. and KIRK, M. T., "Influence of Elastic Modulus
on the Lubrication of Point Contacts", Lubrication and Wear,
Proc. Instn. Mech. Engrs., 1963, pp.181-89.

33. ROBERTS, A. D. and SWALES, P. D., "The Elasto-Hydrodynamic
Lubrication of a highly Elastic Cylindrical Surface", Brit. J.
App. Phys. (J. Phys. D.), 1969, 2 (2), pp.1317-26.

34. SWALES, P. D., DOWSON, D. and LATHAM, J. L., "Theoretical and
Experimental Observations of the Behaviour of Soft Elastic

Materials under Elastohydrodynamic Conditions", Symp.
Elastohydrodynamic Lubrication, Instn. Mech. Engrs., 1972,
pp.22-28.

35. JAGGER, E. T. and WALKER, P. S., "Further Studies of the
Lubrication of Synthetic Rubber Rotary Shaft Seals". Proc.
Instn. Mech. Engrs., 1966-67, 181 (1), pp.191-204.

36. DOWSON, D. and TAYLOR, C. M., "Elastohydrodynamic Lubrication
of Circular Plate Thrust Bearings", J. Lubrication Technology,
Trans. A.S.M.E., 1967, 89F, pp.237-244.

37. CASTELLI, V., RIGHTMIRE, G. K. and FULLER, D. D., "Investigation
of a Hydrostatic, Axisymmetric Compliant-Surface Thrust Bearing",
ibid, pp.510-20.

38. BENNETT, A., "Hydrodynamic Lubrication of Soft Solids", M.Sc.
Thesis, University of Durham, 1969.

39. BENNETT, A. and HIGGINSON, G. R., "Hydrodynamic Lubrication of
Soft Solids", J. Mech. Eng. Sc., 1970, 12 (3), pp.218-222.

40. HIGGINSON, G. R., "The Theoretical effects of Elastic Deformation
of the Bearing Liner on Journal Bearing Performance", Proc.
Instn. Mech. Engrs., 1965-66, 180 (3B), pp.31-38.

41. O'DONOGHUE, J., BRIGHTON, D. K. and HOOKE, C. J., "The Effect
of Elastic Distortions on Journal Bearing Performance, J.
Lubrication Technology, Trans. A.S.M.E., 1967, 89 (F),
pp.409-417.

42. HOOKE, C. J., BRIGHTON, D. K. and O'DONOGHUE, J., "The Effect
of Elastic Distortions on the Performance of Thin Shell
Bearings", Proc. Instn. Mech. Engrs., 1966-67, 181 (3B),
pp.63-69.

43. BRIGHTON, D. K., HOOKE, C. J. and O'DONOGHUE, J., "Theoretical
and Experimental Investigation of the Effect of Elastic

Distortions on the Performance of Journal Bearings", Proc. Instn.
Mech. Engrs., 1967-68, 182 (3N), pp.194-200.

44. BRIGHTON, D. K., HOOKE, C. J. and O'DONOGHUE, J. P., "Distortion
of a Squeeze Film Bearing", Proc. Instn. Mech. Engrs.; 1968-69,
183 (3P), pp.15-20.

45. HOOKE, C. J. and O'DONOGHUE, J. P., "Elastohydrodynamic
Lubrication of Soft, Highly Deformed Contacts", J. Mech. Eng.
Sci., 1972, 14 (1), pp. 34-48.

46. BAGLIN, K. P. and ARCHARD, J. F., "Analytic Solution of the
Elastohydrodynamic Lubrication of Materials of Low Elastic
Modulus", Symp. E.H.L. (Leeds), Instn. Mech. Engrs., 1972,
pp.13-21.

47. DOWSON, D. and HIGGINSON, G. R., "A Numerical Solution to the
Elasto-Hydrodynamic Problem", J. Mech. Eng. Sci., 1959, 1 (1),
pp. 6-15.

48. DOWSON, D. and HIGGINSON, G. R., "Elasto-Hydrodynamic Lubrication",
Pergamon Press, 1966.

49. DRUTOWSKI, R. C., "Contact Elasticity of Seal Elastomers",
J. Lubrication Technology, Trans. A.S.M.E., 1968, pp.478-83.

50. HERTZ, H. R., "Miscellaneous Papers", Macmillan, 1896.

51. IRONS, B. M., "Numerical Integration Applied to Finite Element
Methods", Int. Symp. Electronic Digtl. Comput. Structl. Engrg.,
Newcastle Univ., 1966.

52. ZIENKIEWICZ, O. C. and CHEUNG, J. K., "The Finite Element Method
in Structural and Continuum Mechanics". McGraw-Hill, 1967.

53. ERGATOUDIS, IRONS, B. M. and ZIENKIEWICZ, "Curved Isoparametric,
"Quadrilateral" Elements for Finite Element Analysis", Int. J.
Solid Structures, 1968, 4, pp.31-42.

54. IRONS, B. M., "Frontal Solution Program for Finite Element Analysis", Int. J. Numerical Methods in Engrg., 1970, 2, pp. 5-32.

55. IRONS, B. M. and DRAPER, K. J., "Lagrange Multiplier Techniques in Structural Analysis", AIAA J., 1965, 3 (6), pp. 1172-74.

56. IRONS, B. M., "Round off Criteria in Direct Stiffness Solutions", AIAA J., 1968, 6 (7), pp.1308-12.

57. BETTESS, P., Private Communication, 1970.